UNIVERSITY OF OKLAHOMA

GRADUATE COLLEGE

THE EFFECT OF STRONG ELECTRIC FIELDS ON TYROSINE HYDROXYLASE ACTIVITY

A DISSERTATION

SUBMITTED TO THE GRADUATE FACULTY

in partial fulfillment of the requirements for the

Degree of

DOCTOR OF PHILOSOPHY

By

KAREN A. JOHNSON

Norman, Oklahoma

2009

THE EFFECT OF STRONG ELECTRIC FIELDS ON TYROSINE HYDROXYLASE ACTIVITY

A DISSERTATION APPROVED FOR THE
DEPARTMENT OF CHEMISTRY AND BIOCHEMISTRY

BY

_____
Dr. C. LeRoy Blank

_____
Dr. Richard Taylor

_____
Dr. Robert White

_____
Dr. Daniel Glatzhofer

_____
Dr. Stewart Ryan

© Copyright by Karen A. Johnson 2009
All Rights Reserved.

Acknowledgments

First, I would like to thank Dr. C. LeRoy Blank for his guidance during my college career. He directed my research as an undergraduate in a summer undergraduate research fellowship program and as a graduate student at the University of Oklahoma and for that I will always be grateful. Dr. Blank's vast knowledge of not only science but innumerable other subjects was of great assistance to me as it has been for all other graduate students that have been a part of his laboratory. Dr. Blank, thank you for putting up with me for so many years. You've become a great friend.

I would next like to thank my husband, Robert, for always being there to listen and help when there were questions that I could not answer. Without you, and your encouragement, I don't know how I could have finished my research and dissertation. I don't have the words to express how thankful I am for having you in my life and all that you've done for me. You make my heart smile.

Finally, I would like to thank my family. To my mother and father, Wanda and Gerry Bailey, and my brother, Kevin Bailey, I am sure you were wondering if this day would ever come, but it has, and I assure you that without your support it would not have been possible. Not only did you help me move numerous times during my college career, but you were always there when my car broke down, or when something else needed done that I didn't know how to do.

Table of Contents

Chapter 1: Tyrosine Hydroxylase

Chapter 2: Liquid Chromatography with Electrochemical Detection

Chapter 3: Tyrosine Hydroxylase-Glutathione-S-Transferase Expression, Purification and Assay for Activity

Chapter 4: Immobilization of TH-GST Fusion Protein on Glutathione-Modified Glass Slides

Chapter 5: Tyrosine Hydroxylase Activity in the Presence of a Strong Electric Field

List of Tables

List of Figures

List of Abbreviations

6-MPH_4	6-Methyl-5,6,7,8-tetrahydropterin
AMP	Adenosine 5'-monophosphate
ATP	Adenosine 5'-triphosphate
BH_4	Tetrahydrobiopterin
BSA	Bovine serum albumin
C	Coulomb
°C	Celsius
cAMP	Adenosine 3',5'-cyclic monophosphate
cDNA	Complimentary deoxyribonucleic acid
cm	Centimeter(s)
CRE	cAMP response element
CREB	cAMP response element binding protein
ddH_2O	Distilled deionized water
DA	Dopamine
D	Electric displacement
DNA	Deoxyribonucleic acid
DOE	Department of Energy
DTT	Dithiothreitol
E	Electric field
EC	Electrochemical detection
E. coli	Escherichia coli

EDTA	Ethylenediaminetraacetic acid
EPI	Epinephrine
ε	Permittivity
ERK1	Extracellular signal-regulated protein kinase 1
ERK2	Extracellular signal-regulated protein kinase 2
eq	Equivalents
F	Farad(s)
g	Gram(s)
g	Gravity
Glu	Glutamate
GΩ	Gigaohm(s)
GSH	Glutathione
GSH-agarose	Glutathione-agarose
GSSG	Glutathione, oxidized
GST	Glutathione-S-transferase
HDV	Hydrodynamic votammogram
His	Histidine
IPTG	Isopropyl β-D-1-thiogalactopyranoside
κ	Dielectric constant
kDa	KilloDalton(s)
K_m	Michaelis-Menton constant
l	length
L	Liter

LB Media	Luria-Bertani media
LC	Liquid chromatography
LCEC	Liquid chromatography with electrochemical detection
L-DOPA	3,4-Dihydroxy-L-phenylalanine
LDR	Linear dynamic range
L-TYR	L-Tyrosine
µg	Microgram
µL	Microliter
µm	Micrometer
M	Molar concentration
mA	MilliAmpere
mg	Milligram
min	Minute(s)
mL	Milliliter
mm	Millimeter
mM	Millimolar
MΩ	Megaohm(s)
mol	Mole(s)
mV	Millivolt
MPTS	3-Mercaptopropyl trimethoxysilane
mV	Millivolt(s)
NE	Norepinephrine
ng	nanogram

NIEHS	National Institute of Environmental Health Sciences
NIH	National Institute of Health
nm	Nanometer(s)
PCR	Polymerase chain reaction
PEEK	Polyetheretherketone
pF	PicoFarad(s)
PKA	Protein kinase A
PKC	Protein kinase C
pmol	picomole
PMSF	Phenylmethylsulfonyl fluoride
psi	Pounds per square inch
PVC	Polyvinyl chloride
Q	Charge
r	Radius
RNA	Ribonucleic acid
rpm	Revolutions per minute
SDS	Sodium dodecyl sulfate
SDS-PAGE	Sodium dodecyl sulfate-polyacrylamide gel electrophoresis
sec	Second(s)
Ser	Serine
σ	Standard deviation
Std Dev	Standard deviation
TEMED	N,N,N',N'-tetramethylethylenediamine

TH	Tyrosine hydroxylase
TH-GST	Tyrosine hydroxylase glutathione-S-transferase fusion protein
Tris	Tris(hydroxymethyl)aminomethane hydrochloride
Tween 20	Polyethylene glycol sorbitan monolaurate
V	Volt
Vdc	Direct current voltage
V_{max}	Maximum velocity (maximum rate of enzymatic reaction)

Abstract

Tyrosine hydroxylase (TH) catalyzes the first and, more importantly, the rate-limiting step in the biosynthetic pathway of the catecholamine neurotransmitters dopamine, norepinephrine and epinephrine. The regulation of the biosynthesis of these neurotransmitters is vital to normal physiological and psychological function. The activity of TH is currently known to be regulated by three mechanisms: two short-term regulatory mechanisms (seconds to minutes), including end-product feedback inhibition and phosphorylation, and one long-term regulatory mechanism (12 to 48 hours), involving transcriptional level expression of additional TH enzyme which becomes available for utilization in the biosynthetic pathway. A proposed fourth type of regulation of TH is derived from the existence of two distinct forms of TH within neurons: cytosolic and neuronal membrane-bound. The proximity of the neuronal membrane-bound form of TH to the two sources of strong electric fields (100,000 V/cm) associated with cell membranes, transmembrane and surface potentials, was hypothesized to change the conformation of TH due to its internal structural electric field susceptibility, i.e., its polarizability. This study has shown that, in fact, TH activity is increased when exposed to an external electric field. Kinetic studies revealed K_m values for both the L-tyrosine substrate and the 2-amino-4-hydroxy-6-methyltetrahydro-pteridine (6-MPH_4) synthetic cofactor increased when TH was exposed to an external electric field. However, even though TH appears less efficient in the presence of an electric field, V_{max} for both L-tyrosine and 6-MPH_4 increase. The turnover number, k_{cat}, of TH for L-tyrosine increased by 27% while the k_{cat} of TH for 6-MPH_4 increased by 41% in the presence of an applied external field.

Tyrosine Hydroxylase

Chapter 1

I. Introduction

The catecholamine neurotransmitters, dopamine, norepinephrine and epinephrine are vital to normal physiological and psychological function.

Catecholamines are involved in a vast range of physiological activities including heart rate, blood pressure, vasodilation, motility and digestion.[1] Deficiencies in dopamine have been shown to play a major role in Parkinson's Disease.[2,3] Catecholamine neurotransmitters also appear to play a significant role in various emotions and emotional disorders including happiness, depression, reward and schizophrenia.[4,5]

Tyrosine hydroxylase (TH) is the enzyme that catalyzes the first and rate-limiting step in the biosynthetic production of catecholamine neurotransmitters. Therefore, regulation or modulation of TH activity can have significant effects on normal biological function.

II. Catecholamine Neurotransmitters

A. Overview

1. Catecholamine Chemical Structure

The term catecholamine is a general description for any chemical which has a basic structure containing a catechol (benzene ring with two adjacent hydroxyl groups) moiety and an amine moiety. These fundamental structural components and the exact structures of the three known catecholamine neurotransmitters are shown in Figure 1-1.

2. Dopamine

Neurons containing dopamine are commonly known as dopaminergic neurons. Within the central nervous system, dopaminergic neurons predominantly occur in three main pathways. The first is the nigrostriatal pathway which originates in the substantia nigra and innervates the caudate nucleus and putamen of the corpus striatum. This pathway facilitates the initiation of voluntary movement, and degeneration of the dopaminergic neurons in this pathway has been implicated in the development of Parkinson's disease.

The second major dopaminergic pathway is the mesocortical pathway which originates in the ventral tegmental area of the midbrain and innervates various regions of the forebrain including the frontal and cingulate cortex, the septum, the nucleus accumbens, and the olfactory tubercle of the limbic system. This pathway is involved in a reward system that reinforces certain adaptive behaviors. It is also implicated in psychiatric disorders such as schizophrenia.[6]

Figure 1-1. Structures of catechol and various catecholamines.

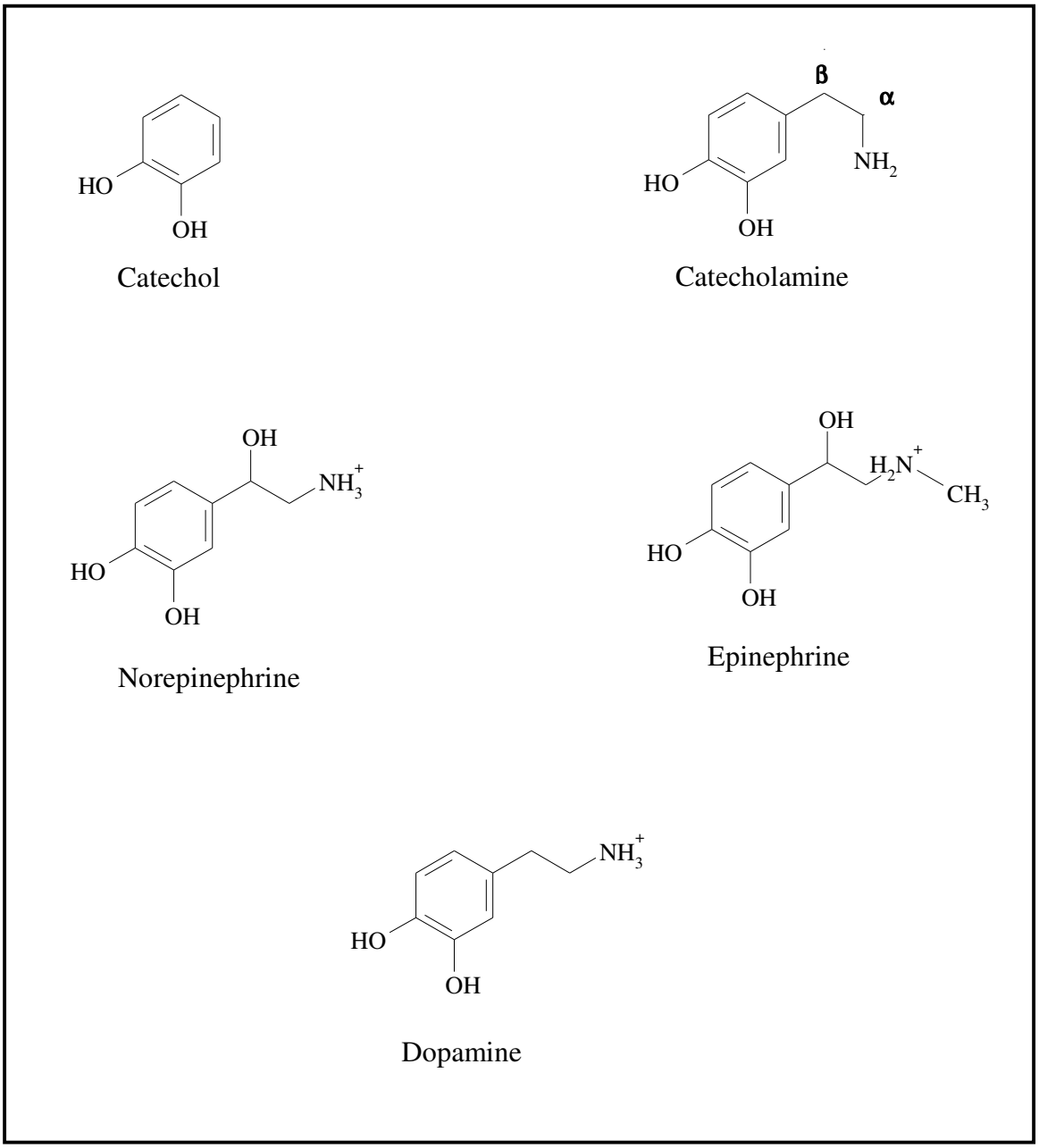

The third is the tuberoinfundibular pathway originating in the hypothalamus and innervating the pituitary and the median eminence. This pathway influences the secretion of hormones such as prolactin which stimulates lactation.[6,7]

Dopaminergic neurons are also found within the olfactory bulb and the retina.

3. Norepinephrine

Neurons containing norepinephrine are commonly known as noradrenergic neurons. Noradrenergic neurons within the central nervous system can be grouped into two major pathways: the dorsal bundle and the ventral bundle. The dorsal bundle originates in the locus ceruleus, which is located adjacent to the fourth ventricle in the pons region of the brain. This bundle innervates the spinal cord, the cerebellum, the cerebral cortex and the hippocampus. The ventral bundle, on the other hand, primarily innervates the brainstem and hypothalamus. The roles of noradrenergic neurons within the CNS are diverse, including involvement in learning, memory, reinforcement, sleep-wake cycle regulation, cerebral blood flow and metablolism.[6,8]

4. Epinephrine

Neurons containing epinephrine are commonly known as adrenergic neurons. Adrenergic neurons originate in the pons and the medulla regions and innervate the brain stem and the hypothalamus. Adrenergic neurons within the central nervous systems have possible roles in neuroendocrine mechanisms and blood pressure control.[7,9]

B. Biosynthesis of Catecholamine Neurotransmitters

1. Biosynthesis Scheme

The immediate precursor to all catecholamine neurotransmitters is L-tyrosine. L-Tyrosine is normally obtained from dietary sources. However, it is officially classified as a nonessential amino acid, since, it can be synthesized from L-phenylalanine which is an essential amino acid.[10]

Common names, alternate structurally related names, and common abbreviations for compounds involved in the biosynthesis of the catecholamine neurotransmitters are given in Table 1-1.

Table 1-1. Catecholamine names and abbreviations.

Common Names	Alternate Structurally Related Names	Abbreviations
L-tyrosine l-tyrosine	3-hydroxy-L-phenylalanine	L-TYR
L-dopa l-dopa	3,4-dihydroxy-L-phenylalanine	L-DOPA
dopamine	dihydroxyphenylethylamine	DA
norepinephrine or noradrenaline	dihydroxyphenylethanolamine	NE
epinephrine or adrenaline	3,4-dihydroxy-N-methyl phenylethanolamine	EPI

The biosynthetic pathways for catecholamine neurotransmitters including enzymes and cofactors involved in each step are illustrated in Figure 1-2.

The first step in the production of catecholamine neurotransmitters is the hydroxylation of L-tyrosine to form L-dopa (3,4-dihydroxy-L-phenylalanine). This reaction is catalyzed by tyrosine hydroxylase (TH). As a consequence, TH is found in all cells that synthesize catecholamines. This normally represents the rate-limiting step in the biosynthesis of these neurotransmitters. We will shortly discuss TH in greater detail.

Dopamine is synthesized by the DOPA decarboxylase-catalyzed removal of the carboxyl group from L-dopa. This enzyme is also capable of decarboxylating all naturally occurring aromatic L-amino acids; therefore, it is additionally known as L-aromatic amino acid decarboxylase. It's a 109 kDA enzyme requiring pyridoxal phosphate (vitamin B6) as a cofactor. It has a K_m value of 0.4 mM.[11] Its low K_m and high V_{max} result in very efficient decarboxylation of L-dopa to dopamine. DOPA decarboxylase is located within the cytosol of all dopaminergic neurons, noradrenergic neurons, and adrenergic neurons.

Norepinephrine is synthesized by the addition of a hydroxyl group to the β-carbon on the side chain of dopamine. This reaction is catalyzed by dopamine β-hydroxylase which requires molecular oxygen and ascorbate as cofactors in addition to Cu^{2+} to facilitate electron transfer in the reaction. It's a 290 kDa enzyme with a K_m of 5 mM and is located within the catecholamine storage vesicles in all noradreneric and adrenergic neurons.

Figure 1-2. Biosynthetic pathway for catecholamine neurotransmitters.

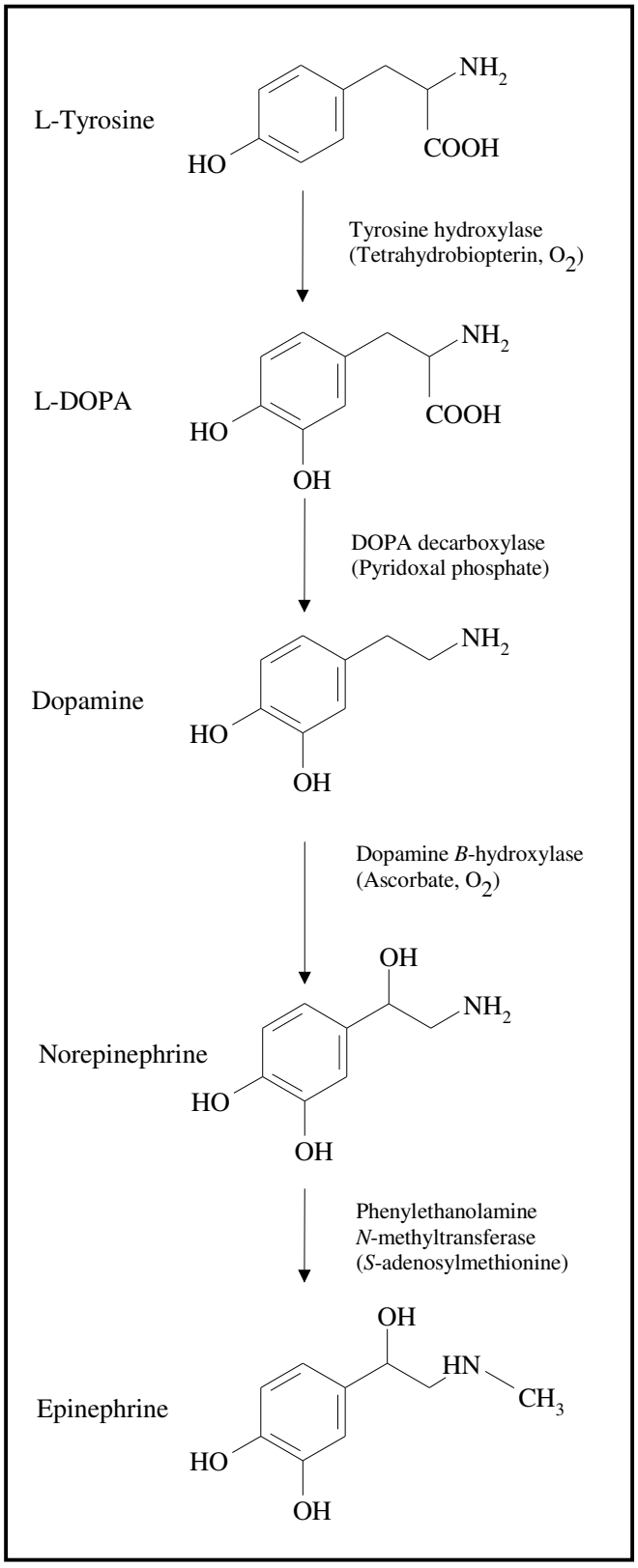

Phenylethanolamine N-methyltransferase catalyzes the addition of a methyl group to the amine group of norepinephrine to create epinephrine. It requires S-adenosyl methionine as a cofactor. It's a 30 kDa enzyme located within the cytosol of adrenergic neurons.

2. The Rate-Limiting Step

Tyrosine hydroxylase requires molecular oxygen, O_2, for conversion of L-tyrosine to L-dopa as well as the cofactor 2-amino-4-hydroxy-6-[1,2-dihydroxypropyl (L-erythro)] pteridine (Figure 1-3). Since 2-amino-4-hydroxy-pteridine is frequently called simply "pterin," this cofactor is also commonly known as tetrahydrobiopterin (BH_4).[12,13]

Figure 1-3. Structure of tetrahydrobiopterin (BH_4).

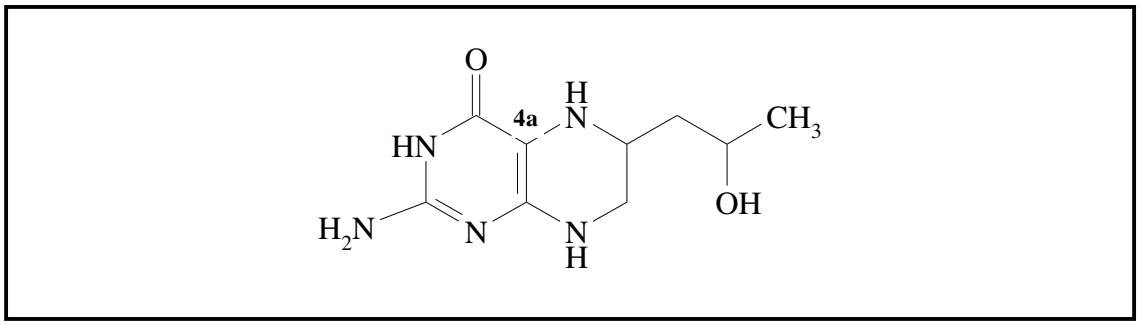

TH also requires ferrous iron for effective conversion of L-tyrosine to L-dopa. Catalytic domain characterization through crystallographic studies has shown that the active site Fe^{2+} is coordinated to the amino acid residues His331, His336 and Glu376.[14]

It has been determined that the substrate and cofactors demonstrate an ordered binding process with BH_4 binding first, followed by molecular oxygen and finally L-tyrosine.[13,15,16]. No reaction occurs until all three are bound.[17] It is thought that BH_4 works in conjunction with the active site Fe^{2+} to activate molecular oxygen.[18] During the hydroxylation reaction, the molecular oxygen serves as the source of the oxygen atom used for the hydroxyl group added to L-tyrosine in producing L-dopa. The remaining oxygen atom from the molecular oxygen is incorporated into the hydroxyl group at the 4a position of BH_4 producing 4a-OH-BH_4.

III. Tyrosine Hydroxylase

A. Structure of Tyrosine Hydroxylase

1. Primary Structure

Human TH consists of 497 amino acids with a molecular weight of 56 kDa. Rat TH, cloned from male Sprague-Dawley rats, consists of 498 amino acids, has a molecular weight of 56 kDa and has shown considerable homology to human TH with 89% of the amino acid sequence being conserved.[19] Due to its relative ease of accessibility and similarity to human TH, rat TH has been used extensively in studies of this enzyme

including the current study. Subsequent references to TH in this dissertation refer to rat TH unless otherwise stated.

The full amino acid sequence of TH can be seen in Figure 1-4. The N-terminal domain, consisting of amino acids 1-155, is commonly identified as the regulatory domain of TH. The catalytic domain is typically associated with amino acid residues 156-456, while the remaining C-terminal amino acid residues, 457-498, have been shown to primarily be important for the tertiary structure.[14] The full amino acid sequence is shown in Figure 1-4.

Figure 1-4. Tyrosine hydroxylase amino acid sequence.

```
        10         20         30         40         50         60
MPTPSAPSPQ PKGFRRAVSE QDAKQAEAVT SPRFIGRRQS LIEDARKERE AAAAAAAAAV

        70         80         90        100        110        120
ASSEPGNPLE AVVFEERDGN AVLNLLFSLR GTKPSSLSRA VKVFETFEAK IHHLETRPAQ

       130        140        150        160        170        180
RPLAGSPHLE YFVRFEVPSG DLAALLSSVR RVSDDVRSAR EDKVPWFPRK VSELDKCHHL

       190        200        210        220        230        240
VTKFDPDLDL DHPGFSDQVY RQRRKLIAEI AFQYKHGEPI PHVEYTAEEI ATWKEVYVTL

       250        260        270        280        290        300
KGLYATHACR EHLEGFQLLE RYCGYREDSI PQLEDVSRFL KERTGFQLRP VAGLLSARDF

       310        320        330        340        350        360
LASLAFRVFQ CTQYIRHASS PMHSPEPDCC HELLGHVPML ADRTFAQFSQ DIGLASLGAS

       370        380        390        400        410        420
DEEIEKLSTV YWFTVEFGLC KQNGELKAYG AGLLSSYGEL LHSLSEEPEV RAFDPDTAAV

       430        440        450        460        470        480
QPYQDQTYQP VYFVSESFND AKDKLRNYAS RIQRPFSVKF DPYTLAIDVL DSPHTIQRSL

       490
EGVQDELHTL AHALSAIS
```

2. Secondary Structures

Goodwill et al.[14] determined that the secondary structures formed in the catalytic domain and the C-terminal structural domain of tyrosine hydroxylase included 14 α-helices and 8 β-strands. A bend in one of these α-helices is responsible for the proximity of His331 to His336 which aids in coordination of the Fe^{2+} at the active site.

3. Tertiary Structure of Catalytic and C-Terminal Domains

An image of the catalytic and extreme C-terminal domains of TH reported by Goodwill et al.[14] is illustrated in Figure 1-5. BH_4 and an Fe^{2+} atom are clearly visible in the active site.

The active site of TH has been described as an α-helical basket with the helices interacting mainly with loops and only loosely with other α-helices. This loose structure may facilitate the enzyme's conformational change needed for activity. The two β-strands and terminal α-helix in the foreground and right side of the image in Figure 1-5 make up the C-terminal structural domain.

Figure 1-5. Image of the catalytic and C-terminal domains of tyrosine hydroxylase.[14,136]

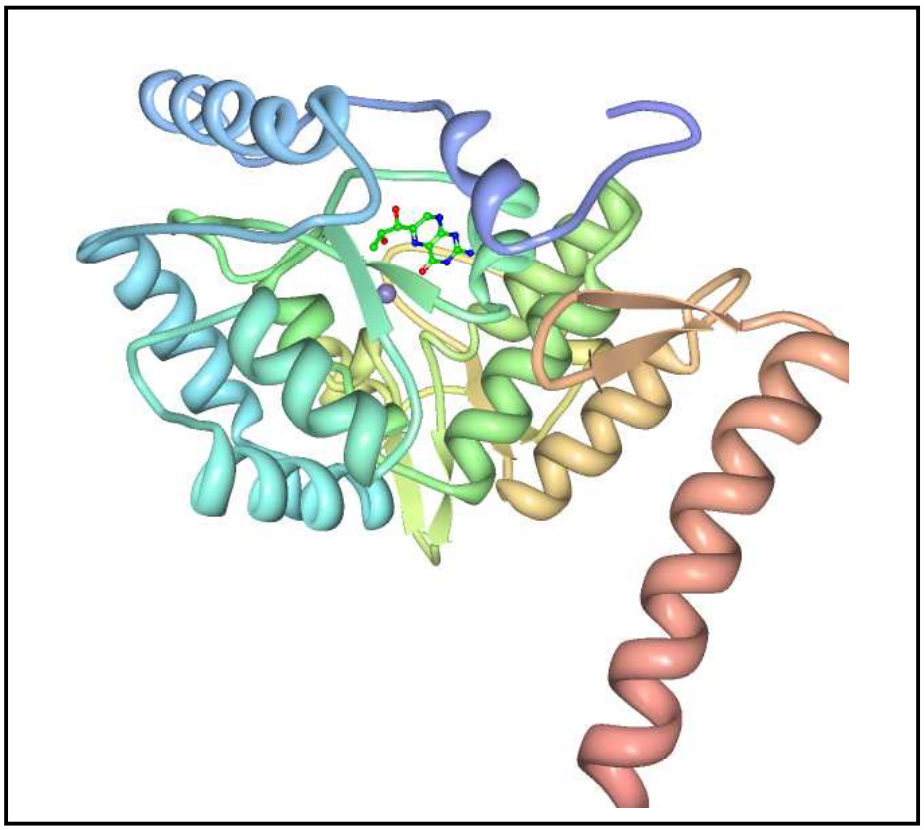

4. Quaternary Structure

The quaternary structure of TH consists of 4 identical monomers; therefore, it is referred to as a homotetramer. Figure 1-6 illustrates this TH tetramer. Figure 1-6 clearly demonstrates the importance of the C-terminal domain of TH in the structure of this homotetramer.

Figure 1-6. Quaternary structure of tyrosine hydroxylase.[14,136]

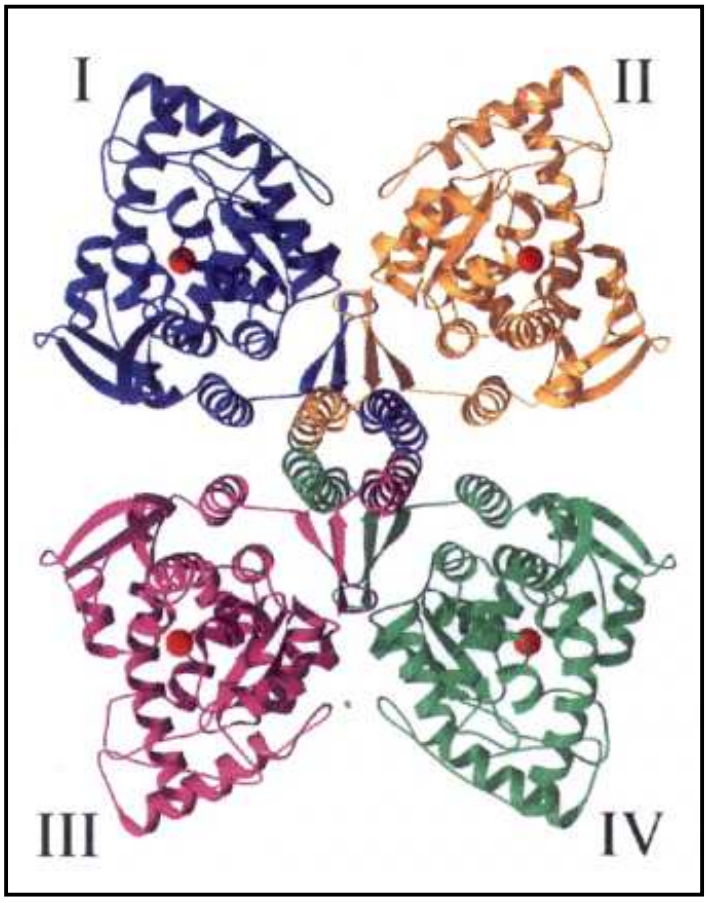

Each of the four monomers is identical. Each contains a catalytically active ferrous atom center and all monomers are catalytically active.[20]

B. Endogenous Regulation of TH Activity

1. Short-Term Regulation

There are two types of short-term regulation of TH activity that occur in the seconds to minutes time frame: product feedback inhibition and enzyme phosphorylation.

a. Feedback Inhibition

When the concentration ratio for the catecholamine neurotransmitter to the BH_4 cofactor is high, catecholamines demonstrate feedback inhibition of TH by competing for the binding site of BH_4.[21,22] Concentrations of $1.0x10^{-4}$ M dopamine, norepinephrine and epinephrine have each been shown to elicit TH activity inhibition of approximately 40%.[23] Higher concentrations of the catecholamine neurotransmitters can result in almost complete blockade of enzymatic activity. However, this feedback inhibition of enzymatic activity is easily reversible. When the concentration ratio of the catecholamine neurotransmitter to BH_4 is returned to a low level, the cofactor again binds to TH initiating normal enzymatic catalysis.

b. Phosphorylation

Phosphorylation is a commonly known method of short-term regulation for numerous enzymes.[24, Lehninger, 1993 #5]

TH is subject to multiple-site serine phosphorylation including Ser8, Ser19, Ser31, Ser40 and Ser153.[21,25,26] However, it has been shown that only Ser19, Ser31 and Ser40 are involved in the regulation of rat TH activity.[27,28] These three serine residues are conserved in human TH.[19] Thus, it is not surprising that the same three serine residues are involved in regulation of human TH.

Figure 1-7 illustrates the phosphorylation of a serine residue. The addition of a bulky, highly charged phosphate group to various serine moieties of TH changes the conformation of the enzyme leading to increased activity via differing effects on the catalytic process.

Figure 1-7. Phosphorylation of serine.

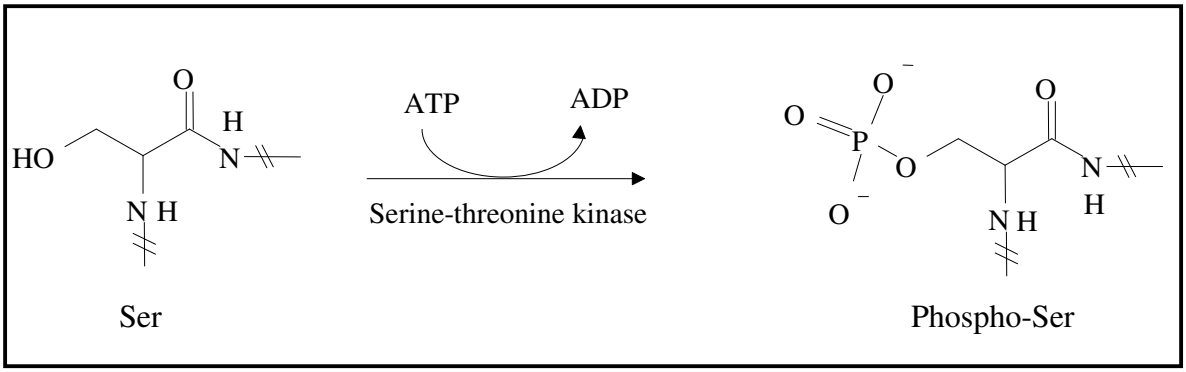

Phosphorylation of TH has been shown to be catalyzed by site-specific enzymes. Phosphorylation of Ser19 involves Ca^{2+}-calmodulin protein kinase II.[29] During increased neuronal activity, Ca^{2+} influx occurs and the intraneuronal concentration of Ca^{2+} increases. By binding to calmodulin, these calcium atoms induce a conformational change in this protein. The conformationally changed calmodulin, in turn, binds to Ca^{2+}-calmodulin protein kinase II. Binding of Ca^{2+}-calmodulin to the kinase results in increased activity of the kinase which enhances phosphorylation of Ser19 in TH.[10] Phosphorylation of Ser19 changes the structure of tyrosine hydroxylase to a conformation more easily accessed by the kinases necessary for the phosyphorylation of Ser40. The rate constant for the phosphorylation of Ser40 was shown to increase 2 to 3-fold if Ser19 had previously been phosphorylated.[30]

Cyclic AMP-dependent protein kinases A and C (PKA and PKC) catalyze the phosphorylation of Ser40.[21] The inactive form of these kinases consist of 4 subunits: 2 inhibitory regulatory domains and 2 catalytic domains. Binding of cAMP to both of the regulatory domains causes a conformational change and release of the catalytic subunits

which are, thereby, activated.[10] Cyclic AMP concentrations increase within neurons due to Ca^{2+}-calmodulin protein kinase II activation and subsequent phosphorylation of adenylyl cyclase, which accelerates the conversion of ATP to cAMP. The increase in cAMP activates the PKA enzyme and the PKC enzyme, both of which, in turn, can and do phosphorylate Ser40, increasing the activity of TH.[31] Phosphorylation of Ser40 reduces the K_m for BH_4 and correspondingly decreases the inhibition feedback due to catecholamine neurotransmitters. By increasing the affinity for limiting amounts of BH_4 and reducing the feedback inhibition, phosphorylation of Ser40 effectively increases the catalytic efficiency of tyrosine hydroxylase.[30,32-34]

Phosphorylation of Ser31 involves extracellular signal-regulated protein kinases 1 and 2 (ERK1 and ERK2).[20,35,36] GTP-binding protein, also known as stimulatory G protein (G_s), is a membrane protein on the extracellular surface of membranes. When a phorbol ester (extracellular signal) binds to G_s, its regulatory subunit is dissociated resulting in the activation of G_s. Activated G_s moves through the plane of the membrane, binding and simultaneously activating the membrane-bound adenylate cyclase. The active site of adenylate cyclase extends into the cytosol. When activated, adenylate cyclase catalyzes the production of cAMP from ATP. The newly formed cAMP then activates PKC.[10] Activation of PKC phosphorylates ERK1 and ERK2 rendering them active and able to phosphorylate TH at Ser31. Phosphorylation of tyrosine hydroxylase at Ser31 increases the activity of TH 1.2 to 2-fold as a consequence of a decreased K_m for BH_4.[20]

2. Long-Term Regulation

a. Regulation of TH Gene Expression

Expression of new TH protein molecules can be promoted by extended catecholaminergic activity and other phenomena.[37,38] This type of regulation is considered long-term, and occurs over a period of 12 - 48 hours.

Briefly, a cAMP response element (CRE) transcription factor is located upstream from the TH gene. Stimulation of adenylyl cyclase (for example, via Ca^{2+}-calmodulin protein kinase activation) increases cAMP production. The increase in cAMP activates PKA. The active catalytic subunits of PKA move into the cell nucleus and phosphorylate the CRE binding protein (CREB), changing its conformation. Activated CREB then binds to the CRE transcription factor promoting transcription of TH mRNA.[6,21,39,40] The new mRNA leaves the nucleus through pores in the nuclear envelope and binds to ribosomes which translate TH mRNA into assembled proteins. These newly assembled proteins then travel down the axon at a typical rate of 20-30 mm/day.[41-44]

3. Understanding Regulation through Michaelis-Menton Kinetics

Since tyrosine hydroxylase activity conforms to Michaelis-Menten kinetics, certain kinetic parameters related to regulation of its activity can be relatively easily determined experimentally.

a. Enzyme Kinetics

There are two general reactions involved in the enzyme-catalyzed conversion of a substrate to a product. The first reaction is the formation of the enzyme-substrate complex (ES) from the free enzyme (E) and the substrate (S) followed by breakdown of

the ES complex to form free enzyme, E, and product, P. These reactions are summarized below.

$$E + S \underset{k_{-1}}{\overset{k_1}{\rightleftharpoons}} ES$$

Equation 1-1

$$ES \underset{k_{-2}}{\overset{k_2}{\rightleftharpoons}} E + P$$

Equation 1-2

In an enzyme kinetic experiment, since the concentration of substrate changes over time, it is usual to focus on the measurement of the initial rate or initial velocity (V_o) of the reaction at a given set of conditions where this change will be negligible.

A plot of [S] versus V_o, with [E] held constant, is illustrated in Figure 1-8. As can be seen, at low [S] the initial velocity is almost directly proportional to [S]. In this region since most of the enzyme is free, as [S] increases Equation 1-1 is driven to the right to form ES with little to none of the reverse reaction happening. Further increases in substrate drive Equation 1-1 even farther to the right until the initial velocity approaches the V_{max} value. V_{max} is observed when virtually all of the enzyme is bound to substrate with essentially no free enzyme remaining. At this point, the enzyme is said to be "saturated" with its substrate with further increases in [S] having no measurable effect on the rate.

Figure 1-8. Substrate concentration effect on initial velocity of an enzyme.

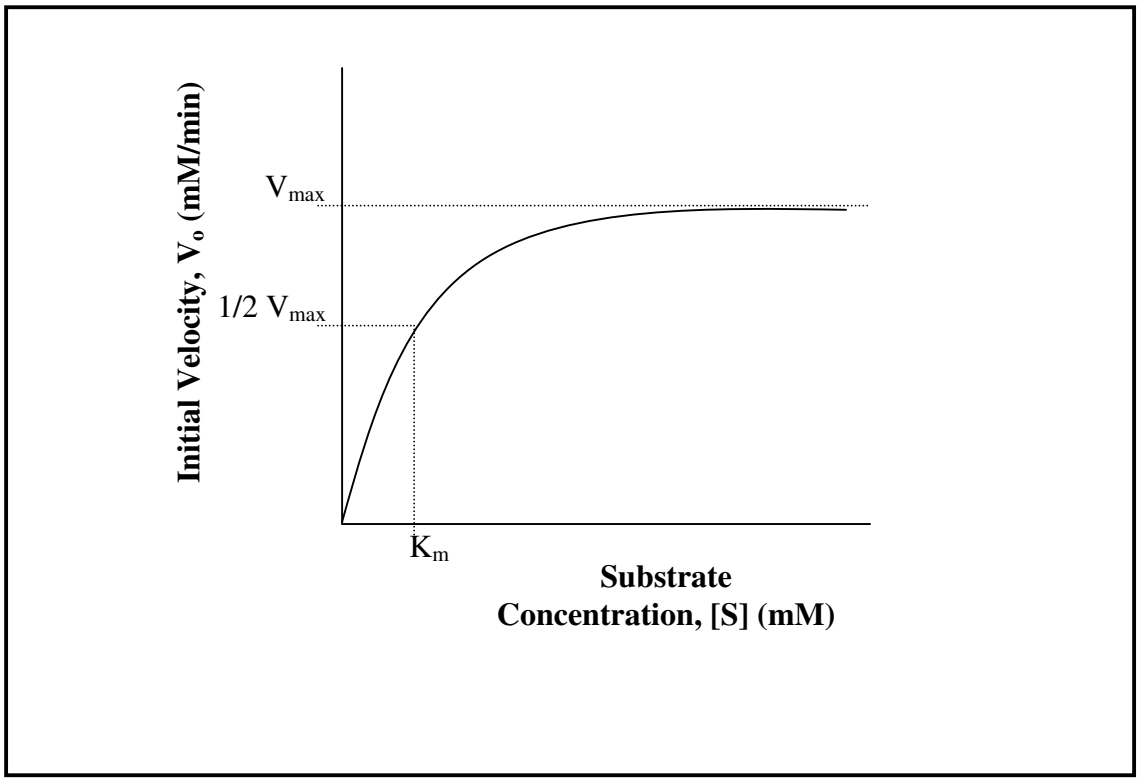

b. Michaelis-Menton Equation

Leonor Michaelis and Maud Menten derived a steady state formula that could easily be used experimentally.[45] Important for their derivation was the assumption that

the breakdown of ES to E and P was the rate-limiting step and that at V_o conditions, [P] is negligible so Equations 1-1 and 1-2 can now be represented by

$$E + S \underset{k_{-1}}{\overset{k_1}{\rightleftharpoons}} ES \xrightarrow{k_2} E + P$$

Equation 1-3

where

$$V_o = k_2[ES]$$ **Equation 1-4**

Since [ES] is not readily measured, Michaelis and Menten derived a formula to eliminate this term using two assumptions. First, the total amount of enzyme, $[E_t]$, is equal to [E] plus [ES]; therefore [ES] equals $[E_t]$ minus [E]. Second, they made the steady state assumption that the rate of formation of ES is equal to the rate of breakdown of ES resulting in

$$[ES] = \frac{[E_t][S]}{[S] + \frac{(k_{-1} + k_2)}{k_1}}$$ **Equation 1-5**

They then replaced the rate constant term with K_m, the Michaelis-Menten constant and since [ES] = $[E_t]$ at V_{max}, V_{max} equals $k_2[E_t]$. The Michaelis-Menten equation then for steady state kinetics is seen to be

$$V_o = \frac{V_{\max}[S]}{[S] + K_m}$$ **Equation 1-6**

c. Lineweaver-Burk Plot

A rearrangement of the Michaelis-Menten equation allows for graphical analysis through simple linear regression

$$\frac{1}{V_o} = \frac{K_m}{V_{\max}}\frac{1}{[S]} + \frac{1}{V_{\max}}$$ **Equation 1-7**

This form of the Michaelis-Menton equation leads to analysis by a so-called double reciprocal plot, also known as a Lineweaver-Burk plot. Figure 1-9 illustrates a typical Lineweaver-Burk plot. By plotting enzymatic data in this manner, K_m and V_{max} are, as seen, readily obtained.

Figure 1-9. Typical Lineweaver-Burk plot.

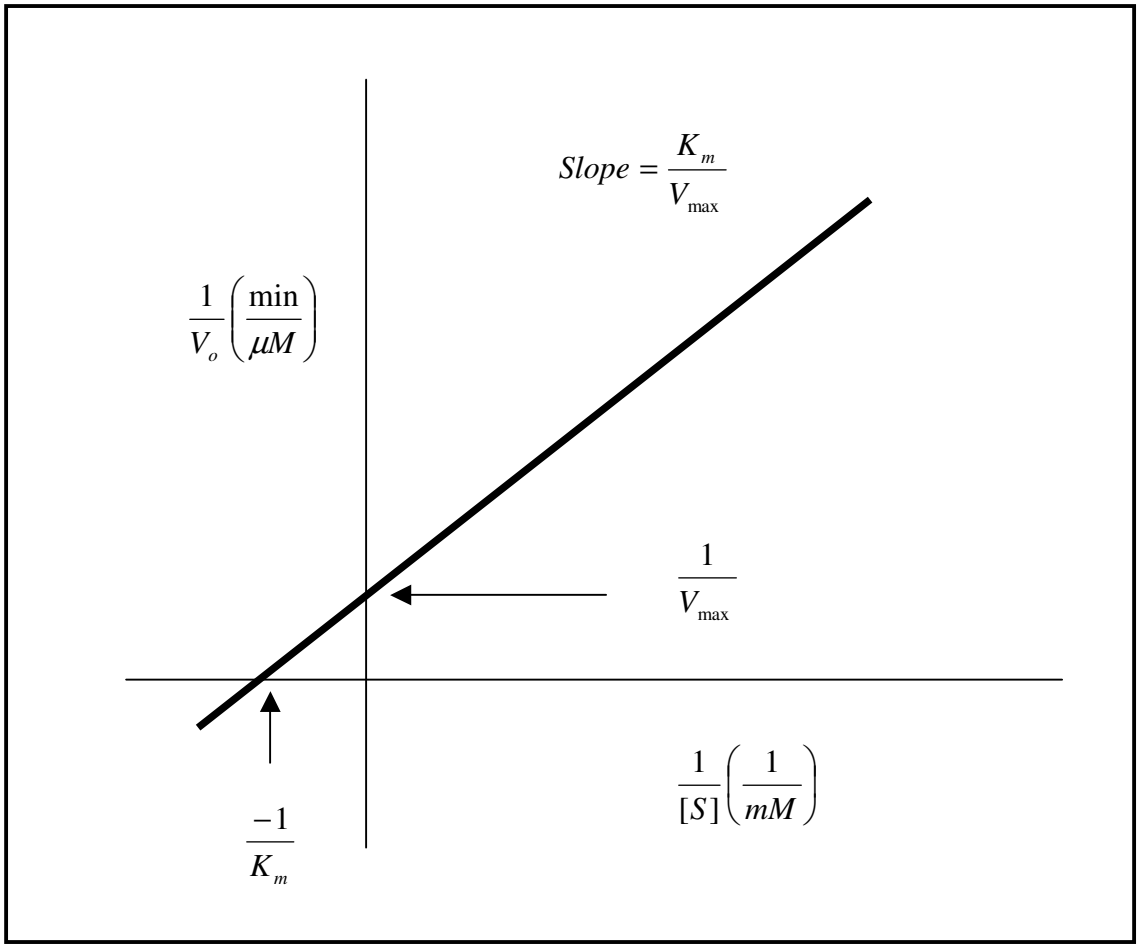

d. K_m and V_{max}

Since k_2 represents the rate constant for the rate-limiting step (conversion of ES to E and P), the value of k_2 is typically much less than k_{-1}. Therefore, the Michaelis-Menton constant can be reduced as

$$K_m = \frac{k_{-1} + k_2}{k_1} \cong \frac{k_{-1}}{k_1} \qquad \textbf{Equation 1-8}$$

The Michaelis-Menton constant, K_m, then, is an indirect measure of the affinity of the enzyme for the substrate. Smaller values of K_m demonstrate better substrate affinity, while larger values of Km indicate lesser substrate affinity. Typical values of K_m range from 10^{-3} to 10^{-6} M.[46] K_m is also equal to the concentration of the substrate necessary to achieve 1/2 V_{max}.

As stated above, V_{max} represents the maximum rate an enzyme can attain when saturated with substrate under the stated conditions.

Another useful kinetic parameter is k_{cat}, which is a first order rate constant for the rate-limiting step of the enzymatic reaction. Experimentally, k_{cat} is calculated using V_{max} and the total concentration of the enzyme, $[E_t]$ as

$$k_{cat} = \frac{V_{\max}}{[E_t]} \qquad \textbf{Equation 1-9}$$

Since k_{cat} represents the number of substrate molecules converted to product per enzyme molecule in a given amount of time when the enzyme is saturated by that substrate, it has been termed the turnover number.

The ratio of V_{max} to K_m is an important kinetic parameter which describes the relative specificity of a fixed amount of the enzyme for its substrate. Events which lead to an increased V_{max} to K_m ratio, for example conformational changes of the enzyme, improve the efficiency of the kinetic mechanism.[46]

IV. Neuronal Membranes

A. Fluid Mosaic Model

It has been well-established that tyrosine hydroxylase exists in two distinct forms within a neuron: cytosolic and membrane-bound.[25,47-53]

The neuronal cell membrane is composed of a phospholipid bilayer similar to the fluid mosaic model proposed by Singer and Nicolson in 1972.[54] In addition to phospholipids, the membrane contains transmembrane (integral) proteins, surface (peripheral) proteins and cholesterol. Figure 1-10 is a representation of the fluid mosaic model of a cell membrane.

Figure 1-10. Fluid mosaic model of a phospholipid bilayer membrane.

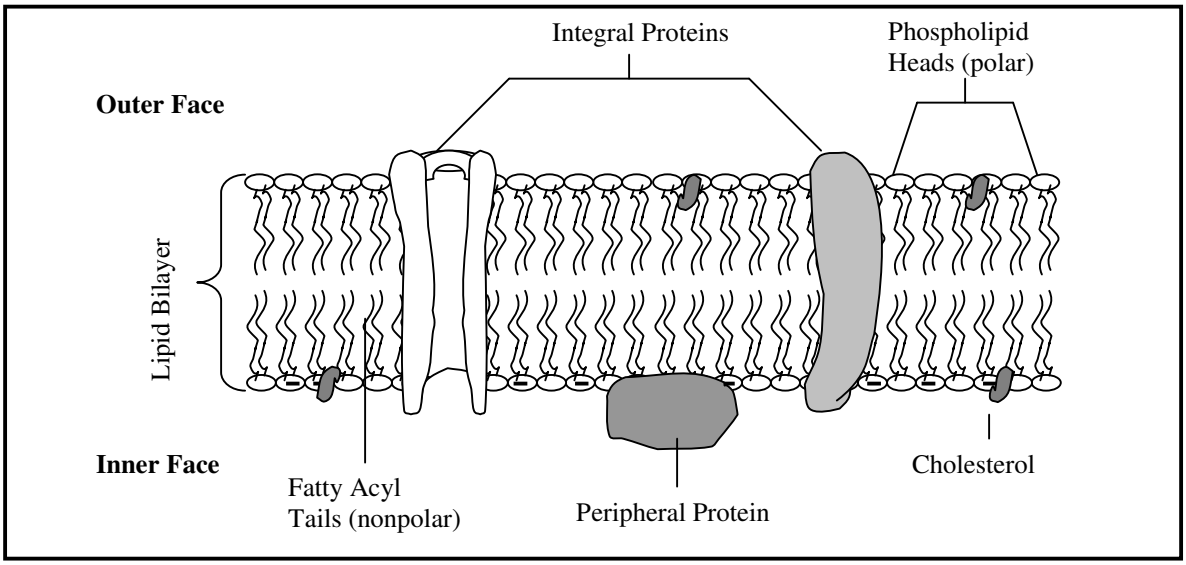

B. Membrane Potentials and Strong Electric Fields

There are two sources of electric fields associated with cell membranes: transmembrane and surface potentials.[55,56]

1. Transmembrane Potentials and Electric Fields

Transmembrane potentials arise from the nonhomogeneous distribution of charged ions on either side of the cell membrane. If the concentrations of all charged species were equal on either side of the membrane, there would be no potential difference across the membrane. However, due to the concentration differences, the charged species are thermodynamically driven to move across the membrane through ion specific pores down their concentration gradients. For example, given two separate KA salt solutions

separated by a cell membrane, if the concentration of K^+ ions outside the membrane is less than the concentration within the cell, K^+ would diffuse from the inside of the cell to the outside of the cell through a K^+ specific pore. This movement of positive charges out of the cell would lead to a net negative charge on the inside of the cell and a net positive charge on the outside of the cell, i.e., the potential difference. The net negative charge on the inside of the cell would attract K^+ ions back through the pore until an equilibrium potential for K^+ (E_{K+}) is reached. The equilibrium potential for an ion, E_{ion}, occurs when movement due to the potential difference is balanced by movement due to the diffusion. The Nernst equation can be used to calculate E_{ion}.

$$E_{ion} = 2.303\frac{RT}{zF}\log\frac{[ion]_o}{[ion]_i} \qquad \textbf{Equation 1-10}$$

In reality, the neuronal membrane is permeable to multiple ions (K^+, Na^+, Ca^{2+}, Cl^-) with varying permeablilities due to separately gated ion-specific channels. Therefore, the simplistic view afforded by Equation 1-9 and any associated calculation of the transmembrane potential is not adequate. Moreover, the resting membrane potential is maintained by ion pumps, such as the sodium-potassium pump and the calcium pump, which establish concentration gradients.[57] Typical concentrations of K^+, Na^+, Ca^{2+} and Cl^- inside the neuron at rest are 100 mM, 15 mM, 0.0002 mM and 13 mM, respectively; while extracellular concentrations for K^+, Na^+, Ca^{2+} and Cl^- are 5 mM, 150 mM, 2 mM and 150 mM, respectively.[41]

The Goldman equation[41,58] more comprehensively accounts for the permeability of each ion and can be used to reasonably estimate the resting membrane potential, V_{rest}.

$$V_{rest} = 2.303\frac{RT}{F}\log\frac{P_{K^+}[K^+]_o + P_{Na^+}[Na^+]_o + P_{Cl^-}[Cl^-]_o}{P_{K^+}[K^+]_i + P_{Na^+}[Na^+]_i + P_{Cl^-}[Cl^-]_i} \quad \textbf{Equation 1-11}$$

where P is the instantaneous relative permeability of an ion and the subscripts o and i denote concentrations outside and inside the cell, respectively. The resting membrane potential can be practically measured by using a voltmeter with a microtip electrode. The tip of the electrode is inserted into the cell while a reference wire is inserted into the extracellular fluid.[41] Such measurements closely correspond with values calculated from Equation 1-11.

The cell membrane can be viewed as a parallel plate capacitor.[59] A parallel plate capacitor consists of two parallel conductive plates of equal but opposite charge a distance of d from each other, where the area of each plate is A and the electric field between the plates is assumed to be uniform. The assumption that the electric field is uniform between the plates is reasonably correct as long as the distance between the plates is small compared to the area of the plates. The potential difference, V_o, across a parallel plate capacitor equals the electric field, E, times the distance between the plates, d

$$V_o = Ed \quad \textbf{Equation 1-12}$$

The electric field, E, across the parallel plate capacitor can thus be calculated as

$$E = \frac{V_o}{d} \qquad \textbf{Equation 1-13}$$

For a parallel plate capacitor with no dielectric, the capacitance, C_o, is

$$C_o = \frac{Q}{V_o} \qquad \textbf{Equation 1-14}$$

where Q is the charge on the capacitor. The charge is the charge density, σ, on the plate multiplied by the area of the plate

$$Q = \sigma A \qquad \textbf{Equation 1-15}$$

The charge density is calculated by

$$\sigma = \varepsilon_o E \qquad \textbf{Equation 1-16}$$

where ε_o is the permittivity of free space (8.8542×10^{-12} C^2/Nm^2). Thus, the capacitance

can be given as

$$C = \frac{\varepsilon_o EA}{V_o} = \frac{\varepsilon_o A}{d} \qquad \textbf{Equation 1-17}$$

Figure 1-11 illustrates a parallel plate capacitor with a dielectric material filling the space between the plates. This situation more closely mimics the situation with a cell membrane, where the membrane serves as a dielectric material. The dielectric material located between the plates is electrically neutral in the absence of an electric field; however, when an electric field is applied across the capacitor, the positive and negative charges within dielectric molecules are displaced. This results in a net positive charge on the surface of the dielectric facing the negative plate and a net negative charge on the surface of the dielectric facing the positive plate. Since the dielectric is a nonconducting material, this surface charge is bound to the molecules.

Figure 1-11. Parallel plate capacitor with a dielectric insert.

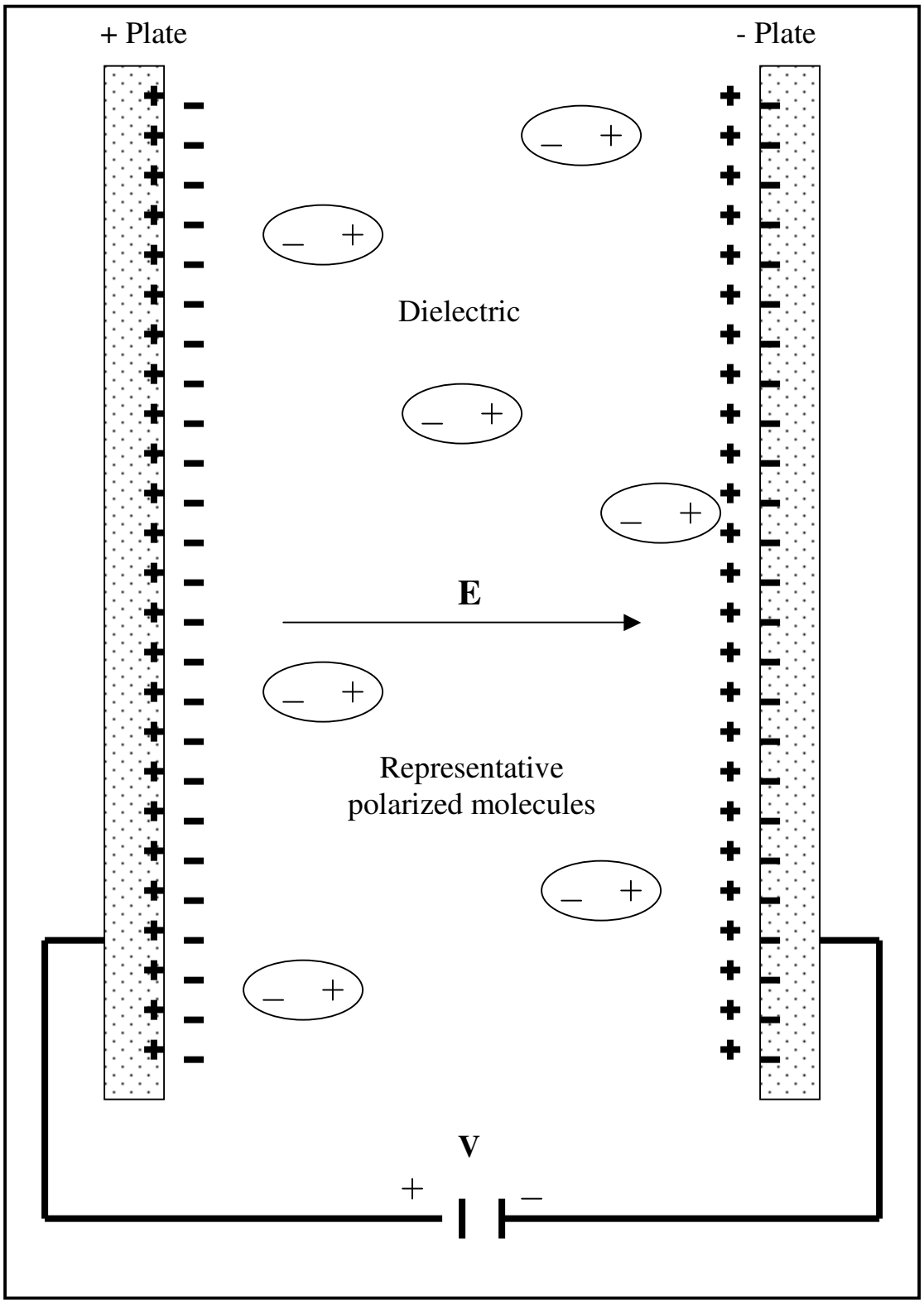

When a dielectric material is placed between the plates of a parallel plate capacitor, keeping all other factors equal, a voltmeter reading decreases across the plates. This voltage can be represented by V and is related to V_o by the following equation

$$V = \frac{V_o}{\kappa} \qquad \textbf{Equation 1-18}$$

where κ is the dielectric constant of the material.

Since the charge on the capacitor does not change, the capacitance can now be calculated by the following equation

$$C = \frac{Q}{V} = \kappa \frac{Q}{V_o} = \kappa C_o \qquad \textbf{Equation 1-19}$$

where C_o represents the capacitance in the absence of the dielectric. Therefore, capacitance is increased by a factor of κ when a dielectric material is inserted into the capacitor.

Substituting Equation 1-16 into Equation 1-18, the capacitance in the presence of a dielectric can then be calculated by

$$C = \kappa \frac{\varepsilon_o A}{d} \qquad \textbf{Equation 1-20}$$

Substituting Equation 1-17 into Equation 1-12, the electric field for a neuronal cell is calculated by

$$E = \frac{\kappa V}{d} \qquad \textbf{Equation 1-21}$$

So, for a cell membrane with a cell wall 7 nm thick,[6] a resting membrane potential of -70 mV[6] and a dielectric constant of 2,[59] the electric field across the membrane would be 2.0×10^5 V/cm.

2. Surface Potentials and Electric Fields

The second source of an electric field associated with a cell membrane is the surface potential. Surface potentials are the potential differences between the surface of the membrane and the bulk solution. The surface potential is usually negative since the surface charge of a synaptic cell membrane arises from the negatively charged phosphatidylserine.[60,61] The magnitude of the electric field drops exponentially as the distance from the cell membrane surface increases. This exponential drop is normally ascribed to the electrical double-layer. Counterions are adsorbed on the surface of the cell membrane in a "non-diffuse" layer which "screens" the surface potential from the bulk of the solution. Further dampening of the surface potential arises from a "diffuse" layer of ions having a charge opposite that of the ions constituting the "non-diffuse" layer. The potential can be estimated mathematically using the formula[61]

$$V = V_o e^{(-x/\lambda)} \qquad \textbf{Equation 1-22}$$

where V is the potential at distance x from the cell membrane, V_o is the surface potential of the cell membrane and λ is the Debye-Hückel length constant for the exponential decay (λ = 1 nm for typical physiological electrolyte concentrations).[61] Since V_o is negative, V is also notably negative relative to the bulk of the solution. The electric field at any point in the diffuse layer can then be estimated by

$$E = \frac{dV}{dx} = (-\frac{1}{\lambda})V_o e^{(-x/\lambda)} \qquad \textbf{Equation 1-23}$$

Assuming that 15% of the phospholipids in the membrane are negatively charged, the estimated surface potential would be -30 mV relative to the bulk of the solution.[61,62] Using the absolute value of this potential for the magnitude of V_o, the exponential decay profile for the surface derived electric field E from the surface of a cell membrane into the bulk of the solution was calculated and is represented in Table 1-2 and the corresponding Figure 1-12.

Table 1-2. Magnitude of the surface derived electric field at various distances from the cell membrane.

Distance from the Cell Membrane (nm)	Electric Field Magnitude (V/cm)	Distance from the Cell Membrane (nm)	Electric Field Magnitude (V/cm)	Distance from the Cell Membrane (nm)	Electric Field Magnitude (V/cm)
0.5	180,000	3.0	15,000	5.75	960
0.75	140,000	3.25	12,000	6.0	750
1.0	110,000	3.5	9,100	6.5	450
1.25	86,000	3.75	7,100	7.0	270
1.5	67,000	4.0	5,500	7.5	170
1.75	52,000	4.25	4,300	8.0	100
2.0	41,000	4.5	3,300	8.5	60
2.25	32,000	4.75	2,600	9.0	40
2.5	25,000	5.0	2,000	10	10
2.75	19,000	5.25	1,600	15	0.09
3.0	15,000	5.5	1,200	20	0.0006

Figure 1-12. Exponential decay of the suface derived electric field near the surface of the cell membrane.

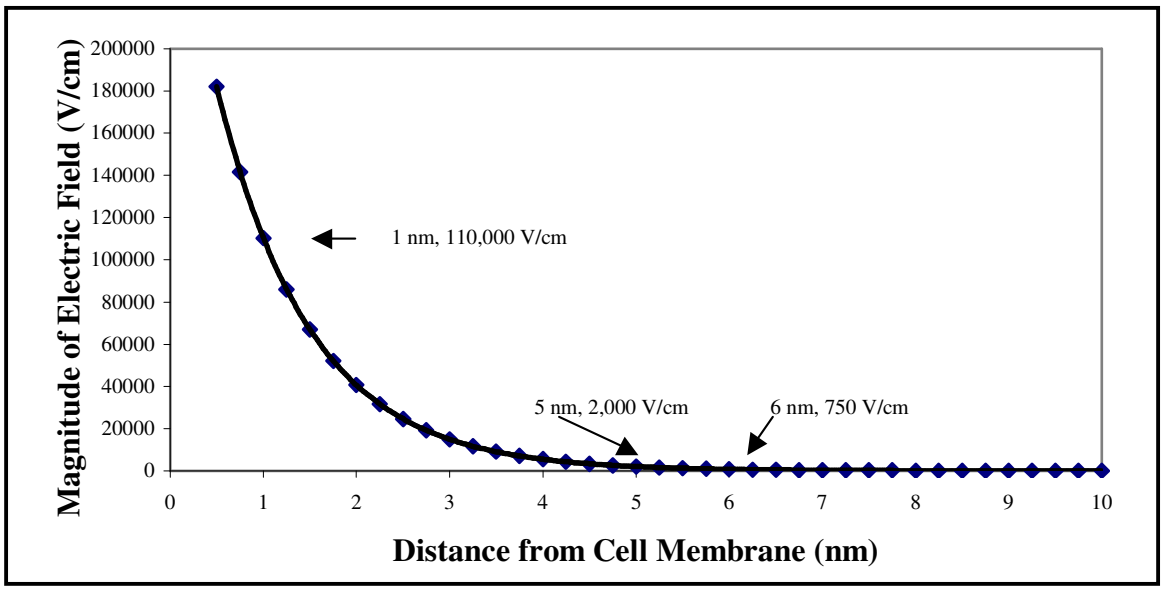

V. Current Study

A. Attachment of TH to Synaptic Membrane

Tyrosine hydroxylase exists in two fundamental forms: cytosolic and membrane-bound. Kuczenski et al.[50] have shown that the membrane-bound form of TH is, in fact, bound to the synaptic membrane.

Thórólfsson et al.[63] have proposed that TH is a specific type of peripheral protein called an amphitropic protein.[64] Amphitropic proteins have two distinct forms within cells: cytosolic and membrane-bound. Thórólfsson et al. have demonstrated that TH belongs to a specific category of amphitropic proteins that bind to membranes through amphipathic α-helices as illustrated in Figure 1-13. The binding of amphipathic helices is thought to be triggered by an electrostatic pull from phosphatidylserine. With its axis parallel to the membrane, the amphipathic helix partitions into the membrane with the hydrophobic side inserted into the bilayer while its hydrophilic side maintains contact with the cytosol. These same authors have shown that the TH binding to the cell membrane involves the two amphipathic N-terminal α-helices comprised of amino acid residues 15-30 and 37-58, respectively. The binding exhibits a dissociation constant of 305 μM.[63]

Figure 1-13. Amphipathic α-helix attachment of a general amphitropic protein to a membrane.

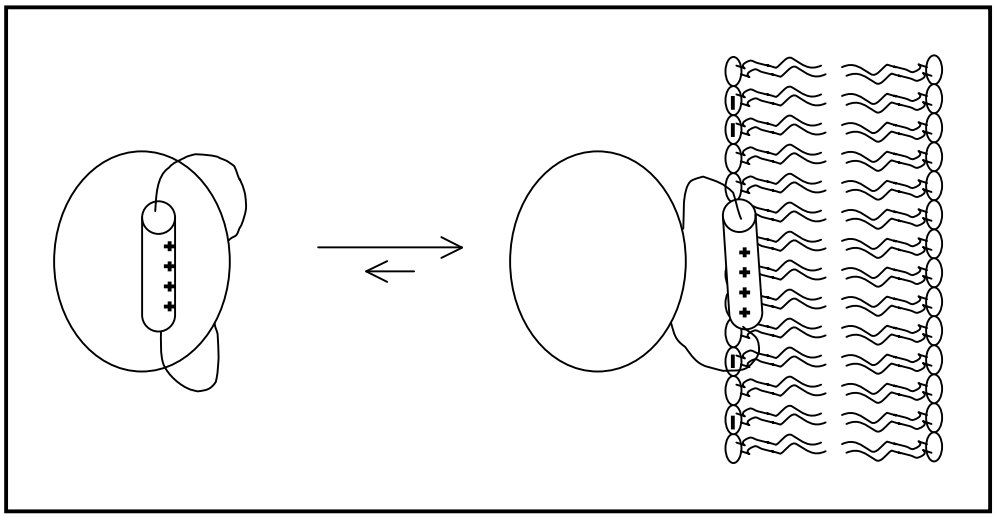

B. Structural Components of Proteins Affected by Electric Fields

Structural components of proteins susceptible to the presence of an applied electric field include ionized moieties, peptide bonds and α-helices, with the latter entities representing very large dipoles.[55,65] The dipole moment of a single peptide bond is 3.5 Debye (D). In an α-helix, these dipole moments are aligned along the axis of the helix, and due to polarization by hydrogen bonds, the aggregate possesses a dipole moment which can be one to two orders of magnitude greater than that of a single peptide bond.[55,65]

In the presence of an electric field, proteins respond in such a way as to increase their dipole moments. This is accomplished by dissociation of ionizable groups,

separation of charges, cooperative alignment of weak dipoles, reorientation of permanent dipoles within the protein, and conformational change(s) leading to an increased overall dipole moment.[56]

C. Proposed Fourth Type of Regulation of TH Activity

Since TH is attached to the cell membrane and its dimensions are roughly 19 nm x 16 nm x 6 nm,[14] the membrane-bound enzyme or substantial parts of the enzyme will be exposed to at least a portion of the electric field existing across the membrane and in the solution immediately adjacent to the surface of the membrane.

The presence of this strong electric field, it was hypothesized, would change the conformation of tyrosine hydroxylase due to its internal structural electric field susceptibility, i.e., its polarizability. Each monomer of tyrosine hydroxylase contains 36 positively charged arginine residues, 23 positively charged lysine residues, 29 negatively charged aspartate residues and 42 negatively charged glutamate residues, which, in aggregate, account for 26% of all of the amino acids in TH. In addition, along with the dipole contribution of all the individual peptide bonds, TH contains 14 α-helices, each of which independently possess very large aggregate dipoles. The presence of an electric field should, thus, clearly result in a conformational change in TH. A conformational change in TH would, subsequently, be predicted to have a measurable effect on its activity.

Liquid Chromatography with Electrochemical Detection

Chapter 2

I. Introduction

To determine the activity of tyrosine hydroxylase in an experimental setting, all components necessary for the conversion of L-tyrosine to L-dopa must be present. As discussed in Chapter 1, tyrosine hydroxylase (TH) requires a tetrahydropterin cofactor, ferrous ion and molecular oxygen to convert L-tyrosine to L-dopa. Other metal chelating and anti-oxidant compounds such as EDTA and sodium bisulfite are also typically necessary when TH is examined in vitro to prevent degradation of the enzyme as well as the product. Following the addition of these necessary components, we were able to routinely monitor the activity of TH by quantifying the production of L-dopa under various experimental conditions.

Prior to any experiments designed to monitor the activity of tyrosine hydroxylase, it was necessary to establish a technique for the routine separation and quantification of any L-dopa that might be present in the experimental incubation mixture. The technique

chosen for this purpose was liquid chromatography with electrochemical detection (LCEC).

II. High Performance Liquid Chromatography

A. Introduction

The separation and detection of chemical compounds is considered by some to be the fundamental basis upon which the field of analytical chemistry is based. Numerous separation techniques are available for use in an analytical laboratory. These can be coupled with any number of detectors for the determination of analytes in a variety of sample types. High performance liquid chromatography (HPLC) is one of the most common separation techniques used today. The first report involving the separation technique known as chromatography was presented by M. S. Tswett in 1903 in a speech he gave at a meeting of the Biological Section of the Warsaw Society of Natural Scientists.[66] In this presentation, he described separation of plant pigments from their leaves using various solvents. He also introduced over 100 adsorbants that could be used to separate plant pigments; he suggested these adsorbants had the additional potential to separate many other mixtures of compounds. However, he did not introduce the term chromatography to describe this technique until 1906.[67] Since that time over 100 years ago, liquid chromatography, and more recently high performance liquid chromatography, has grown considerably in its application to a wide variety of analytical problems. It is

now extensively employed in various fields of research including biochemistry [68] and in environmental chemistry.[69]

B. LC Instrumentation

Basic liquid chromatography instrumentation consist of a mobile phase reservoir, a pump, stainless steel tubing and fittings, a sample injector, a separation column, a detector, and a recording device as illustrated in Figure 2-1.

Figure 2-1. Liquid chromatograph system components.

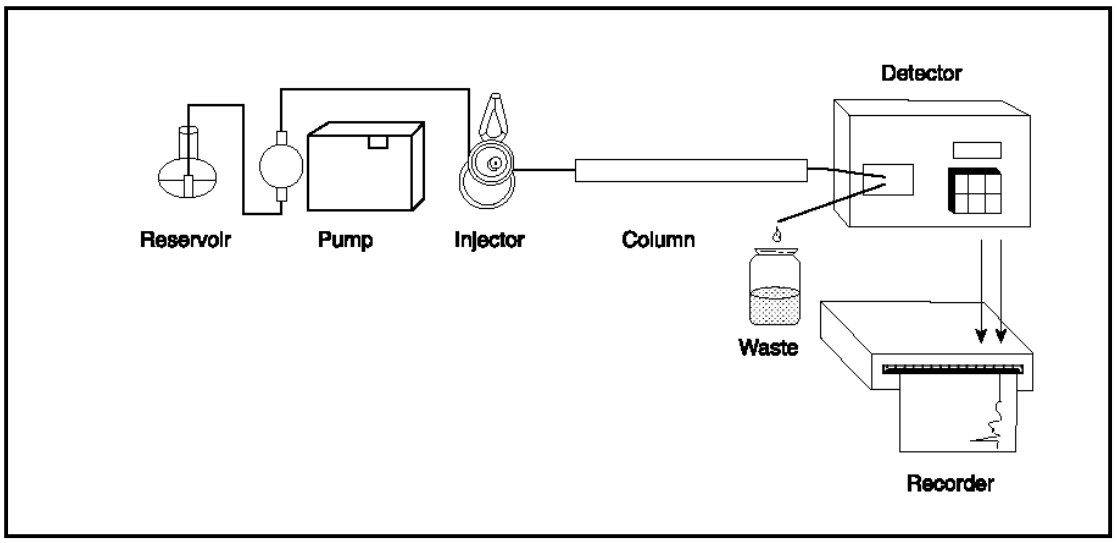

The heart of the LC system is the analytical separation column. Typically composed of a stainless steel tube packed with particles under high pressure, the analytical column is designed to retain various analyte molecule(s) depending on the

chemistry of the compound(s) in question. The analytical column in the LC setup is perhaps the most studied and variable component of such a system. Today, a wide variety of LC columns are available, providing an analyst with the capability to perform nearly any separation desired. The theory behind LC separations is briefly discussed in the following sections.

C. Analyte Separation

The dynamic distribution of analytes of interest between a stationary phase and a liquid mobile phase represents the basic principle of all liquied chromatographic separations. The time required for the elution of an analyte is dependent on the amount of time spent by the analyte in or adsorbed on the stationary phase of the column versus the amount of time spent traveling along with the mobile phase. In reversed-phase liquid chromatography, the column packing material is coated with nonpolar moieties while the mobile phase is typically a relatively polar aqueous solution. A small sample of an analyte mixture is introduced into the column through the sample injector. The components of the mixture are carried through the column where they partition between the stationary phase and the mobile phase according to their individual polarities. Those components that are more nonpolar are retained on the column more extensively than are those components that are more polar. Hence, the most polar components will be eluted from the column first.

Adequate separation of a given set of analytes by LC requires the utilization of proper chromatographic conditions. The distribution equilibria involved in

chromatography can be represented by a simple equation that involves the transfer of the analyte between the mobile and stationary phases. For example, for analyte A

$$A_{mobile} \rightleftharpoons A_{stationary}$$

Equation 2-1

where A_{mobile} and $A_{stationary}$ represent the analyte within the mobile phase and stationary phase, respectively.

The distribution constant (K_c) is defined as the ratio of the concentration of the analyte in the stationary phase, C_s, to the concentration of an analyte in the mobile phase, C_m. This equilibrium constant is given as

$$K_c = \frac{C_s}{C_m}$$

Equation 2-2

Alternatively, the distibution constant can be written as

$$K_c = \frac{n_s V_m}{n_m V_s}$$

Equation 2-3

where n_s and n_m are the number of moles of the compound of interest in the stationary and mobile phases, respectively, and V_s and V_m are the volumes of the stationary and the mobile phases, respectively. A typical LC chromatogram can be seen in Figure 2-2 below.

Figure 2-2. Representative LC chromatogram.

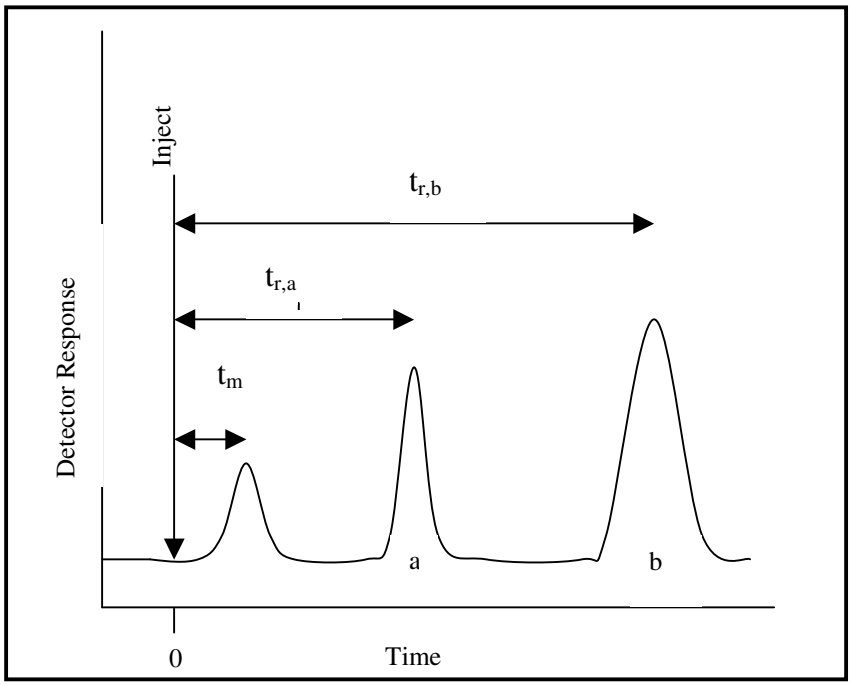

Another useful retention parameter related to analyte partition in LC is the retention factor (k'). The retention factor is defined as the ratio of the volumes of the analyte in the stationary and the mobile phases multiplied by the distibution constant, as can be seen below

$$k' = \frac{K_c V_s}{V_m} = \frac{n_s}{n_m} \qquad \textbf{Equation 2-4}$$

The separation factor (R), which describes the fraction of an analyte in the mobile phase at any given time, can be expressed as

$$R = \frac{n_m}{n_s + n_m} = \frac{1}{1 + k'} \qquad \textbf{Equation 2-5}$$

Using this equation, the length of the column (L) and the linear velocity of the mobile phase (υ), the observed retention time (t_r) of an analyte can be expressed as

$$t_r = \frac{L}{\upsilon R} \qquad \textbf{Equation 2-6}$$

Retention time is more commonly defined as the time it takes an analyte to reach the detector following injection. The time necessary for an unretained analyte, commonly referred to as the solvent front, to reach the detector following injection is designated as t_m and can be expressed similarly as

$$t_m = \frac{L}{\upsilon} \qquad \textbf{Equation 2-7}$$

Substituting equations 2-5 and 2-7 into 2-6 results in a practical means for calculation of the retention factor from typical chromatographic results.

$$k' = \frac{t_r - t_m}{t_m} \qquad \textbf{Equation 2-8}$$

Since t_r and t_m are readily obtained from a chromatogram, the retention factor becomes readily determined. This parameter serves as a very useful tool for optimizing chromatographic conditions. In fact, the retention factor is considered by many to be more important than the retention time itself because it should be a constant from one LC system to the next, relatively independent of flow rate, column length, and other variables if one uses the same column packing material, same mobile phase and same temperature.

D. Column Characterization

1. Column Efficiency

Unlike retention time and retention factor, which are related to individual analytes, column efficiency is an important parameter that more broadly defines the separation power of the chromatographic setup. The column efficiency in an LC separation is defined by the number of theoretical plates. A greater number of theoretical plates indicates greater column efficiency. A theoretical plate is a hypothetical region contained within the column where analyte partitioning theoretically achieves equilibrium between the stationary and mobile phases. Although the theoretical plate is imaginary in reality, an analyte can be perceived to move through an analytical column in an incremental fashion, taking time to achieve equilibrium between the stationary and mobile phase within each theoretical plate. Following equilibrium, the mobile phase then moves the analyte down the column to interact with the stationary phase in the next

theoretical plate. These processes of analyte absorption into or adsorption onto the stationary phase, mobile phase movement, and subsequent desorption into the flowing mobile phase are all repeated multiple times until the analyte exits the column. Thus, an analyte more strongly attracted to the stationary phase in each such hypothetical equilibrium will require longer to move through the column. From an alternative kinetic analysis of solute adsorption/desorption, the more time an analyte spends adsorbed onto the stationary phase the longer it takes for that analyte to travel the length of the column, resulting in an increased retention time (t_r). An equation for calculation of the number of theoretical plates (N) for a given column is provided by

$$N = \frac{L}{H} \qquad \textbf{Equation 2-9}$$

where H represents the height equivalent to a theoretical plate (HETP) and L represents the length of the column. The plate height would obviously be very small for a column with greater efficiency. Typical numbers of theoretical plates found in modern analytical LC columns range from 3,000–100,000. In some situations, even less than 3,000 plates is more than sufficient for successful analysis. If the chromatographic peak is assumed to be Gaussian in shape, the plate height can be calculated as[70]

$$H = \frac{\sigma^2}{L} \qquad \textbf{Equation 2-10}$$

where σ represents the standard deviation, σ^2 represents the variance of the peak, and σ has units of length. For a Gaussion peak, about 96% of its area is included within ±2σ of the peak maximum.

Routinely, chromatograms are recorded as a response parameter versus time following sample injection rather than response versus distance of analyte migration. Therefore, the standard deviation and variance for chromatograms are denoted in units of time as τ and τ^2, respectively, to denote the difference in the abscissa. The relationship between τ and σ is

$$\tau = \frac{\sigma}{\upsilon} = \frac{t_r \sigma}{L} \qquad \textbf{Equation 2-11}$$

As stated above, 96% of the area of a Guassian peak is contained within ±2s.d. from the maximum of the peak, where the standard deviation in terms of time is now τ. And, 96% of the area under the peak will be encompassed by the region of t_r ±2τ. The width measured at the base of the peak is

$$W = 4\tau \qquad \textbf{Equation 2-12}$$

Substituting equation 2-12 into 2-11 and solving for σ we obtain

$$\sigma = \frac{LW}{4t_r} \qquad \textbf{Equation 2-13}$$

Substituting equation 2-13 into 2-10 yields

$$H = \frac{LW^2}{16{t_r}^2} \qquad \textbf{Equation 2-14}$$

Substitution of Equation 2-14 into 2-9 shows that the number of theoretical plates, N, can now be readily calculated from easily accessible chromatographic parameters,

$$N = 16\left(\frac{t_r}{W}\right)^2 \qquad \textbf{Equation 2-15}$$

2. Analyte Resolution

Resolution between two analytes is defined as the ratio of the distance between the centers of the two chromatography peaks, divided by the average width (measured at the base of the peak) of those peaks. In general, increasing the length of the column, and therefore the number of theoretical plates, increases the resolution of two adjacent analytes. In theory, any required separation can be achieved, given a column of sufficient length and availability of the associated increase in time required for the separation to occur. The resolution (R_s) is calculated as

$$R_s = \frac{t_{r,b} - t_{r,a}}{0.5(W_a + W_b)} \qquad \textbf{Equation 2-16}$$

where $t_{r,a}$ and $t_{r,b}$ are the retention times and W_a and W_b are the base widths of analytes a and b, respectively. A resolution of 1.5 demonstrates "complete" resolution between two analyte peaks. A resolution value exceeding 1.0 between two analyte peaks is normally accepted as providing sufficient resolution for typical analytical purposes where the analytes are present in roughly equal concentrations. For greater disparities in concentrations, larger values of R_s are necessary.

III. Electrochemical Detection

A. Introduction

The electrochemical detector responds to substances that are either oxidizable or reducible at the selected applied potential. The measured electrical output arises from a current flow due to an electrochemical reaction occurring at the surface of the working electrode. The first published reports of an electrochemical detector for LC involved catecholamine research and preceded the commercial version by more than a year.[71,72] A commercially available electrochemical detector for liquid chromatography was introduced by Bioanalytical Systems Inc. (West Lafayette, IN) in 1974.[73] The development of this detector was in response to the need for an improved detector for analyzing aromatic amino acid metabolites in the mammalian nervous system.[73,74] EC detection has now been successfully employed for more than thirty years for this purpose. The choice of EC detection for the current studies was made relatively easy

when considering its extensive prior use for the detection of these compounds by our laboratory and other laboratories.

B. Amperometry

Amperometry is defined as the measure of a produced electrical current. Typically the current is measured as a function of time. In LCEC systems, the current is produced when an analyte is either oxidized or reduced, and the resulting amperometric signal is recorded. The amperometric signal in LCEC indirectly reflects the amount of electroactive chemical instantaneously eluting from the liquid chromatograph.

Electrochemical detectors are simply working electrodes in a standard three-electrode system used in conjunction with a potentiostat. The potentiostat both controls the applied voltage between the working and reference electrodes while measuring the current flowing between the working and auxiliary electrodes.

1. Three-Electrode System

Figure 2-3 illustrates the physical arrangement of the three fundamental electrodes in our system and the relationship of these electrodes to each other.

Referring to the following illustration, the separated analyte components exit the bottom of the LC column in the liquid chromatographic mobile phase and enter the thin-layer flow-through electrochemical cell. This thin-layer portion of the cell contains a

Figure 2-3. Thin-layer flow-through electrochemical detector system.

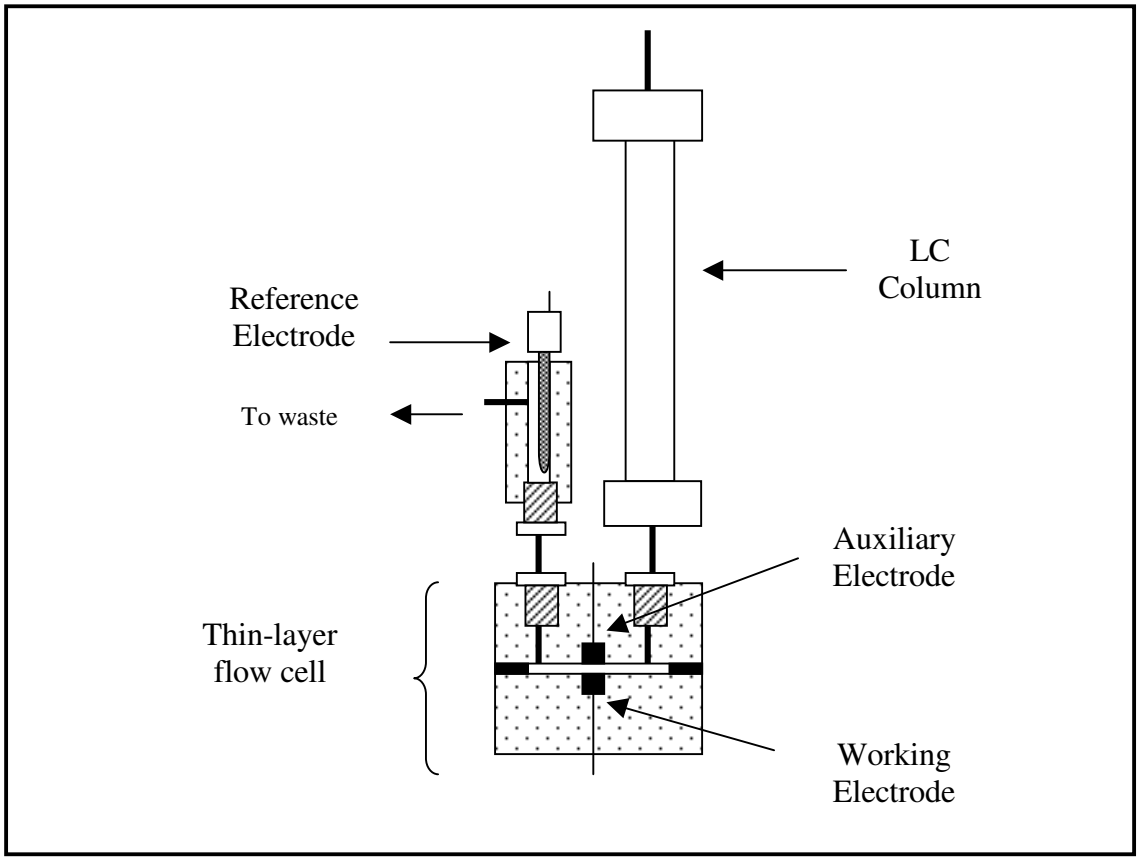

vitreous ("glassy") carbon working electrode embedded in a PEEK (polyetheretherketone) block. Glassy carbon is widely used as the working electrode in electrochemical detectors due to its excellent electrochemical properties. It consists of a smooth, renewable surface, and is virtually free of impurities.[73] PEEK exhibits almost complete inertness under a wide range of conditions. While the working electrode is embedded in the lower PEEK block of the flow-through portion of the cell, the auxiliary electrode (stainless steel) is embedded in the upper PEEK block in direct opposition to the working electrode. The upper and lower PEEK blocks are separated by a 50 μm

Teflon® (DuPont, Wilmington, DE) membrane containing a channel for solution flow. The reference electrode in the electrochemical detector shown is located in its own separate holder downstream from the thin-layer cell. In the three-electrode system, the mobile phase also serves as the electrochemical supporting electrolyte. The electrochemical reaction proceeds as the analyte passes over the surface of the working electrode. The electrode surface becomes virtually depleted of the analyte of interest. As a consequence, a concentration gradient is established between the electrode surface and the bulk of the mobile phase solution flowing through the cell. The created gradient causes the analyte of interest to diffuse from the flowing solution into the depleted zone at a rate proportional to its bulk concentration in the mobile phase. The current generated at the working electrode surface is directly determined by the rate at which the analyte reaches the electrode surface and is, thus, directly proportional to the concentration of the analyte in the mobile phase.

The arrangement of the auxiliary electrode to the working electrode is designed to reduce the iR drop of the system. In a flow-through cell, since the flow is parallel to the surface of the electrode, if the auxiliary electrode were located substantially downstream from the working electrode, the iR drop could cause the potential difference at the downstream edge of the working electrode to be considerably greater than the potential at the upstream edge, resulting in a decreased ability to oxidize the analyte upstream and, ultimately, non-uniformity in the detector response. By placing the auxiliary electrode directly across from the working electrode, the iR drop is minimized due to the extremely small gap in the channel. Therefore, the potential is relatively uniform across the entire surface of the working electrode.[73]

2. Current Measurement

The potentiostat is designed to apply a user selected potential to the working electrode. As the analyte flows over the working electrode, if the applied potential is sufficient, the analyte is either oxidized or reduced resulting in an electrical current between the working electrode and auxiliary electrode. The produced current is then recorded by the potentiostat. As the concentration of the analyte changes in the band eluted from the LC column, so does the current. This results in a typical gaussian shaped chromatographic elution peak that can be recorded and analyzed.

This type of amperometry is governed by Faraday's Law

$$Q = nFN \qquad \textbf{Equartion 2-17}$$

where Q is the charge (C), n is the number of electrons involved in the reaction, F is Faraday's constant (9.65×10^4 C/eq) and N is the number of moles converted to product. The instantaneous current is then

$$i = \frac{dQ}{dt} = nF\frac{dN}{dt} = 9.65x10^4 \times (equivalents\ converted\ \ per\ \mathrm{sec}ond) \qquad \textbf{Equation 2-18}$$

Since the applied potential is normally set to create a surface concentration near zero for the analyte, the rate of the reaction (υ) is solely governed by the mass transfer rate (υ_{mt}) of the analyte from the bulk of the thin layer solution to the surface of the working electrode; therefore,

$$\upsilon = \upsilon_{mt} = \frac{i}{nFA} \qquad \textbf{Equation 2-19}$$

where A is the area of the working electrode.

Assuming a Nernstian diffusion layer near the surface of the electrode where mass transfer occurs only by diffusion, the flux of the analyte (mol sec^{-1} cm^{-2}) at the surface of the electrode would be

$$J(x = 0) = D\left(\frac{\partial C}{\partial x}\right)_{x=0} = \frac{i}{nFA} \qquad \textbf{Equation 2-20}$$

where (x = 0) represents the distance x measured from the surface of the electrode, D is the diffusion coefficient (cm^2/sec) and ∂C/∂x is the concentration gradient. Therefore, the current at the surface of the electrode is

$$i = nFAD\left(\frac{\partial C}{\partial x}\right)_{x=0} \qquad \textbf{Equation 2-21}$$

However, since the analyte is flowing past the electrode surface in the mobile phase, mass transport is considerably assisted by forced convection.[74] Weber and Purdy[75] derived a more comprehensive equation that represents the current at the surface of such a convection aided amperometric electrode

$$i = 1.467nFCW_e\left(\frac{DL}{b}\right)^{2/3}\left(\frac{U}{W_c}\right)^{1/3} \qquad \textbf{Equation 2-22}$$

where C is the bulk concentration of the analyte (mol/cm^3), W_e is the width (cm) of the electrode perpendicular to the direction of flow, L is the length (cm) of the electrode in the direction of flow, b is the depth (cm) of the fluid channel, U is the flow rate (cm^3/sec), and W_c is the width (cm) of the fluid channel.

IV. LCEC Use for Measuring Tyrosine Hydroxylase Activity

The use of LCEC has been previously established for the quantification of TH activity. The first published report for this use came from our laboratory in 1976.[76] Since then, LCEC has been extensively used in research involved with TH from various biological matrices.[77-81] Considering the long history of success when used in work of this type, LCEC was chosen for the detection of TH activity in our current experiments.

Tyrosine Hydroxylase-Glutathione-S-Transferase Expression, Purification and Assay for Activity

Chapter 3

I. Introduction

Our studies required a form of tyrosine hydroxylase (TH) which was capable of being physically immobilized on a solid glass surface. For this reason we employed the combination of TH as a fusion protein with glutathione-S-transferase (GST). The GST portion of this protein, as will be seen, offers a convenient mechanism to convert the TH into an immobilized form. Since the fusion form of these two enzymes was not commercially available, it was necessary to express and purify this protein in-house using recombinant DNA technology.[82]

Briefly, expression was accomplished using BL21 E. coli (DE3) as the bacterial host for TH cDNA ligated pGEX vector.[82,83] Purification of TH-GST was accomplished through the use of sonication and glutathione-agarose (GSH-agarose).[84-88] Sodium dodecyl sulfate-polyacrylamide gel electrophoresis (SDS-PAGE) was

employed to monitor the expression and purification of TH-GST throughout the procedure.[89,90]

Finally, the purified, expressed protein was assayed for TH activity using appropriate incubation and LCEC detection of the product. This method allowed for the in-house production of a fusion protein that ultimately made the investigation of TH activity in large, applied electric fields possible.

II. Background

Glutathione-S-transferases are detoxifying enzymes found in all living organisms. Their main function is to catalyze the detoxification of electrophilic compounds such as drugs, herbicides and insecticides by adding a glutathione moiety to these compounds. [91,92] Attachment of the thiol group of the glutathione (GSH, γ-glutamyl-L-cysteinyl-glycine) compounds leads to increased solubility of the molecules which facilitates excretion of these toxic compounds.[93-95]

Since the affinity of glutathione-S-transferase for glutathione is so high,[96] expressed glutathione-S-transferase and glutathione-S-transferase fusion proteins can be purified in a fairly straightforward procedure using affinity chromatography with GSH previously immobilized on the stationary phase.[86-88,97,98] The most readily available glutathione-modified support is agarose.[84] GSH-agarose can be used in either a column or a batch mode for purification of the fused protein. In the batch mode, the fusion protein, GSH agarose beads, and a buffer are mixed together as a slurry in a centrifugation tube. In the column mode, the solution containing GST or a GST fusion

protein is slowly passed through a column loaded with the GSH-agarose. GST binds to the GSH-agarose support while contaminants remain in the mobile phase and eventually exit the column. A buffer is used to wash away contaminants leaving only the GST fusion protein attached to the support. With a column, the wash buffer and contaminants are eluted, while with the batch method, the slurry is centrifuged and the buffer decanted. With either method, the GST may be eluted by treatment with an appropriate solution, e.g. a concentrated glutathione solution. Alternatively, the purified enzyme can be used while still attached to the support.

There are two common methods for elution of GST-fused proteins from a glutathione support structure. The first is to elute the combined fusion protein by adding a concentrated glutathione solution to displace the protein from the support.[86-88] The second is to cleave only the desired protein from the glutathione-S-transferase fused combination by adding a selective cleaving agent.[99]

The initial and most crucial step in TH-GST production was obtaining a bacterial culture that could be used to express this protein. Fortunately, an E. coli culture which had been transformed to express tyrosine hydroxylase as a fusion protein with glutathione-S-transferase was available from within the department.[100] The original expression vector was notably obtained from Dr. Donald M. Kuhn from the Department of Psychiatry and Behavioral Neurosciences and Center for Molecular Medicine and Genetics at Wayne State University School of Medicine in Detroit, Michigan.[82] Dr. Kuhn's group used TH RNA from male Sprague-Dawley rat brains to transcribe the cDNA that was ligated in-frame into pGEX-4T-2 (GE Lifesciences). pGEX expresses proteins as fusion proteins with GST, which was ideal for this work.[101,102]

As illustrated in Figure 3-1, DNA cloning is accomplished by first obtaining the gene of interest using restriction endonucleases that recognize specific cleavage sites. The vector of choice is cleaved using the same restriction endonucleases to ensure the gene of interest will contain complimentary ends to the vector. The inserts are then ligated with DNA ligase to create the recombinant vector.

Figure 3-1. DNA cloning.

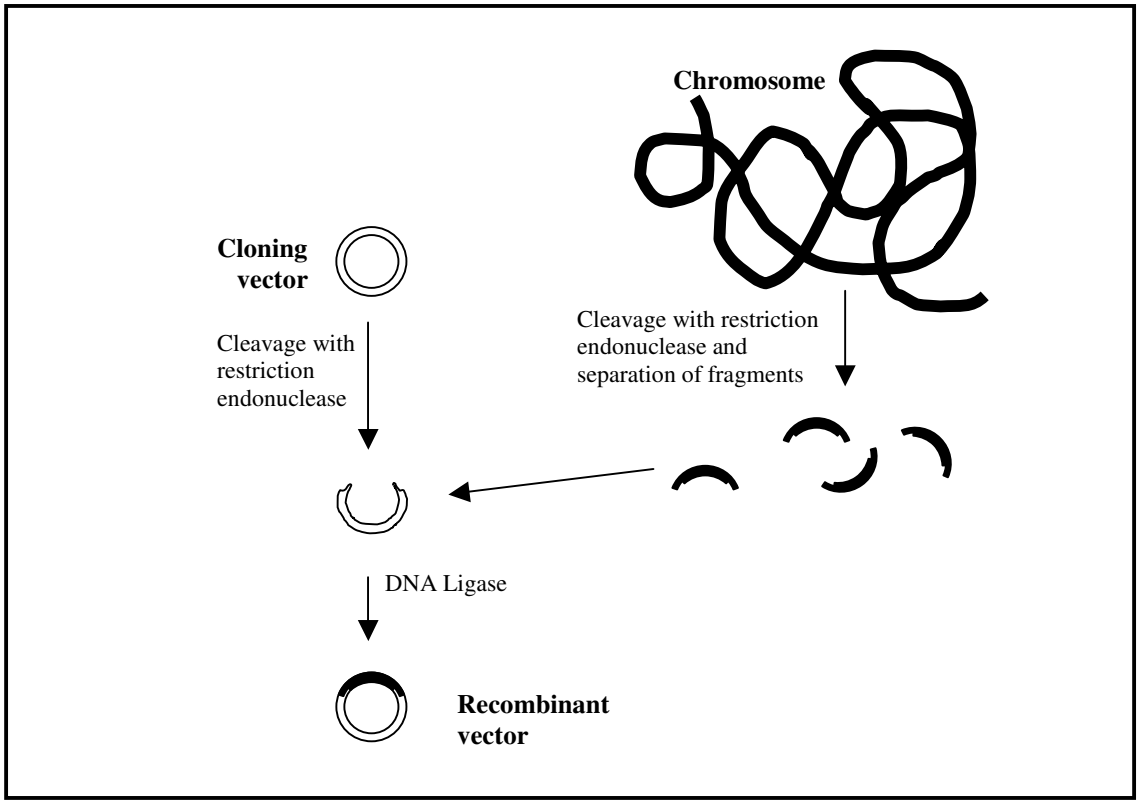

The vector used in the current study involved a few more steps. First, rat TH RNA was reverse transcribed to synthesize cDNA.[82] pGEX vectors contain SmaI and XhoI restriction sites;[83] therefore, it was necessary to encode the TH cDNA with these same restriction sites to ensure insertion into the pGEX vector. Polymerase chain reaction technology (PCR) was used to amplify the amount of cDNA. The PCR primers that were used were specifically chosen because they contained SmaI and XhoI restriction sites.[82]

Figure 3-2 illustrates the specific vector used, pGEX-4T-2.[83] The origin of replication, ori, is located near the bottom of the drawn vector. Downstream from the ori is the lac operon which is negatively regulated by the lac repressor bound to its operator. The repressor can be displaced from the operator by the lac inducer, allolactose, which binds to the lac repressor causing a conformational change. This conformational change allows the repressor to release from the operator initiating transcription.[10] Downstream from the lac operon and immediately upstream from the GST gene is an additional promoter, Ptac. Ptac is a hybrid promoter derived from the sequence of the lac operon but has been shown to be 11 times more efficient than the lac promoter.[103] The nucleotide sequence shown at the top of the illustration is immediately downstream from the GST gene. This sequence shows the thrombin cleavage site, which can be used post-expression to cleave the protein of interest from GST. This sequence also contains the SmaI and XhoI restriction sites which will create the insertion site for the TH cDNA. Downstream from the insertion site is the stop codon. On the right side of the vector can been seen the ampicillin resistance gene.[83]

Figure 3-2. pGEX-4T-2 vector.

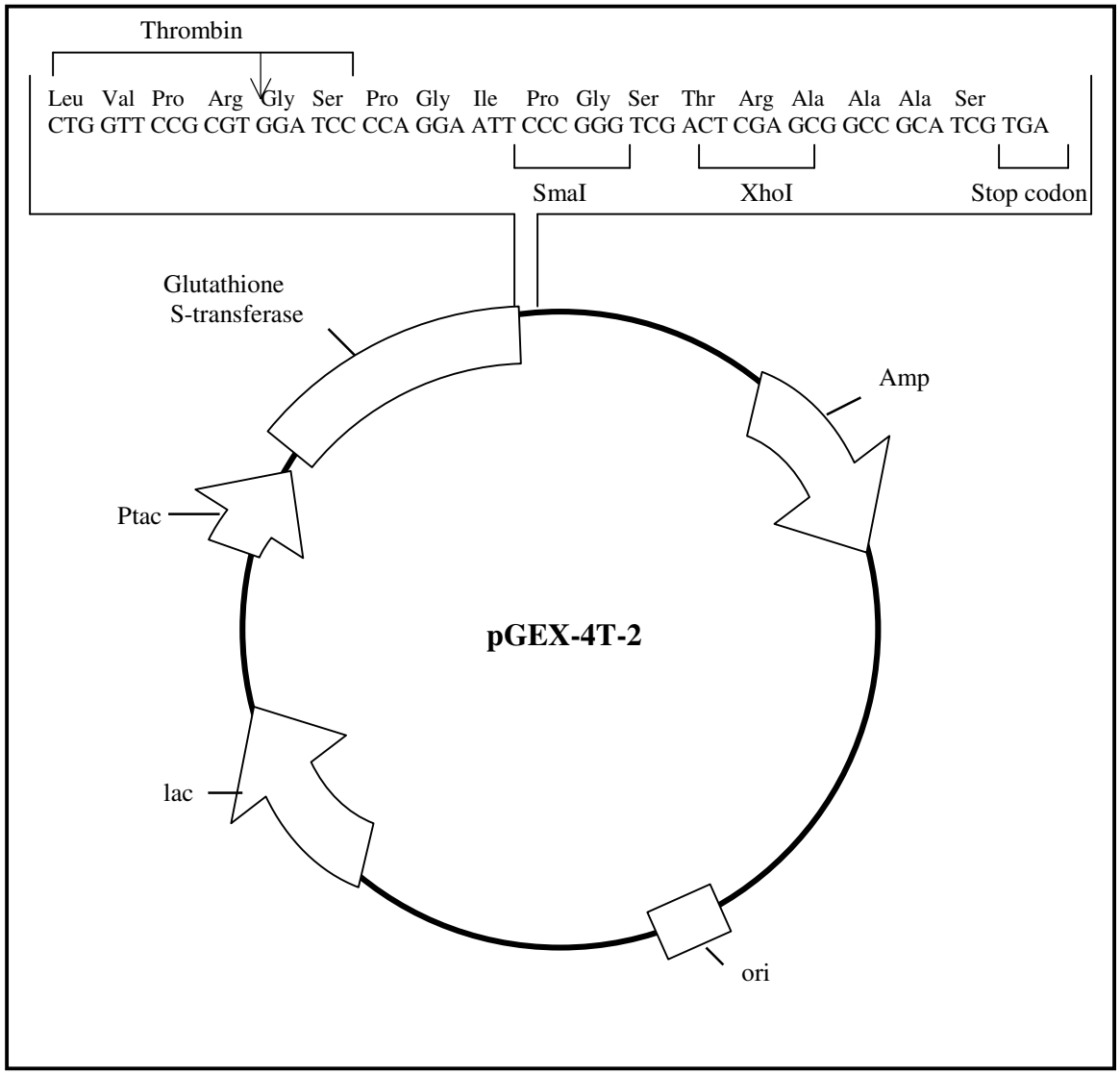

The pGEX-TH expression vector was transfected into BL21(DE3) E. coli cells through heat shock.[100] This particular strain of E. coli is ampicillin resistant and contains defective *lon* and *ompT* proteases. [104] BL21 E. coli was chosen as the

expression host because it has been successfully used on multiple prior occassions to express proteins in their native, active conformations.[105-108]

Once the transformed bacterial stock was obtained, a modified version of Dr. Kuhn's production procedure was employed for expressing and purifying TH-GST.[82] This method utilizes Luria-Bertani (LB) Media containing ampicillin for the growth of the transformed E. coli culture. LB consists of tryptone, yeast extract and sodium chloride adjusted to pH 7.2. BL21 and other derived strains of E. coli lack vitamin B complex. The yeast extract contains vitamin B complex and also, along with tryptone, provides nitrogen, sulfur and carbon. The sodium ions aid in membrane transport and help to maintain osmotic equilibrium of the medium.[109] The conditions, temperature, ampicillin and media are relatively specific for BL21 E. coli and will substantially inhibit the growth of other bacteria.[110]

The culture was incubated at 37°C while shaking until an absorbance of 1.2 at 600 nm in a 1.00 cm cell was obtained which corresponded to the maximum growth potential of the culture. The spectrophotometer was used to determine an approximate number of cells within the culture. The absorbance of light is affected by the turbidity of the solution. Bacterial growth occurs in a logarithmic fashion. Therefore, a plot of absorbance versus time yields a straight line. By matching the absorbance to plate counts of the same culture, this relationship can be used for estimations of bacterial concentrations during culture growth.[110]

When maximum growth potential of the E. coli culture had been attained, the transcription of the pGEX vector was induced by the addition of isopropyl β-D-1-thiogalactopyranoside (IPTG). IPTG is structurally related to allolactose and can

bind to the repressor which then releases the tac promoter initiating TH-GST expression.[83] IPTG is commonly used as a substitute for allolactose and has been proven to be 11 times more efficient. This increased efficiency is due to the fact that allolactose can be used as a carbon source by the bacterial host.[10]

Following induction of the transcription of the pGEX vector, the culture was centrifuged, the supernatant was discarded, and the resulting pellet was washed to remove the remaining incubation broth.

The isolated E. coli cells were resuspended in Tris buffer which contained dithiothreitol (DTT), phenylmethylsulfonyl fluoride (PMSF) and leupeptin and subsequently sonicated. DTT is used to ensure that all thiol groups in the protein remain in a reduced state, which helps to preserve the activity of the enzyme.[111,112] Both PMSF and leupeptin were added as protease inhibitors.[113-115] During sonication, the intact E. coli membranes are reduced to small membrane fragments freeing the contents of the cell including TH-GST and other debris. Following sonication, this mixture was centrifuged to pelletize the membrane fragments. This completed the first step in the purification process for the expressed TH-GST enzyme.

The supernatant from the above centrifugation was added to glutathione-agarose beads in batches and incubated at 4°C while shaking. Following an additional centrifugation step, the beads were washed with Tris buffer, the mixture was centrifuged, and the supernatant was discarded. This wash step was performed a total of three times.

It had been previously shown that leaving TH attached to GST does not alter its activity. [82] This preserved activity was very helpful for the development of the techniques utilized in the following chapters. TH-GST bound to the glutathione-agarose

beads (referred to as TH-agarose) was employed for all further assays associated with the enzyme preparation and purification procedures.

The induction and purification of TH-GST was monitored using sodium dodecyl sulfate-polyacrylamide gel electrophoresis (SDS-PAGE).[116,117] In this technique, SDS binds to all available proteins. One molecule of SDS binds to two amino acids. This gives the protein a net negative charge. SDS dramatically affects the conformation of proteins so that most proteins have a similar shape following treatment. This ensures that proteins will have comparable mass to charge ratios allowing for separation by molecular weight when loaded on a polyacrylamide gel and applying an electrical potential. In this way, smaller proteins migrate more quickly through the gel than larger proteins.

The polyacrylamide gel is created by copolymerizing acrylamide with N,N'-methylene-bisacrylamide. The reaction is catalyzed by the addition of ammonium persulfate, an agent that generates free radicals by photodecomposition. This formation of free radicals is catalyzed by N,N,N',N'-tetramethylethylenediamine (TEMED). The amount of acrylamide added to the gel mixture is inversely proportional to the size of the pores created in the gel matrix.[89]

When the SDS-modified proteins are added to the gel and a current is applied, the smaller proteins travel more quickly through the gel matrix while larger proteins are more hindered leading to the separation of the proteins by mass. Standard molecular weight markers are employed in SDS-PAGE.[10] These standards are proteins of known molecular weight, which provide a reference for locating the protein of interest in the subsequent lanes. To visualize the proteins within the gel, a protein dye, Coomassie

brilliant blue, is added to the gel after the separation is completed. The negatively charged dye binds to the positively charged amino acids within the proteins, changing the dye from red (λ_{max} = 465 nm) to blue (λ_{max} = 595 nm), but does not bind to the gel. [10,118]

The Bradford Assay was used to determine the concentration of TH-GST produced from the expression process.[89,119] This assay utilized Coomassie brilliant blue as a dye for the TH-GST protein. A standard curve was separately produced using bovine serum albumin. Since the response curve for a wide range of proteins is nearly identical, bovine serum album is routinely used as the standard protein for such determinations.[89] The concentration of TH-GST was then quantified by comparison to the calibration curve.

Once TH-GST was successfully expressed, an enzymatic assay was performed to determine the TH activity. The method employed was a modified method of one developed in-house.[120] The experiment was performed in six 12x100 mm test tubes. The 6 tubes consisted of two controls (a standard and a blank) and 4 purified TH activity samples. Both the standard and the blank were prepared with boiled enzyme. Boiling the enzyme rendered it inactive. It was vital to prepare all controls in the same matrix as the unknowns so that any matrix effects would be eliminated. The standard was prepared with an accurately known concentration of L-dopa. The blank was employed to account for any non-enzymatic production of L-dopa. The standard was used as a one-point calibration curve to allow for determination of the concentration of L-dopa produced in the unknown samples.

Instead of the very expensive natural cofactor, BH_4, a much less expensive and more readily available synthetic cofactor, 2-amino-4-hydroxy-6-methyltetrahydro-pteridine (6-MPH_4) was employed in our studies. This synthetic cofactor has been used extensively in investigations of the activity of TH and has been shown to have very similar kinetic properties to BH_4.[12,13,17,19]

The experiment was performed by initially combining all of the components necessary for the hydroxylation of L-tyrosine to L-dopa excluding L-tyrosine itself in the two control and four experimental test tubes. The added components and their final concentrations consisted of 0.40 M acetate buffer (pH 6.00), 0.10 mM ferrous sulfate, 2.0 mM 6-MPH_4, 0.050 M 2-mercaptoethanol (to maintain reducing conditions for protein thiols), 1.3×10^{-5} M isoproterenol (as the internal standard), the TH-agarose and 200 ng/mL L-dopa in the standard sample. The test tubes were capped and placed in a 37°C incubation chamber for 30 minutes of preincubation to achieve the desired reaction temperature of 37°C. Once the desired reaction temperature was achieved, 0.50 mM L-tyrosine marked the beginning of the assay incubation. Termination of the reaction was accomplished by the addition of 0.26 M perchloric acid after a reaction time of 20 minutes while 0.023 M sodium bisulfite and 2.0 mM EDTA were added to inhibit any possible oxidation of the newly formed L-dopa.

The L-dopa was quantified by LCEC. 10 μL of the resultant assay solution was directly injected into the LCEC for the analysis of L-dopa.

III. Experimental Design and Methods

A. Chemicals and Solutions

1. Chemicals

Doubly deionized water (ddH_2O) was used to prepare all aqueous solutions. A wall-mounted Milli-Q® Ultrapure Water System (Millipore® Corporation, El Paso, TX) was used to produce the ddH_2O from water previously subjected to reverse osmosis (RO).

Each of the chemicals used for the expression, purification and activity assays are listed in Table 3-1 along with their purity and the company from which they were obtained.

Table 3-1. Chemicals used in protein expression, purification and activity assays including their purities/grades and sources.

Chemical	Purity/Grade	Company	Location
Acetic acid, glacial	ACS	Mallinckrodt	Paris, KY
Acrylamide	Ultrapure Bioreagent	Bio-Rad	Hercules, CA
Ammonium persulfate	Ultrapure Bioreagent	Bio-Rad	Hercules, CA
Ampicillin, sodium salt	Biotechnology Grade	Fisher Biotech	Fair Lawn, PA
Bromphenol blue	—	Bio-Rad	Hercules, CA
Citric acid, monohydrate	ACS	Sigma	St Louis, MO
Coomassie Brilliant Blue Stain	—	Bio-Rad	Hercules, CA
Coomassie Destain Solution	—	Bio-Rad	Hercules, CA
3,4-Dihydroxy-L-phenylalanine	>99%	Sigma	St Louis, MO
Disodium ethylenediamine-tetraacetic acid dihydrate	>99%	Sigma	St Louis, MO
Dithiothreitol	Ultrapure	Amersham Life Sciences	Fairfield, CT
Ferrous sulfate heptahydrate	ACS	Matheson Coleman	East Rutherford, NJ
Glycerol	ACS	Fisher	Fair Lawn, NJ
Hydrochloric acid, conc.	GR	EM Science	Gibbstown, NJ
Isopropanol, anhydrous	99.50%	Sigma	St Louis, MO
Isopropyl β-D-1-thiogalactopyranoside	Molecular Biology Grade	Gold Biotechnology Inc.	St Louis, MO

Table 3-1. Continued.

Chemical	Purity/Grade	Company	Location
Isoproterenol hydrochloride	98%	Aldrich	Milwaukee, WI
Luria-Bertani Media (LB)	Molecular Biology Grade	Beckton Dickson & Co	Sparks, MD
Leupeptin hemisulfate salt	>90% (HPLC)	Sigma	St Louis, MO
2-Mercaptoethanol	>99%	Sigma	St Louis, MO
N,N'-methylenebisacrylamide	Ultrapure Bioreagent	Bio-Rad	Hercules, CA
6-Methyl-5,6,7,8-tetrahydropterin dihydrochloride	>99%	Fluka	Switzerland
Perchloric acid	AR	Mallinckrodt	Paris, KY
Phenylmethylsulfonyl fluoride	>99% GC	Sigma	St Louis, MO
Sodium acetate trihydrate	ACS	EM Science	Gibbstown, NJ
Sodium dodecylsulfate	Ultrapure Bioreagent	Bio-Rad	Hercules, CA
Sodium hydroxide	Analytical	Mallinckrodt	Paris, KY
TEMED	Ultrapure Bioreagent	Bio-Rad	Hercules, CA
Tris-(hydroxymethyl)aminomethane free base (Tris)	Molecular Biology Grade	Sigma	St Louis, MO
L-Tyrosine	>99%	Sigma	St Louis, MO

2. Luria-Bertani (LB) Media

LB media was prepared from a powdered concentrate obtained from Sigma Aldrich (St. Louis, MO). This solution was used within two weeks of the preparation date. To 1.00 L ddH_2O, 20.0 g of LB concentrate was added. The concentrate consisted of tryptone, yeast extract and sodium chloride. The measured pH of the solution was 7.20. The flask was covered with a piece of aluminum foil to which a small piece of autoclave tape was affixed and placed in a Hirayama HA-300MII autoclave (Amerex Instruments, Inc. Lafayette, CA) set at 120°C for 20 minutes. The autoclave was used to sterilize the LB media before inoculation with our transformed E. coli stock to minimize growth of foreign bacteria.

3. 1.0 M Dithiothreitol Stock Solution

A 1.00 M dithiothreitol (DTT) stock solution was prepared by adding 15.5 mg DTT to a 1.50 mL Flex-Tube® (Eppendorf®, Brinkmann Instruments, Inc., Westbury, NY) containing 100 µL ddH_2O and mixing well. This solution was prepared immediately before use.

4. 50% (v/v) Glycerol Stock Solution

A 50% (v/v) stock solution of glycerol was prepared by adding 250 mL of glycerol to a 500 mL volumetric flask and diluting to the mark with ddH_2O and mixing well. The solution was transferred to a 500 mL stock bottle, covered with a piece of aluminum foil to which a small piece of autoclave tape was affixed and placed in a

Hirayama HA-300MII autoclave (Amerex Instruments, Inc. Lafayette, CA) set at 120°C for 20 minutes to minimize subsequent growth of foreign bacteria.

5. 10% (v/v) Glycerol Wash Solution

A 10% (v/v) glycerol wash solution was made by adding 40.0 mL of sterilized ddH_2O to 10.0 mL of sterilized 50% (v/v) glycerol. This solution was kept in an ice water bath until used and was prepared fresh before each analysis.

6. 5.0 mg/mL Leupeptin Stock Solution

A 5.0 mg/mL leupeptin stock solution was made by injecting 1.00 mL ddH_2O directly into the manufacturer's septum-sealed vial containing 5.0 mg leupeptin. After mixing, this stock solution was divided into twenty 50 µL aliquots and stored in 1.50 mL Flex-Tubes® (Eppendorf®, Brinkmann Instruments, Inc., Westbury, NY) at -20°C to be used within 6 months.

7. 50.0 mM Phenylmethylsulfonyl Fluoride

Due to its instability, the phenylmethylsulfonyl fluoride (PMSF) stock solution was made immediately prior to use. Specifically, a 50.0 mM solution was made by adding 8.71 mg PMSF to 1.00 mL of anhydrous isopropanol in a 1.50 mL Flex-Tube® (Eppendorf®, Brinkmann Instruments, Inc., Westbury, NY), mixed, and stored on ice until used.

8. 0.050 M Tris Sonication Buffer (pH 7.40)

Immediately prior to use, 0.050 M Tris buffer pH 7.40 containing 1.0 mM DTT and 1 μg/mL leupeptin was made and stored on ice. The buffer was made by adding 0.30 g Tris to 50.0 mL of ddH_2O and adjusting the pH to 7.40 with concentrated HCl using an Orion Model SA720 pH meter with an Orion PerpHecT 9206BN electrode (Orion Research, Inc., Beverly, MA). To complete the buffer, 50 μL of the 1.0 M DTT stock and 10 μL of the 5.0 mg/mL leupeptin stock were added, and the combination was mixed well.

9. 4xTris Buffer (0.5 M Tris with 0.4% (w/v) SDS)

A 0.50 M Tris buffer containing 0.40 % (w/v) SDS was prepared by adding 6.05 g Tris to a 100 mL volumetric flask and diluting with ddH_2O. The solution was adjusted to pH 6.80 with hydrochloric acid and filtered through a Pall, GH Polypro, 47 mm, 0.45 μm hydrophilic membrane filter (Pall Life Sciences Corp., Ann Arbor, MI). Following filtration, 0.40 g SDS was added to the Tris solution. This solution was prepared immediately before use.

10. 30% (w/v) Acrylamide/0.8% (w/v) Bisacrylamide

To a 100 mL volumetric flask, 30.0 g acrylamide and 0.80 g bisacrylamide were added, and diluted to the mark with ddH_2O, and mixed well. The solution was filter through a Pall, GH Polypro, 47 mm, 0.45 μm hydrophilic membrane filter (Pall Life Sciences Corp., Ann Arbor, MI). This solution was prepared immediately before use.

11. 10 % (w/v) Ammonium Persulfate

This solution was prepared by adding 50.0 mg ammonium persulfate to 500 µL of ddH_2O and mixing the combination. This solution was prepared immediately before use.

12. 2xSDS Sample Buffer (0.25 M Tris with 0.2% (w/v) SDS)

SDS sample buffer was prepared by adding 25.0 mL 4xTris buffer, 20.0 mL glycerol, 4.0 g SDS, 3.1 g DTT, and 1.0 mg bromphenol blue tracking dye to a 100 mL volumetric flask, diluting to the mark with ddH_2O and mixing. This solution was diluted as needed.

13. 4xTris Electrophoresis Buffer (1.5 M Tris with 0.4% (w/v) SDS)

A 1.50 M Tris buffer containing 0.4 (w/v) SDS was prepared by adding 91.0 g Tris to a 500 mL volumetric flask and diluting to the mark. The solution was adjusted to pH 8.80 with conc. HCl with stirring and filtered through a 0.45 µm filter. To this solution, 2.0 g SDS was added. This solution was thoroughly mixed and, subsequently, diluted as needed.

14. 2.0 M Acetate Buffer (pH 6.40)

Stock acetate buffer (2.0 M) was prepared by adding 27.22 g $C_2H_3O_2Na \cdot 3H_2O$ to a 100 mL volumetric flask and diluting to the mark with ddH_2O. The pH was adjusted, while stirring, to 6.40 with glacial acetic acid. 1.20 mL aliquots were stored in 1.50 mL Flex-Tubes® (Eppendorf®, Brinkmann Instruments, Inc., Westbury, NY) at –80°C until needed for analysis.

15. 1.0 mM Ferrous Sulfate Solution

Stock ferrous sulfate (1.0 mM) was prepared fresh daily by adding 2.78 g $FeSO_4$ to a 10.0 mL volumetric flask, diluting to the mark with ddH_2O and mixing.

16. 2.0 M Stock Perchloric Acid

Stock perchloric acid (2.0 M) was prepared by adding 21.5 mL of conc. $HClO_4$ to a 100 mL volumetric flask, diluting to the mark with ddH_2O and mixing. 1.00 mL aliquots were stored in 1.50 mL Flex-Tubes® (Eppendorf®, Brinkmann Instruments, Inc., Westbury, NY) at –80°C until used in assays.

17. 0.30 M Sodium Bisulfite and 0.030 M Ethylenediaminetraacetic acid (EDTA)

A stock sodium bisulfite (0.30 M) solution containing EDTA (0.030 M) solution was prepared by adding 1.43 g $Na_2S_20_5$ and 0.56 g EDTA to a 50.0 mL volumetric flask, diluting to the mark with ddH_2O and mixing. 1.00 mL aliquots were stored in 1.50 mL Flex-Tubes® (Eppendorf®, Brinkmann Instruments, Inc., Westbury, NY) at –80°C until used in assays.

18. $1.30x10^{-4}$ M Stock Isoproterenol

A 1.0 M HCl solution was initially prepared by diluting 21.7 mL conc. HCl to 250.0 mL with ddH_2O in a volumetric flask and mixing. This 1.0 M HCl solution was used to adjust the pH of 1.0 L ddH_20 to 4.00 with stirring to create $1.0x10^{-4}$ M HCl. A 1.0 mM stock isoproterenol solution was prepared by adding 2.48 mg of the HCl salt to a 10.0 mL volumetric flask, diluting with $1.0x10^{-4}$ M HCl and mixing. The $1.30x10^{-4}$ M

isoproterenol solution was prepared by adding 1.30 mL of the 1.0 mM solution to a 10.0 mL volumetric flask, diluting to the mark with $1.0x10^{-4}$ M HCl and mixing. This solution was prepared the day of use. The $1.0x10^{-4}$ M HCl solution was made by first preparing a 1.0 M HCl solution.

19. 2.50 mM L-Tyrosine (L-TYR)

L-Tyrosine was prepared by dilution from a stock solution on the day of use. First, a 25.0 mM solution was prepared by adding 45.30 mg to a 10.0 mL volumetric flask and diluting to the mark with 1.0 M HCl and mixing. The 2.50 mM solution was then prepared by adding 1.00 mL of the 25.0 mM solution to a 10.0 mL volumetric flask and diluting with $1x10^{-4}$ M HCl.

20. 20.0 M 6-Methyl-5,6,7,8-tetrahydropterin (6-MPH_4) and 0.50 M 2-Mercaptoethanol

A stock solution containing 6-MPH_4 (20.0 mM) and 2-mercaptoethanol (0.50 M) solution was prepared by adding 5.08 mg 6-MPH_4 and 34.97 µL of 14.3 M 2-mercaptoethanol to a 1.00 mL volumetric flask, diluting with ddH_2O and mixing. This solution was prepared fresh on the day of use.

21. 6400 ng/mL 3,4-Dihydroxy-L-phenylalanine (L-dopa)

Stock L-dopa (6400 ng/mL) was made in a stepwise process on the day of use. First, a 1 µg/mL solution was prepared in $1.0x10^{-4}$ M HCl. The 6400 ng/mL solution was then prepared by adding 640 µL of the 1.0 mg/ 10.0 mL solution to a 10.0 mL volumetric flask, diluting with $1.0x10^{-4}$ M HCl and mixing.

22. LC Mobile Phase

The mobile phase used was specifically designed for the separation of catecholamines. This solution was prepared by adding 10.51 g citric acid, 13.61 g sodium acetate, 4.80 g sodium hydroxide and 2.17 mL acetic acid to a 2.00 L volumetric flask, diluting to the mark with ddH_2O, and stirring until homogeneous. The pH was adjusted to 5.18 with conc. HCl before filtering through a Pall, GH Polypro, 47 mm, 0.45 μm hydrophilic membrane filter (Pall Life Sciences Corp., Ann Arbor, MI).

B. TH-GST Expression

1. BL21 E. Coli Culture Growth

a. Initial Culture Growth

Ten milliliters of LB media, containing 100 μg/mL ampicillin, was placed in a 50.0 mL Pyrex® Fernbach culture flask (Corning, Inc., Corning, NY) and inoculated with transformed BL21 E. coli cells. The inoculated media was incubated at 37°C and shaken at 250 rpm for approximately 18 hours in an Innova 4330 refrigerator/incubator shaker (New Brunswick Scientific, Edison, NJ). This initial growth phase in a small amount of media was necessary due to the use of a miniscule quantity of cells initially for inoculation.

b. Mother Culture Storage

After the 18 hour incubation time, a 0.70 mL aliquot of the culture was placed in a sterile Nalgene® cryogenic vial (Nalgene® Labware, Rochester, NY) with 0.30 mL of 50% (v/v) glycerol and stored at -80°C until needed for future cultures.

c. Culture Growth

The remaining 9.30 mL of the initial culture was used to inoculate 1.00 L of LB media containing 100 µg/mL ampicillin in a 2800 mL Pyrex® Fernbach culture flask (Corning, Inc., Corning, NY). This mixture was incubated at 37°C and shaken at 250 rpm in the aforementioned shaker until an absorbance of 1.2 units in a 1 cm cell at 600 nm using a Beckman DU® 640 spectrophotometer was obtained (Beckman Coulter, Inc., Fullerton, CA). Once an absorbance of 1.2 units was reached, a 50 µL sample was placed in a 1.50 mL Flex-Tube® (Eppendorf®, Brinkmann Instruments, Inc., Westbury, NY) and spun at 13,400 x g in an Eppendorf® MiniSpin Microcentrifuge (Eppendorf®, Brinkmann Instruments, Inc., Westbury, NY) for 1 minute. The supernatant was decanted and discarded. The pellet, containing pre-induced BL21 E. coli, was frozen at -20°C until all samples were collected for electrophoresis.

2. TH-GST Induction, Initial Purification and Storage

a. TH-GST Induction

Expression of TH-GST was induced by adding 24.0 mg of IPTG to 1.00 L of LB media containing the transformed BL21 E. coli culture (IPTG concentration of 0.1 mM).

Induction occurred for 2 hours at 30°C while shaking at 250 rpm in an Innova 4330 refrigerator/incubator shaker (New Brunswick Scientific, Edison, NJ). After the 2 hour induction period, a 50 μL sample was placed in a 1.50 mL Flex-Tube® (Eppendorf®, Brinkmann Instruments, Inc., Westbury, NY) and spun at 13,400 x g in an Eppendorf® MiniSpin Microcentrifuge (Eppendorf®, Brinkmann Instruments, Inc., Westbury, NY) for 1 minute. The supernatant was decanted and discarded. The pellet, containing induced BL21 E. coli, was frozen at -20°C until all samples were collected for electrophoresis.

b. Pelletization of Induced BL21 E. coli

The induced BL21 E. coli was transferred to a 1.00 L centrifuge bottle. The culture was pelletized using a Beckman J6-HC centrifuge and Beckman JS 4.2 rotor (Beckman Coulter, Inc., Fullerton, CA) at 4°C and 10,000 x g for 30 minutes. The supernatant was discarded.

c. Induced BL21 E. coli Wash

The induced BL21 E. coli pellet was resuspended and washed with 50.0 mL of ice-cold 10% (v/v) glycerol. A mechanical pipet was used to aid in the resuspension process by repeatedly filling and expelling the pipet with the suspension.

d. Pelletization of Washed, Induced BL21 E. coli

The suspension of washed, induced BL21 E. coli was transferred to a 100 mL centrifuge tube. The culture was pelletized using a Beckman J2-HS centrifuge and Beckman JS 4.2 rotor (Beckman Coulter, Inc., Fullerton, CA) at 4°C and 10,000 x g for 30 minutes. The supernatant was discarded.

e. Storage of Induced BL21 E. coli

The pellet from the previous step was resuspended in ice-cold 25.0 mL 10% (v/v) glycerol, aliquoted into 15 mL Fisherbrand screwcap tubes and frozen at -80°C until needed on assay day.

C. TH-GST Purification

It is important to note that, once the purification process described below had begun, the procedure was carried to completion ultimately resulting in an assay without any subsequent intermediate storage steps.

1. Cell Lysis by Sonication

a. Preparation of Induced BL21 E. coli

The induced BL21 E. coli pellet was thawed on ice and then transferred to 1.50 mL Flex-Tubes® (Eppendorf®, Brinkmann Instruments, Inc., Westbury, NY) and spun at

8,000 x g in an Eppendorf® MiniSpin Microcentrifuge (Eppendorf®, Brinkmann Instruments, Inc., Westbury, NY) for 10 minutes. The supernatant was discarded. The pellet was then resuspended in 1.20 mL of the Tris sonication buffer. A mechanical pipet was used to aid in the resuspension process.

b. Sonication

Immediately prior to sonication, 10 μL of the 50.0 mM PMSF stock solution was added to the tube which was suspended in an ice water bath. A Misonix Inc. Ultrasonic Processor XL with a microtip (Farmingdale, NY) was used at a setting of 3.5 corresponding to 35% maximal output for 15 seconds with a 45 second interval before the subsequent sonication step. This was repeated three more times for a total of 60 seconds of sonication. An additional 10 μL of the 50.0 mM PMSF stock solution was added post-sonication.

2. Purification

a. Pelletization of Membrane Debris

After sonication was completed, the Flex-Tube® was spun at 10,000 x g in an Eppendorf® MiniSpin Microcentrifuge (Eppendorf®, Brinkmann Instruments, Inc., Westbury, NY) for 30 minutes at 4°C and the tubes were reserved for use of the supernatant in step (c) below.

b. Preparation of Glutathione Agarose Beads

Seventy mg glutathione-agarose beads (Sigma-Aldrich St. Louis, MO) were weighed and placed into a 15.0 mL Fisherbrand screwcap tube, 14.0 mL ddH_2O was added and the mixture was allowed to sit overnight at 4°C. The swelled beads were pipetted into two different flex tubes labeled "boiled" and "un-boiled." The beads were centrifuged at 3000 x g for 1 minute, and the water was decanted. The pellets were rinsed with 500 µL ddH_2O and centrifuged again. This process of rinsing followed by centrifugation and decanting was repeated a total three times. Finally, the pellet was rinsed once with 500 µL 0.050 M Tris buffer pH 7.40, centrifuged, and decanted.

c. TH-GST Attachment to Glutathione Agarose Beads

Once the membrane debris had been palletized from step (a) above, half of the supernatant was added to the "boiled" beads and half to the "un-boiled" beads. The Flex-Tubes® were then placed on a Rocker II Model 260350 (Boekel Scientific, Feasterville, PA) set at 20 cycles/min and incubated at 4°C for 30 minutes.

d. Excess TH-GST Supernatant Removal

The agarose beads were centrifuged at 3000 x g for 1 minute at 4°C using an Eppendorf® MiniSpin Microcentrifuge (Eppendorf®, Brinkmann Instruments, Inc., Westbury, NY), decanted, and rinsed with 500 µL of 0.050 M Tris buffer pH 7.40. Rinsing, followed by centrifugation and decanting was repeated twice. The beads were finally diluted to 1 mL with 0.050 M Tris buffer pH 7.40. Individual 50 µL samples of the agarose bead suspensions were taken following each rinse step and placed in 1.50 mL

Flex-Tubes® (Eppendorf®, Brinkmann Instruments, Inc., Westbury, NY). These samples were stored at -20°C for later analysis by electrophoresis.

e. Preparation of TH-GST Agarose for Assay Standards and Blanks

The purified TH-GST agarose in the "boiled" Flex-Tube® was added to boiling water for 30 minutes prior to use in the assay. If any solution evaporated during this process, 0.050 M Tris buffer pH 7.40 was added to bring the total volume back to 1.00 mL.

D. Protein Quantfication using Bradford Assay

Prior to analysis of the purified protein by electrophoresis, it was necessary to quantify the amount of protein in each sample to ensure none were too concentrated for the process. The total amount of protein loaded per well should be less than 10 μg to ensure adequate band resolution. As can be seen below, a standard curve was prepared using bovine serum albumin in order to quantify the TH samples we collected during the purification process.

1. Bovine Serum Albumin Bradford Assay Process

a. BSA Standard Solutions

Bio-Rad stock BSA solution (Bio-Rad Inc., Hercules, CA) was used to create a standard curve. Since the initial stock solution concentration was 1 mg/mL BSA it was

diluted 1:10 with ddH_2O to create a 0.10 mg/mL BSA solution. This resultant solution was used to create calibration standards by adding 20 µL, 40 µL, 60 µL, 80 µL, 100 µL, and 120 µL of the 1 mg/mL BSA to enough ddH_2O to create 800 µL of solution. The final calibrator concentrations, following the addition of 200 µL of dye reagent in the following step were, 2 µg/mL, 4 µg/mL, 6 µg/mL, 8 µg/mL, 10 µg/mL, and 12 µg/mL BSA, respectively.

b. BSA Standard Curve

Prior to the absorbance readings, 200 µL of BioRad dye reagent was added to each calibrator standard and allowed to develop for 5 minutes at room temperature. A Beckman DU® 640 spectrophotometer (Beckman Coulter, Inc., Fullerton, CA) was used to determine the absorbance of each of the BSA standard solutions in a 1.0 cm cell at a wavelength of 595 nm.

2. TH-GST Bradford Assay Process

a. TH-GST Solution

To an Eppendorf® tube containing 800 µL ddH_2O was added 1 µL of each sample to be analyzed by gel electrophoresis, and the combination was mixed.

b. TH-GST Absorbance

Prior to spectrophotometric analysis, 200 µL of BioRad dye reagent was added to the TH-GST solution. This mixture developed for 5 minutes at room temperature. A

Beckman DU® 640 spectrophotometer (Beckman Coulter, Inc., Fullerton, CA) was then used to determine the absorbance in a 1.0 cm cell at a wavelength of 595 nm.

E. Electrophoresis

1. Preparation of Gel

a. Casting Sandwich

The electrophoresis gel was prepared in a casting sandwich made up of two 14 cm x 0.75 mm spacers and two 14 x 14 cm glass plates attached together in an apparatus known as a casting stand. The spacers were arranged with the long axis oriented vertically between the two glass slides and located physically at the two horizontal ends of the slides, forming a sandwich. The constructed sandwich was placed into the vertical casting stand with the two spacers positioned on the left and right edges (as opposed to the top and bottom). The bottom of the holder was composed of a rubber layer; thus the inserted sandwich now formed a casting mold which had a rectangular opening on the top.

b. 10% Polyacrylamide Separation Gel

The separation gel was prepared by mixing 5.00 mL 30% acrylamide/0.8% bisacrylamide, 3.75 mL 4xTris buffer and 6.25 mL distilled water. Immediately prior to use, 50 µL 10% (w/v) ammonium persulfate and 10 µL TEMED were added to the gel

mixture. The solution was quickly mixed by manually swirling the flask. A Pasteur pipet was used to fill the void in the casting sandwich with the gel up to a height of approximately 11 cm leaving a space of ca. 3 cm on the top. A 1.0 cm layer of isobutyl alcohol was added to the top of the gel solution to provide a protective layer against atmospheric oxygen. Oxygen was eliminated because its presence would inhibit gel polymerization. Additionally, isobutyl alcohol created a flat surface at the top of the gel. Polymerization occurred during a 30 minute incubation period at room temperature.

c. 5% Polyacrylamide Stacking Gel

Following polymerization, the isobutyl alcohol layer was poured off the top of the separation gel, and the gel was rinsed with ddH_2O. This was done in preparation for addition of the ca. 2 cm layer of stacking gel which would rest on top of the separation gel. The stacking gel was then prepared by mixing 0.65 mL 30% acrylamide/0.8% bisacrylamide, 1.25 mL of 4xTris buffer and 3.05 mL distilled water. Just before use, 25 µL 10% ammonium persulfate and 5 µL TEMED were added to the stacking gel solution. The solution was quickly mixed by manually swirling the flask. A Pasteur pipet was used for the addition of the stacking gel solution to the top of the separation gel until its height was within 1 cm of the top of the glass plates. A 10-well 0.75 mm comb was inserted into the top of the stacking gel to form 10 sample wells. Polymerization of the stacking gel occurred over a 30 minute incubation period at room temperature. The greatly reduced concentration of polyacrylamide in the stacking gel layer results in subsequently larger pore sizes within the gel matrix. When the electrical potential is applied across the gel, the proteins move through the stacking gel at a very rapid and

virtually identical rate; however, when they reach the much more dense separation gel, the proteins immediately experience a relatively very large resistance to movement, which concentrates the samples at the beginning of the separation gel. This concentration of the proteins increases the subsequent resolution of the technique. Once the proteins enter the separation gel, they are separated by their mass.

2. Protein Sample Preparation

The TH-GST samples collected during expression and purification of the enzyme were prepared for electrophoresis by diluting 1:1 (v/v) with 2xSDS sample buffer. Pelleted samples were prepared by adding 50 µL of 1xSDS sample buffer. A Benchmark™ pre-stained protein ladder (Invitrogen Corporation, Carlsbad, CA) sample was prepared by diluting 25 µL of the sample with 25 µL 2xSDS sample buffer. All of the samples were then denatured by heating for 3 to 5 minutes in a 100°C water bath.

3. Loading and Separation of Samples

The casting stand containing the newly prepared electrophoresis gel/glass plate sandwich was locked into a separation chamber. The sample well comb was removed from the gel and the sample wells were filled with 1xSDS electrophoresis buffer. The separation chamber was filled with enough 1xSDS electrophoresis buffer to cover the top of the gel. Twenty five µL of each protein sample was loaded into individual wells. An EC Apparatus Model EC 135 power supply (EC Apparatus Corporation, St. Petersburg, FL) was connected to the separation chamber and run at 10 mA of constant current until the tracking dye in the samples entered the separation gel. The current was then

increased to 15 mA and held constant until the tracking dye reached the bottom of the gel.

4. Protein Visualization by Staining

a. Preparation of Gel

The separation chamber was disassembled and the gel sandwich was removed. A spacer was removed and used to pry one of the glass plates from the surface of the gel. The edge of the glass plate was then used to cut the stacking gel from the top of the separating gel.

b. Protein Staining

The separation gel was placed in 20 x 20 cm polypropylene container and covered with a Coomassie Brilliant Blue stain solution. The mixture was then placed on a Rocker II Model 260350 (Boekel Scientific, Feasterville, PA) for 3 to 4 hours where it oscillated at 15 cycles/min at room temperature.

c. Gel Destaining

The Coomassie stain was poured off of the separation gel, and the gel was covered with destain solution. The gel was then placed back on the rocker for ca. 12 hr at 15 cycles/min. During the 12 hr destaining process, the destain solution was removed and replaced 3 to 4 times periodically until the protein bands were stained and the background was clear.

d. Protein Analysis

The resultant stained gel was analyzed for assessment of proteins present and their associated masses by comparison to the standard proteins.

F. TH-GST Activity Assay

Each TH activity experiment included eight test tubes: four controls (2 standards and 2 blanks) and four activity samples. The standards were prepared at a concentration of 200 ng/mL L-dopa and were used for quantitative assessment of the unknown samples. The logistics of the experiments are illustrated in Figure 3-3. The details are explained below.

Figure 3-3. TH activity experiment logistics.

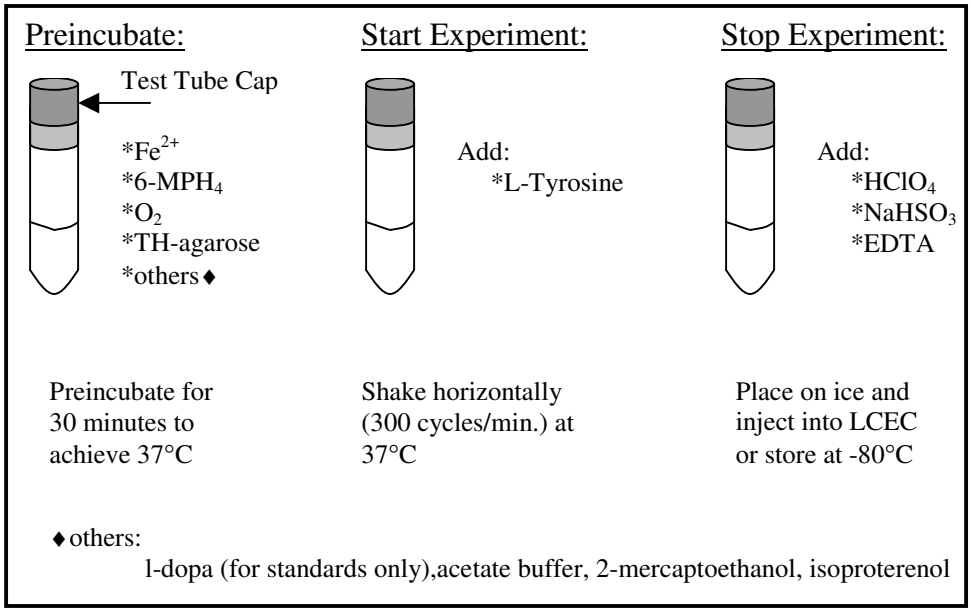

1. Preincubation of Assay Components

Prior to each activity assay, all the components necessary for the hydroxylation of L-tyrosine to L-dopa, excluding the L-tyrosine itself were combined in a test tube, capped and preincubated for 25 min to achieve the optimum reaction temperature of 37°C. Incubation was accomplished in a Sherer Controlled Environment Chamber Model CEL 37-14 (Sherer-Gillett Co., Marshall, MI) using an Eberbach Model 6010 shaker set at 300 cycles/minute. The constituents and the amounts used in the preincubation solutions for standards, blanks and unknown samples are found in Table 3-2.

Table 3-2. Preincubation solution constituents.

Component	Stock Concentration	Assay Concentration	Standard (µL)	Blank (µL)	Activity Samples (µL)
Acetate Buffer	2.0 M	0.40 M	200	200	200
Fe^{2+}	1.0 mM	0.10 mM	100	100	100
6-MPH_4 & 2-Mercaptoethanol	20.0 mM & 0.50 M	2.00 mM & 0.050 M	100	100	100
Isoproterenol	$1.30x10^{-4}$ M	$1.30x10^{-5}$ M	100	100	100
ddH_2O			163	200	200
L-dopa	6400 ng/mL	200 ng/mL	37.5	0	0
TH-GST attached to glutathione agarose			100 boiled	100 boiled	100

2. TH-GST Activity Experiment Initialization

Once the assay components had been equilibrated to 37°C, 200 µL of 2.50 mM L-tyrosine (0.50 mM final assay concentration) was added to begin the activity assay. The conversion of L-tyrosine to L-dopa was allowed to proceed for 20 minutes.

3. Termination of Activity

Perchloric acid was added to terminate the assay, while sodium bisulfite and EDTA were simultaneously added to prevent oxidation of the newly formed L-dopa. Table 3-3 describes the termination and preservation constituent additions.

Table 3-3. Termination and preservation constituents.

Component	Stock Concentration	Assay Concentration	Standard (µL)	Blank (µL)	Activity Samples (µL)
$HClO_4$	2.0 M	0.26 M	200	200	200
$NaHSO_3$ & EDTA	0.30 M & 0.030 M	0.023 M & 0.0023 M	100	100	100

4. Storage of Activity Assay Samples

Following termination of activity, all assay experiment samples were immediately placed on ice to await quantitation by LCEC. If quantitation was not performed immediately, the samples were stored at -80°C until LCEC analysis could be undertaken.

G. LCEC Quantification of TH-GST Activity

All assay and calibration solutions were kept on ice until injected into the LCEC system. In order to obtain comprehensive statistical information, each solution was injected multiple times.

1. Instrumentation

The LCEC system employed for this work was assembled in-house. The constituents of this system included a Milton Roy Minipump (Milton Roy Co., Ivyland, PA) connected to a Mark III pulse dampener (Alltech Scientific Co., Deerfield, IL) and a Noshok pressure gauge (Noshok, Berea, OH) with a 0-6000 psi range. A Rheodyne Model 7125 sample injector (Rheodyne, Oak Harbor, WA) with a Rheodyne stainless steel, 10 μL sample loop was included for sample introduction. All tubing was 0.005" i.d. and made from stainless steel.

We packed the column in-house using a 10 cm x 4 mm stainless steel column having an internal diameter of mm. The stationary phase was Alltech Adsorboshphere C18 Reversed Phase 3.0 μm packing material (Alltech, Deerfield, IL) A slurry containing 1.80 g packing material in 25 mL acetone was sonicated for 15 minutes to ensure suspension of the packing material. The suspension was placed in the slurry reservoir of a Haskel (Burbank, CA) column packing unit which utilized a reciprocating plunger pump with an outlet:inlet pressure amplification of 122:1. The solvent reservoir was filled with 500 mL of acetone. The column was packed at 6000-7200 psi until most of the solvent reservoir acetone was consumed. This process usually required 15 to

20 minutes. The column was removed from the column slurry reservoir, assemble and flushed with 40:60 acetonitrile:water for one hour prior to subsequent analytical use.

A Great Plains Labs potentiostat (Great Plains Labs, Norman, OK) was used in combination with a BASi Model MF-1000 dual 3 mm glassy carbon working electrode (Bioanalytical Systems Inc., West Lafayette, IN). Additionally a BASi Model MF-1093 auxiliary electrode and a BASi Model RE-4 Ag/AgCl reference electrode were used to complete the 3-electrode system. Output from the potentiostat was recorded on a Cole Parmer Model 0156 strip chart recorder (Cole Parmer Instrument Co. Chicago, IL).

2. LCEC Characterization

a. Hydrodynamic Voltammograms (HDVs)

The chemical structures of L-tyrosine and L-dopa are quite similar leading to nearly identical retention times of 2.65 and 2.67 minutes, respectively. Therefore, hydrodynamic voltammograms were completed for each compound to determine the optimum applied potential for the potentiostat. The hydrodynamic voltammogram for L-tyrosine was obtained by injecting 10 μL of a 5 μM stock solution at a intial potential of +0.500 V six times. The potential was then changed by +50 mV and the stock standard was reinjected six times so that data at the new potential was obtained. This process was repeated until all possible applied potentials were investigated and responses from no signal to a relative maximum signal were obtained. The data was then plotted as peak height vs. applied potential. This process was then repeated for L-dopa starting

using injections of 10 µL of a 5 µM solution at an applied potential of 0.000 V. The results are illustrated in Fig 3-4.

Figure 3-4. Hydrodynamic voltammograms for L-tyrosine and L-dopa.

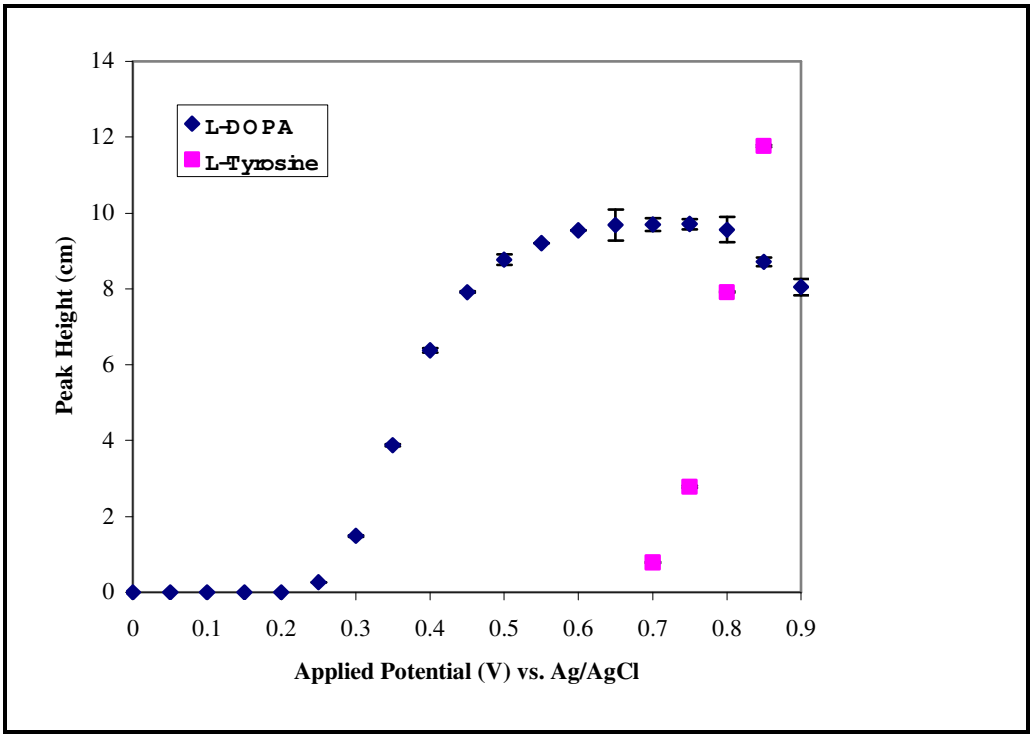

As can be seen in Figure 3-4, the optimum response for L-dopa occurs at approximately +0.550 to +0.750 volts. Additionally, in the lower end of this potential region (+0.550 V) there is a minimal response for L-tyrosine. The concentration of L-tyrosine in a typical incubation sample, however, is on the order of 1000 times greater than the concentration of the L-dopa product. Thus, to prevent, or at least minimize, interference from L-tyrosine during the quantitation of L-dopa, an applied potential of

+0.55 V vs. Ag/AgCl was selected for all routine analyses. As shown in the HDVs, this potential gave a favorable response for L-dopa without substantial interference from L-tyrosine.

b. LCEC Operating Parameters

LC flow rate optimization was accomplished by varying the flow rate from 0.50 to 1.50 mL/min. The flow rate selected for routine use was 1.20 mL/min. This rate provided excellent separation of all analytes of interest, while keeping the time required for a single sample to a modest 8 minutes. The chart recorder speed was set at 2.0 cm/min. Pressure readings at this flow rate were typically around 1500 psi. As described above, the potentiostat was set at +0.55V vs. Ag/AgCl. A representative chromatogram is shown in Figure 3-5.

Figure 3-5. Representative chromatogram of assay components.

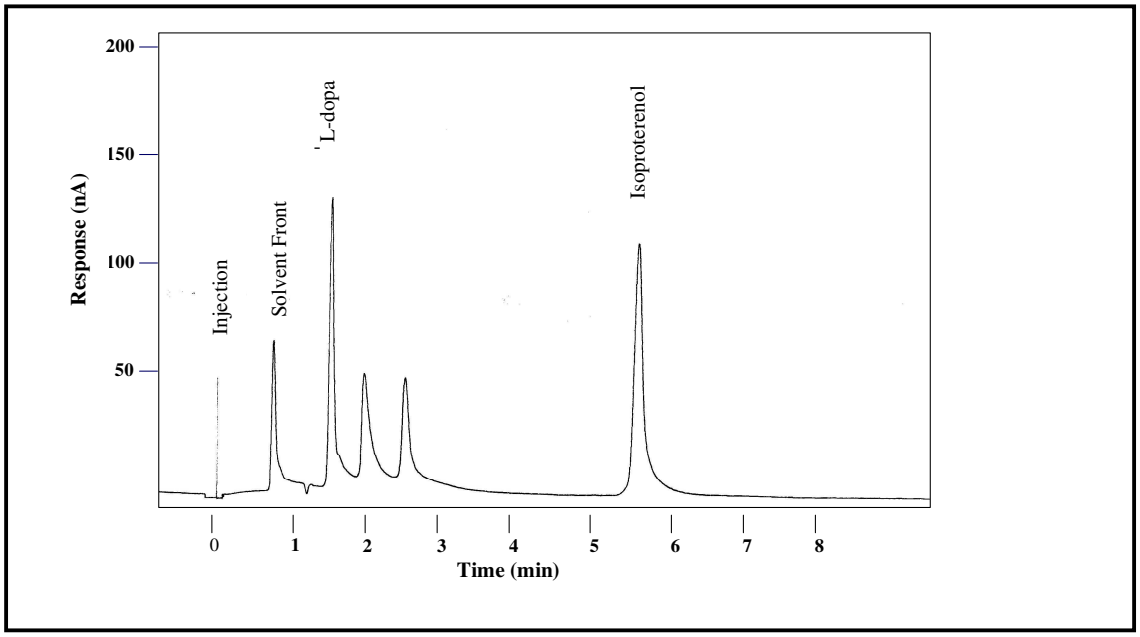

c. Column Characterization

The retention time and calculated number of theoretical plates for L-dopa were 2.6 min and 4400, respectively. The resolution of the L-dopa peak from 2-mercaptoethanol, its nearest eluting neighbor, was typically 2. Background noise was not an issue in the activity ranges investigated. The limit of detection (LOD) was defined as the lowest concentration peak with a signal to noise ratio ≥ 5. For this LCEC system the LOD was determined to be 12.5 ng/mL L-dopa (0.063 μM) when the injection volume was 10 μL.

d. Linear Dynamic Range (LDR)

The LDR for L-dopa was 12.5 - 6400 ng/mL (0.0633 - 32.5 μM) when using 10 μL injections. The correlation coefficient exceeded 0.99. Non-linearity was observed at concentrations ≥ 12800 ng/mL (64.9 μM).

e. Standard Curve Preparation

A standard curve, or calibration curve, was prepared for quantitation of the L-dopa produced during the activity assay. Standard curves were prepared using the same stock solutions and in precisely the same manner as the activity assay samples. Preparation in this manner minimizes any unknown matrix considerations. The constituents of the standard curve are described in Table 3-4. Each of these components was added as described in Section F, Figure 3-3 (TH activity experiment logistics).

Table 3-4. Standard curve constituents.

Component	Stock Conc.	Assay Conc.	800 ng/mL (µL)	400 ng/mL (µL)	200 ng/mL (µL)	100 ng/mL (µL)	50 ng/mL (µL)
Acetate Buffer	2.0 M	0.40 M	200	200	200	200	200
Fe^{2+}	1.0 mM	0.10 mM	100	100	100	100	100
6-MPH_4 & 2-Mercapto-ethanol	20.0 mM & 0.50 M	2.00 mM & 0.050 M	100	100	100	100	100
Isoproterenol	$1.30x10^{-4}$ M	$1.30x10^{-5}$ M	100	100	100	100	100
ddH_2O			150	225	263	281	291
L-dopa	6400 ng/mL		150	75	37.5	18.75	9.38
L-tyrosine	2.50 mM	0.50 mM	200	200	200	200	200
$HClO_4$	2.0 M	0.26 M	200	200	200	200	200
$NaHSO_3$ & EDTA	0.30 M & 0.030 M	0.023 M & 0.0023 M	100	100	100	100	100

A response factor was calculated for each standard curve sample as the ratio of the peak height for L-dopa to the peak height of isoproterenol, the internal standard. Standard curves were prepared by plotting a linear regression of the analyte/internal standard response factor versus the analyte concentration for the calibrators, and used to determine the concentrations of L-dopa in all assay samples. A new standard calibration curve was produced on the day of each analysis. A typical standard curve is shown in Figure 3-6. Each standard concentration was injected four times. The average ± standard deviation is plotted for each concentration. As can be seen in this figure, we were able to obtain linear standard curves for the quantitation of our assay samples.

Figure 3-6. Typical standard curve.

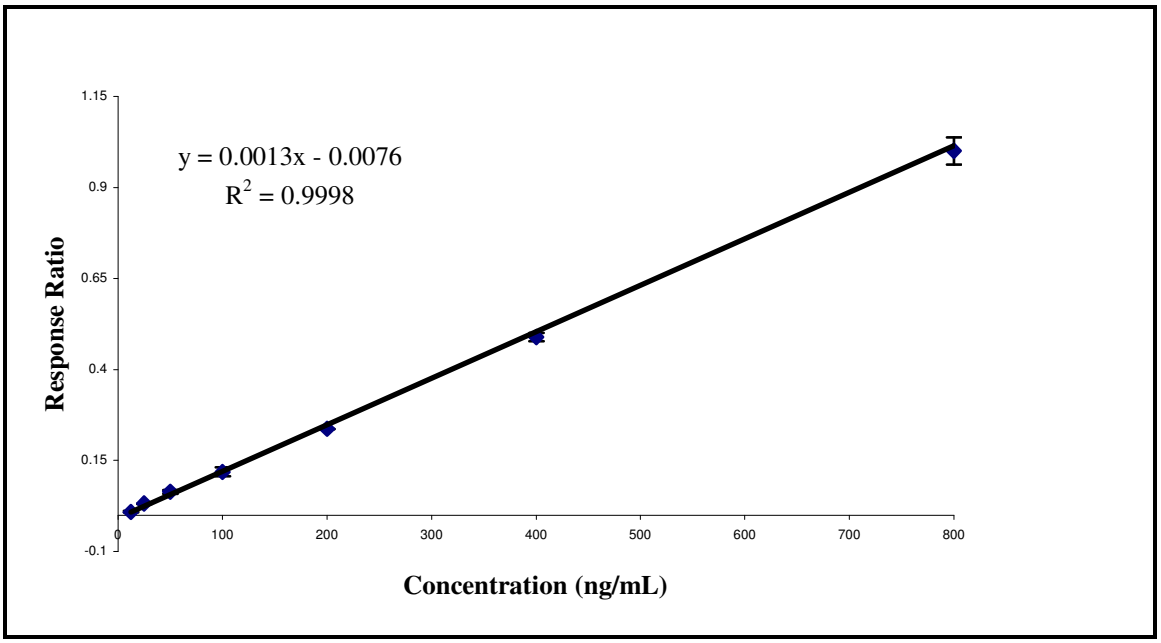

IV. Results and Discussion

A. Results

1. Preincubation Time for TH Assays

Prior to any assays for activity, it was necessary to determine the amount of time required to preincubate the assay solution to attain 37°C. As Figure 3-8 illustrates, a typical assay solution in a typical incubation tube reaches 37°C within 25 minutes. It is also clear that the incubator subsequently maintains the solution at this temperature.

Figure 3-7. Assay solution temperature.

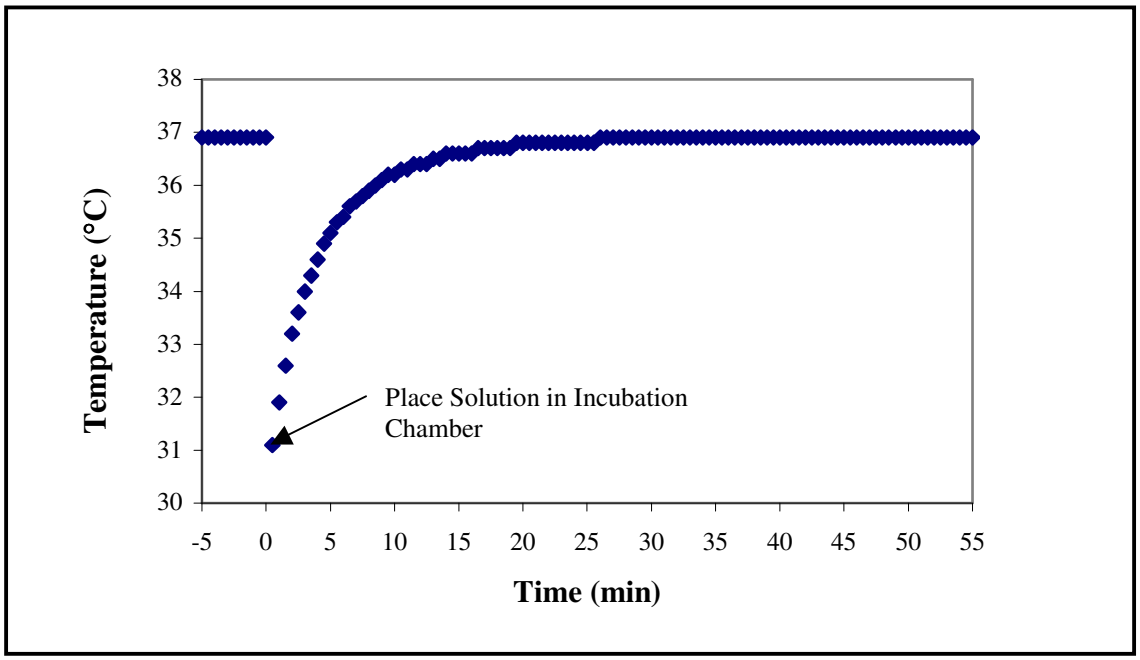

2. TH Assay for Activity of Purified TH-GST.

The initial activity assays were performed while the TH-GST remained attached to the agarose support structure. Following the initial assay experiment for the activity of TH in the supernatate of the cell lysis no enzyme activity was detected. An investigation was undertaken to determine whether the problem had occurred in the sonication process or in the enzyme storage procedures.

3. Successful TH Assay for Activity of Purified TH-GST.

Once sonication and purification of TH-GST had been proven successful, the investigation into why the purified enzyme was inactive led to an extensive literature search, after which it became apparent that freeze/thaw cycles could degrade the enzyme

rendering it inactive. Therefore, instead of proceeding with enzyme expression and purification through the lysis step, and then storage of the whole cell lysate in 10% glycerol at -20°C until use in an activity assay, a change was made to store the whole, induced E. coli cells prior to sonication in 10% glycerol. Whole E. coli were divided into aliquots so that it was necessary to only thaw the precise amount needed for a single assay. Sonication occurred only on the morning of the assay. As can be seen in Table 3-5, this modification to the procedure resulted in active TH-GST attached to the glutathione agarose support. An ANOVA of the four samples shows no significant difference, $F(3,16) = 0.762$, $p = 0.05$.

Table 3-5. Successful TH assay results following procedural modification.

Sample*	TH Activity**
1	3245 ± 26
2	3224 ± 28
3	3219 ± 31
4	3237 ± 36

* Individual samples prepared individually by sonicating whole E. coli cells, isolating TH-GST in supernatant, attaching TH-GST to agarose beads, and washing the beads three times prior to taking an aliquot for assay

** Activity shown as ng L-dopa produced (mean ± s.d.; n=5)

4. Investigation of TH-GST Fusion Protein Expression and Purification

To monitor the expression and purification of TH-GST, we also employed SDS-PAGE. The specific samples monitored from the individual steps of the expression and purification process were chosen to first show that TH-GST was successfully being expressed and to demonstrate the separation/purification of TH-GST from cell debris and other constituents from the whole cell lysate.

A typical gel was constructed to contain 10 sample lanes. In order to identify the bands associated with TH-GST, lanes #1 and #10 were loaded with molecular weight markers (proteins of known molecular weight). The samples from the expression and purification process were loaded in lanes #2 through #9 in the order in which they were taken from the expression and purification process.

The original sonication conditions consisted of 40% maximal output for 5 sec with a following 45 sec resting period in which the cells were stored on ice. This on/off sonication sequence was repeated for four cycles. However, the subsequent SDS-PAGE gel showed no TH-GST in the supernatant fraction postsonication; therefore, the E. coli cells were perhaps still predominantly intact post-sonication and, as a result, TH-GST was not liberated into the supernatant solution. We subsequently attempted sonication at 40% maximal output for 30 seconds with 30 second resting intervals for 2 cycles. Following electrophoresis this second method showed liberation of TH-GST; however, the enzyme assays still revealed no activity. Since the SDS-PAGE gel showed that TH-GST was present in the supernatant fraction postsonication, it was apparent that the sonication successfully lysed the E. coli cells; however, the possibility existed that the sonication was too vigorous which caused heating and degradation of the enzyme. A

third modification employed 15 seconds of sonication at 35% maximal output with 45 second resting intervals for 4 cycles. This modification resulted in less heating; however, the enzyme assays still demonstrated no activity.

The electrophoresis gel in Figure 3-8 illustrates this process for a successful expression, sonication and purifaction sequence. In the figure, as stated above, lanes #1 and #10 contain molecular weight markers. Lane #2 is a sample taken after induction. Lane #3 is a sample taken just before induction. [Note: the sample for lane #3 obviously preceded that for lane #2 in the actual processing sequence.] Lane #4 is a sample from the whole cell lysate. Another sample of the whole cell lysate was obtained, centrifuged and separated into pellet and supernatant fractions. Lane #5 corresponds to the pellet fraction. Lane #6 corresponds to the supernatant fraction. Lane #7, #8 and #9 contain samples purified with glutathione agarose. Lane #7 was obtained following the first rinse cycle, lane #8 was obtained following the second rinse cycle and lane #9 was obtained following the third rinse cycle. The final lane, lane # 10, as mentioned above contains the same molecular weight markers as analyzed for lane #1.

Figure 3-8. Electrophoresis gel for tyrosine hydroxylase purification process.

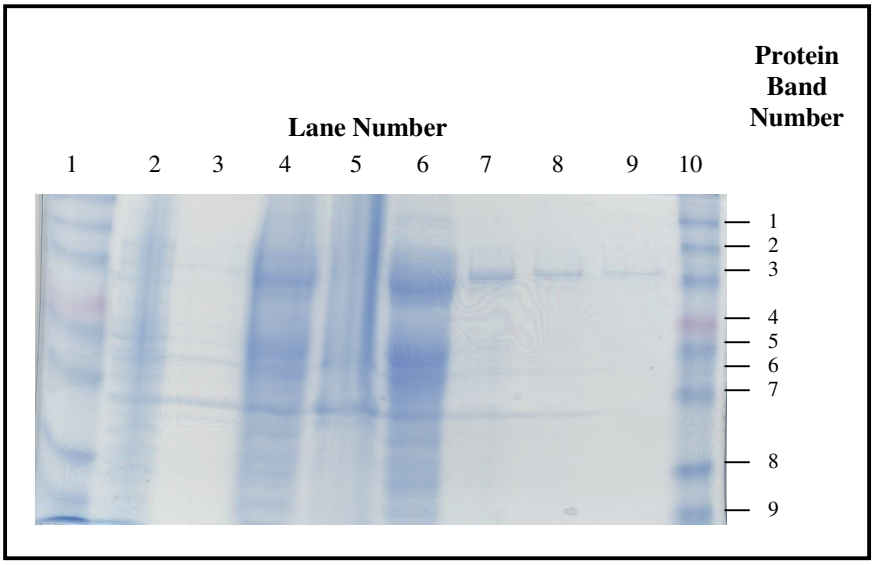

The molecular weights for the Benchmark™ pre-stained protein ladder (1st and last lanes) are listed in Table 3-6 along with the molecular weight of the targeted TH-GST fusion protein (82 kDa).

The band associated with TH-GST is faintly visible in lane #2 of Figure 3-7, which corresponds to the postinduction whole cell lysate. A corresponding band appears in every subsequent postinduction lane except lane #5, corresponding to the pellet from the whole cell lysate, indicating the successful expression of TH-GST. The supernatant fraction of the whole cell lysate, a sample of which is shown in lane #6, was selected for subsequent purification of TH-GST. The presence of a single band in the sample in lane #9 representing the final rinse cycle in enzyme purification with glutathione-agarose, clearly demonstrates that the resulting TH-GST is reasonably free of contaminants.

Table 3-6. Molecular weight of Benchmark™ proteins and the targeted TH-GST.

Protein Band Number	Molecular Weight (kDa)
1	182
2	116
TH-GST	**82**
3	82
4	64
5	49
6	37
7	26
8	19

We quantified the amount of protein in individual samples using the Bradford assay. During expression, typical washed pellets of E. coli following induction, weighed between 6 and 8 g. Analysis via the Bradford Assay revealed a typical value of 1 μg TH-GST/ g postinduction pellet.

5. Storage of Assay Solutions and L-Dopa Produced at -80°C

Due to the extensive amount of time invested when performing a single assay, an experiment was performed to determine which of the stock assay solutions could be prepared and stored prior to the assay. The typical assay involved thawing stored E. coli cells, preparing sonication buffer and its components, sonicating the E. coli, purifying

TH-GST, preparing assay solutions, performing the assay, preparing the LCEC, running a standard curve and finally injecting the assay solutions. The enzyme purification process alone took up to 8 hours. Therefore, it was immediately evident that any solutions that could be prepared prior to analysis would save valuable time. The stock assay solutions initially investigated were the 2.0 M acetate buffer (pH 6.40), 2.0 M $HClO_4$, and the combined $NaHSO_3$ and EDTA solutions. Each solution was prepared and aliquoted into individual 1.50 mL Eppendorf tubes and stored at -80°C. Independent assays using these stored solutions were individually conducted. It was determined that each of these solutions could be stored up to 30 days with no appreciable difference in assay results.

The stability of the L-dopa produced during the assay was also investigated. If shown to be stable at -80°C, samples could be conveniently analyzed after the date of the assay. Assay solutions were separately aliquoted into four individual 1.50 mL Eppindorf tubes and stored at -80°C to be evaluated the day of the experiment (zero days of storage), 24 hours after the experiment, 7 days after the experiment and 30 days after the experiment. As shown in Table 3-7, it was determined that the concentration of L-dopa did not significantly change after storage for up to one month at -80°C, $F(3,16) = 1.719$, $p = 0.05$.

Table 3-7. L-Dopa stability following 30-day storage at -80°C.

Days of Storage	TH Activity*
0	3997 ± 25
1	3986 ± 16
7	4015 ± 19
30	4004 ± 22

* Activity shown as ng L-dopa produced (mean ± s.d.; n=5) following incubation for 20 min

6. Storage of TH-GST within Whole E. coli

Long term storage conditions were investigated to determine the length of time the enzyme could be stored at -80°C as the induced whole cells prior to sonication in 10% glycerol and retain activity. As Table 3-8 illustrates, the enzyme could be stored in this form for approximately one year with no appreciable loss of activity, $t(8) = 0.767$, $p = 0.05$.

Table 3-8. TH activity following 1-year enzyme storage at -80°C.

Days of Storage	TH Activity*
0	2895 ± 20
362	2904 ± 17

* Activity shown as ng L-dopa produced (mean ± s.d.; n=5) following incubation for 20 min

V. Conclusions

The ultimate goal of this work was to investigate the activity of TH when exposed to a strong electric field. To accomplish this, it was necessary to initially devise a method of binding the enzyme to an orientable support structure. Since GST fusion proteins are readily attached to glutathione supports, we intended to employ an orientable, glutathione support structure. A TH-GST fusion protein could then be attached to this orientable surface for the investigations within strong electric fields.

TH-GST was not commercially available; therefore, we needed to express and purify this protein in-house using recombinant DNA technology. Through investigations of sonication and storage procedures, active TH-GST was successfully expressed and purified with glutathione-agarose. These investigations demonstrated that under the proper storage conditions, expressed TH-GST could be stored as the induced whole cells at -80°C for up to one year without appreciable loss of activity. This enabled the expression of large amounts of this intermediate form of the enzyme at a time, limiting the number of times needed to perform the initial steps in this time-consuming procedure.

Appropriate LCEC procedures for the determination of TH activity were established and routinely employed.

The TH activity investigations were undertaken with the TH-GST being attached to glutathione agarose. The demonstration that the immobilized enzyme possessed and maintained the fundamental TH activity provided confidence that we would be able to observe the TH activity when the fusion protein was subsequently immobilized on glass slides and exposed to large electric fields.

Immobilization of TH-GST Fusion Protein on Glutathione-Modified Glass Slides

Chapter 4

I. Introduction

The ultimate goal of this work was to investigate the activity of TH when the enzyme is exposed to a strong electric field. To limit the number of variables involved in such an experiment, it was first necessary to control the orientation of the enzyme within the electric field; therefore, a glutathione support structure was developed in-house that was loosely based on previous work.[121] The technique was originally intended for DNA microarray technology; however, it served our needs extraordinarily well.

As mentioned in Chapter 3, glutathione-S-transferase and glutathione-S-transferase fusion proteins could be purified using a support containing covalently attached glutathione. The most readily available glutathione-modified support is agarose beads which can be used in a column or in a batch made. The affinity of glutathione-S-transferase for glutathione is very high.[96] Thus, the lysate containing the fusion protein needed only to be incubated with the glutathione-agarose, the beads washed with a buffer

to remove contaminants, and the immobilized GST fusion protein was obtained in a form firmly attached to the support.

Our initial assays demonstrated that it was feasible to leave the TH-GST bound to the glutathione-agarose and still obtain functional enzyme activity. The next logical step was to modify a rigid and flat surface, which could be later placed in an electric field with a controlled orientation, to mimic the glutathione-agarose support structure. In theory, one surface of a flat support could be modified to contain covalently attached glutathione. If accomplished, this support could be used to purify the enzyme, and also orient the enzyme within the electric field. The support chosen to be modified was an ordinary, readily available microscope slide.

II. Background

The use of thiol/disulfide exchange reactions to attach substrates to silane-modified solid surfaces is a well established technique which has many applications including covalent chromatography, DNA microarrays and protein microarrays.[122-125] Rogers et al.[121] employed silanized microscope slides as a coupling agent for the immobilization of oligonucleotides to be used as DNA probes.

The silanization reagent 3-mercaptopropyltrimethoxysilane (MPTS) can be seen in Figure 4-1. This molecule, after cleavage of the methoxy groups by water, effectively reacts with free hydroxyl groups on glass surfaces. The free pendant thiol group remains and is available to subsequently react with a disulfide through a thiol/disulfide reaction.

Figure 4-1. 3-Mercaptopropyl trimethoxysilane (MPTS).

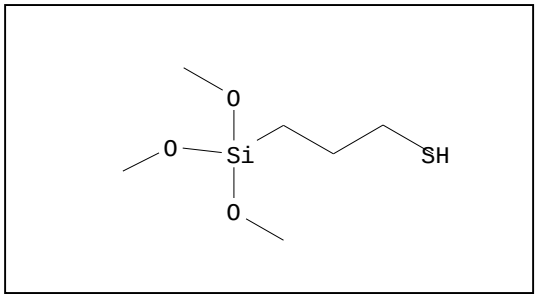

Figure 4-2 illustrates[126] the silanization scheme for modification of glass slides with MPTS. A 1% (v/v) MPTS and 16 mM acetic acid solution in 95% ethanol was stirred for 5 minutes to allow for the protonation and acid-catalyzed hydrolysis of the methoxy groups and condensation of the resultant silanols. This restricted time frame was necessary to limit the amount of condensation in order to maintain water solubility. The microscope slides were cleaned and activated using a 25% (v/v) ammonia solution. The activation involved exposure of hydroxyl groups on the surface of the slides. The cleaned and activated microscope slides were added to the silanol solution. The silanol condensate hydrogen bonded to the hydroxyl groups on the surface of the glass slides. Curing in a heated vacuum oven covalently attached the silane layer to the microscope slides. This silanization process left the thiol group of the silane available for further reaction.

Figure 4-2. MPTS-modification of microscope slides.

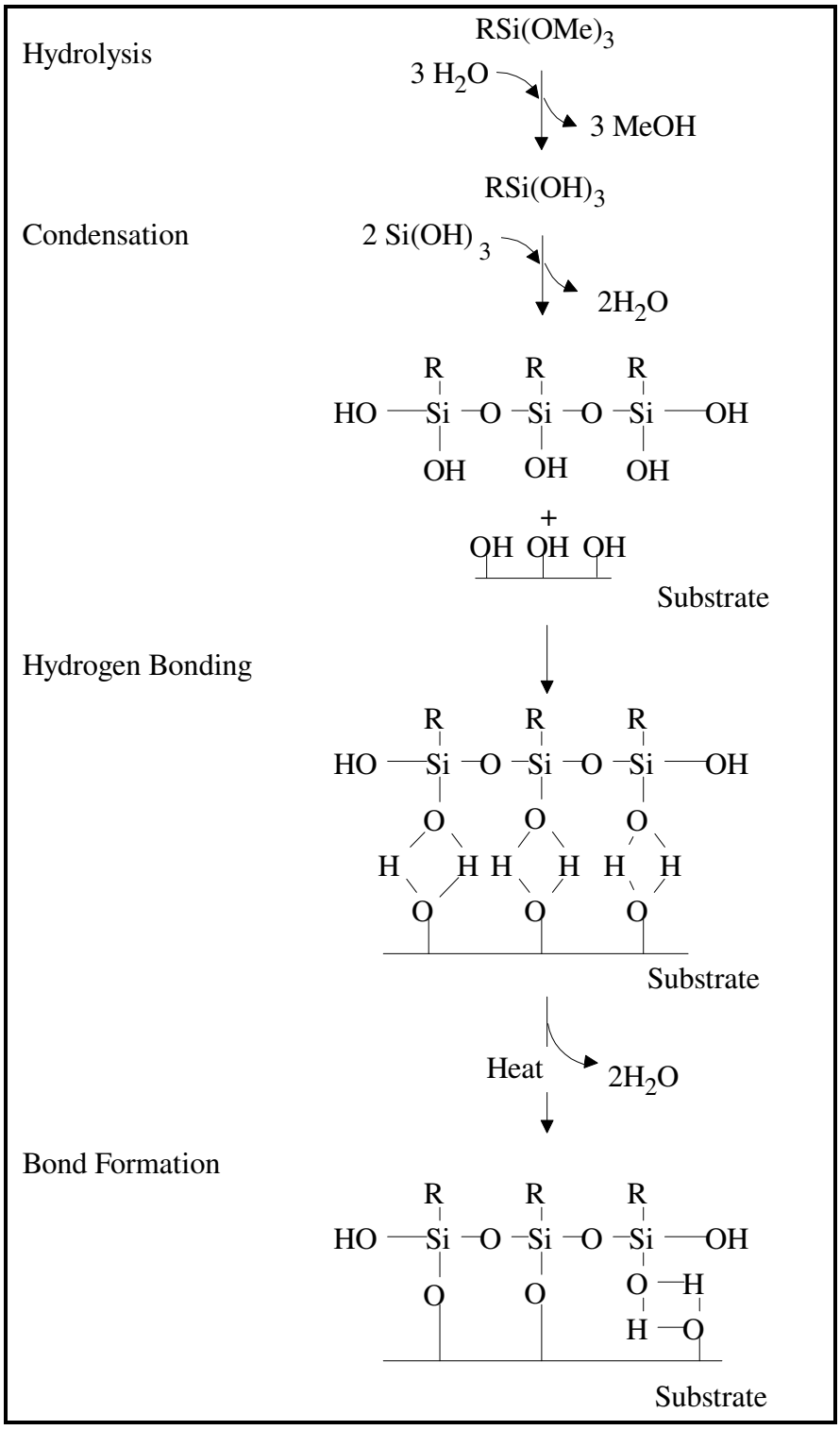

Rogers et al.[121] employed the thiol from MPTS to covalently attach 5'-disulfide-modified oligonucleotides to microscope slides through a thiol/disulfide exchange reaction as can be seen in Figure 4-3.

Figure 4-3. Covalent attachment of oligonucleotides to MPTS-modified glass slides.

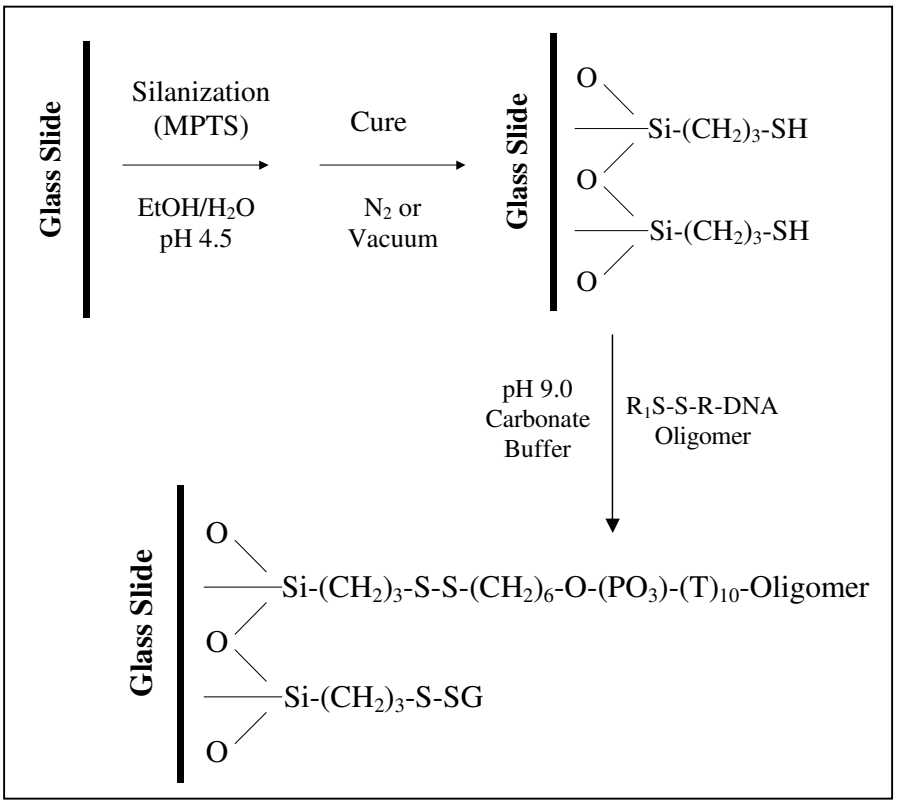

In the current study, this same technique was employed, as mentioned, to modify the surface of microscope slides with MPTS. However, it was imperative for our purposes to modify only one surface of the slide. By simply modifying one surface, the slide could mimic the inside surface of a neuronal cell wall where TH would normally be attached in vivo. Prior to silanization of the microscope slides, one surface was covered,

as well as the edges, with duct tape. We then proceeded with the silanization scheme described above, removing the tape before curing the slides in the vacuum oven.

After silanization, the functionalities of MPTS and oxidized L-glutathione (GSSG) were used to covalently attach an L-glutathione moiety to the microscope slides. Figure 4-4 illustrates the disulfide bond of oxidized L-glutathione necessary for the thiol/disulfide exchange reaction.

Figure 4-4. Oxidized L-glutathione (GSSG).

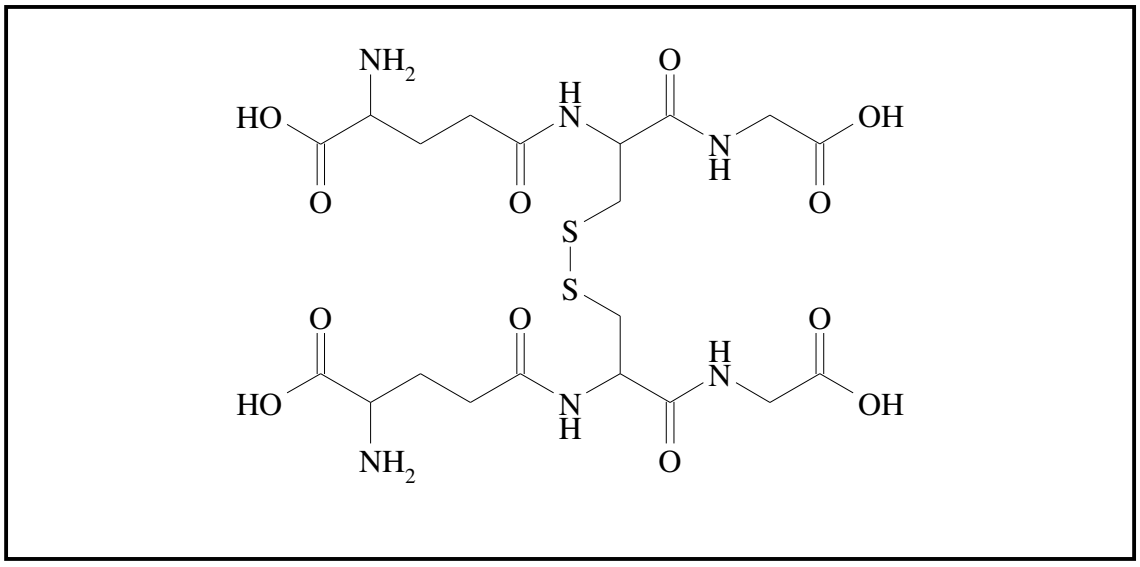

Figure 4-5 illustrates the covalent attachment of L-glutathione to the MPTS-modified microscope slides.

Figure 4-5. Covalent attachment of L-glutathione to MPTS-modified glass slides.

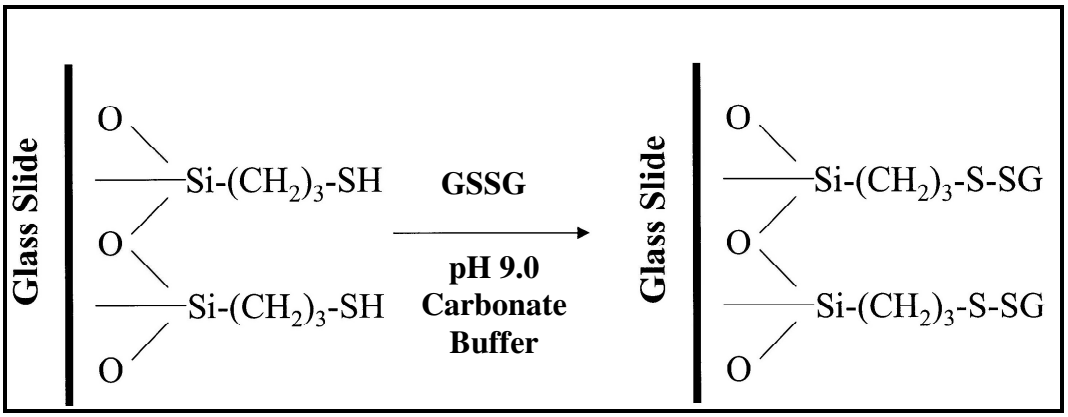

This L-glutathione-modified microscope slide could hopefully then be used in precisely the same manner as L-glutathione-agarose. By incubating the lysate solution from the expression of TH-GST with the L-glutathione-modified slides, the enzyme would attach to the slides and could subsequently be purified through rinsing with an appropriate buffer. Figure 4-6 illustrates the proposed bonding of TH-GST to L-glutathione-modified slides.

Figure 4-6. TH-GST association to L-glutathione-modified slides.

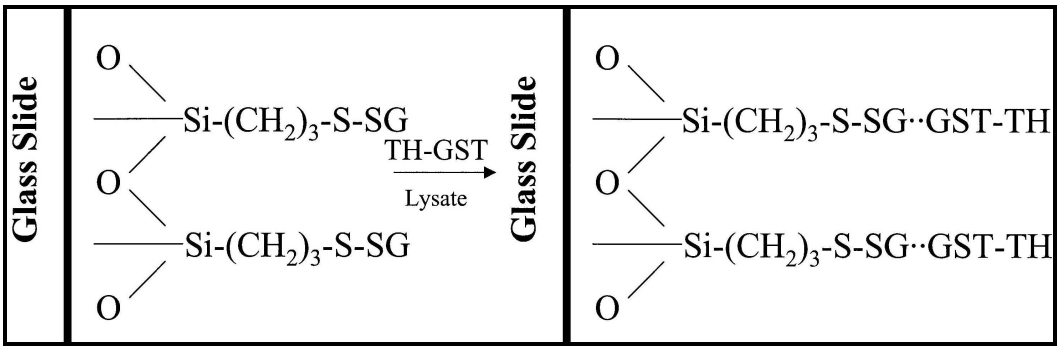

Microscope slides modified by treatment with GSSG were then analyzed for TH activity using the previously described procedure used for the modified agarose beads, as discussed in Chapter 3. Briefly, to attach and purify TH-GST, the whole cell lysate was incubated with the slides at 4°C for 30 minutes while rocking at 20 cycles per minute on a Rocker II Model 260350 platform rocker (Boekel Scientific, Feasterville, PA). The lysate was then removed by washing with Tris buffer. The slides were used immediately for determining the activity of TH-GST through incubation with the appropriate TH assay components in an incubation chamber at 37°C. The results were quantified using the LCEC procedure outlined in Chapter 3.

III. Experimental Design and Methods

A. Chemicals and Solutions

1. Chemicals

Double deionized water (ddH_2O) was used to prepare all aqueous solutions. A wall-mounted Milli-Q® Ultrapure Water System (Millipore® Corporation, El Paso, TX) was used to create the ddH_2O from water previously subjected to reverse osmosis (RO).

All of the chemicals used for preparation of the glass slides and attachment of the fusion protein to the glass slides are listed in Table 4-1 along with their purity and the company from which they were purchased. All of the chemicals used for expression and purification of TH-GST and TH activity assays are listed in Chapter 3, Section III-A.

All solutions were freshly prepared on the day of use unless otherwise noted.

Table 4-1. Chemicals used for the modification of glass slides.

Chemical	Purity/ Grade	Company	Location
Acetic acid, glacial	ACS plus	Fisher	Fair Lawn, PA
Ammonium hydroxide	ACS	Fisher	Fair Lawn, PA
Ethanol	95%	Aaper Alcohol	Shelbyville, KY
Ethanol, anhydrous	200 Proof	Aaper Alcohol	Shelbyville, KY
L-Glutathione, oxidized	>99%	Sigma	St. Louis, MO
Hydrochloric acid	GR	EMScience	Gibbstown, NJ
3-Mercaptopropyltrimethoxysilane (MPTS)		Gelest Inc.	Morrisville, PA
Sodium bicarbonate	ACS cert.	Fisher	Fair Lawn, PA
Sodium chloride	Analytical	Mallinckrodt	Paris, KY
Sodium hydroxide	Analytical	Mallinckrodt	Paris, KY
Tris-(hydroxymethyl)aminomethane free base (Tris)	Molecular Biology Grade	Sigma	St Louis, MO
Tween 20		Sigma	St. Louis, MO

2. 16.0 mM Acetic Acid in 95% Ethanol

This 16.0 mM acetic acid solution was made by adding 942 μL of glacial acetic acid to 1.00 L 95% ethanol with thorough mixing. The measured pH was 4.50. This

solution, prepared on the day of use, was bubbled with argon for 20 minutes before use to remove free oxygen..

3. 1% (v/v) 3-Mercaptopropyltrimethoxysilane (MPTS), 16.0 mM Acetic Acid in 95% Ethanol

To 693 mL of argon-bubbled 16.0 mM acetic acid in ethanol was added 7.00 mL MPTS and mixed well. This solution was stirred for 5 minutes prior to use to allow for hydrolysis and silanol formation. This solution was used immediately after preparation.

4. 500 mM Sodium Bicarbonate Buffer pH 9.00 with 25 μM Oxidized L-Glutathione

A 500 mM $NaHCO_3$ buffer was prepared by adding 23.1 g $NaHCO_3$ to 550 mL of ddH_2O with thorough mixing. A concentrated solution of sodium hydroxide was used to adjust the pH to 9.00 using a Orion Model SA720 pH meter with an Orion PerpHecT 9206BN electrode (Orion Research, Inc., Beverly, MA).. The solution was cooled to 4°C and bubbled with argon for 20 minutes prior to the addition of 8.42 mg oxidized L-glutathione (GSSG) with thorough mixing. This solution was used immediately after preparation.

5. 10.0 mM Tris Buffer pH 7.50 with 150 mM Sodium Chloride and 0.050% (v/v) Tween 20

Tris buffer (10.0 mM) was prepared by adding 0.303 g Tris and 2.19 g NaCl to 250 mL ddH_2O. Concentrated HCl was used to adjust the pH to 7.50. Finally, 1.25 mL of 10% Tween 20 was added. This rinse solution was stored at 4°C overnight before use.

B. Microscope Slide Preparation

1. Microscope Slide Scoring Device

Before the mictroscope slides were used for enzyme immobilization, they were cut to an appropriate size by careful scoring and breaking. The assay test tubes in which TH activity was assessed were 12x75 mm while the original microscope slides were 25x75 mm. Polypropylene caps that extended into the test tubes would be used to seal each tube and hold the slides in the proper orientation during the experiment. But, due to the size of the assay tubes, it was necessary to initially cut each slide to a size of 10x65 mm.

In a collaboration with Plastic Design Inc. (Plastic Design Inc., Sapulpa, OK), a microscope cutting guide was created to ensure that all slides were cut uniformly. The slide cutting guide was made from an aluminum plate with a 2x25x75 mm slot cut into one edge. To this was affixed a strip of aluminum near the inner edge of the 2x25x75 mm slot to be used as the glass scoring guide. The guide was designed and made to be used with a Designer II glass cutter (Wale Apparatus Co., Hellertown, PA).

2. Microscope Slide Scoring and Cutting

The microscope slides were inserted into the slot, underneath the glass scoring guide. Each original 25x75 mm slide could theoretically produce two 10x65 mm slides. Using a Designer II glass cutter (Wale Apparatus Co., Hellertown, PA) with the scoring apparatus, we were able to score the slide, remove it, rotate it 180°, slide it back into the guide and score it a second time. This allowed for the routine production of two

10x75 mm slides with minimal waste. One end of each 10x75 mm slide was then placed in the cutting guide pointing toward the middle of the device and scored to create the proper length of uniform 10x65 mm slides. The uniformity of these slides was a key factor in the success of this work.

3. Microscope Slide Cleaning and Hydroxyl Group Activation

The newly cut microscope slides were cleaned and surface hydroxyl groups were activated by soaking in 100 mL Nalgene® (Thermo Fisher Scientific, Rochester, NY) beakers filled with 25% (v/v) NH_4OH for 12 hours. The slides were then rinsed with running ddH2O for 10 minutes.

4. Silanization Barrier

It was necessary to silanize one side of each slide while simultaneously preventing silanization of the other side and the four edges. To accomplish this, the rinsed slides were blotted dry with Kimwipes® (Kimberly-Clark, Roswell, GA) and Duck brand duct tape (Henkel Consumer Adhesives, Inc., Avon, OH) was used to adhere to one side of the slide and the four edges, leaving only one side exposed. The slides were then cleaned again using the procedure in step 3, above.

5. Silanization Procedure

The cleaned and rinsed slides were rinsed with anhydrous ethanol and blotted with KimWipes® to remove any trace of water from the surface. The water-free slides were placed in 100 mL Nalgene® beakers taking care to not allow any overlap. The

slides were covered with freshly prepared 1% (v/v) MPTS solution and allowed to incubate at room temperature for 30 minutes. Following the 30 minute incubation, any excess MPTS was removed from the slides by briefly rinsing with a 16 mM acetic acid solution.

The adhesive tape was removed from each slide. The slides were then transferred to 100 mL Pyrex® beakers (Fisher Scientific Co., Pittsburgh, PA). Ten slides were added to each beaker taking care to not overlap the faces of the microscope slides: for mechanical support in the following step, the slides were arranged in a criss-crossed manner. The beakers containg the slides were placed in a Napco Model 5831 vacuum oven (Napco Scientific Co., Tualatin, OR) set to a temperature of 150°C and a vacuum pressure of 80 kPa. After 2 hours, the oven was turned off, and the slides were allowed to cool under vacuum for an additional 2 hours.

6. Glutathione Attachment and Modified Slide Storage

a. Glutathione Attachment

Oxidized L-glutathione solution kept at a temperature of 4°C was added to the 100 mL Pyrex® beakers containing the silanized microscope slides. The beakers were immediately covered and sealed with parafilm and placed on a Rocker II Model 260350 platform rocker (Boekel Scientific, Feasterville, PA) in a 4°C cold room for 8-12 hrs overnight. The rocker was set to mix the slides at a rate of 20 cycles/minute.

b. Rinse Slides

The oxidized L-glutathione solution was removed, and the slides were rinsed three times with the pH 7.50 10 mM Tris rinse solution that also contained NaCl and Tween 20.

c. Storage

L-Glutathione-modified microscope slides were stored in a dessicator at 4°C until used in an experiment. The shelf life of slides stored in this manner was shown to be at least one month, but most were normally consumed within 3 weeks.

C. TH-GST Purification

TH-GST was expressed and stored precisely as described in Chapter 3 for L-glutathione-agarose purification. The expressed enzyme was stored within the whole, induced E. coli cells at -80°C until needed for an experiment. Due to the nature of TH-GST, once the purification process had begun, it was carried out through use in the activity experiment without any storage steps.

1. Cell Lysis by Sonication

a. Preparation of Induced BL21 E. coli

The stored pellet was thawed on ice, typically requiring 10 minutes, transferred to 1.5 mL Flex-Tubes® (Eppendorf®, Brinkmann Instruments, Inc., Westbury, NY), and

spun at 8,000 x g in an Eppendorf® MiniSpin Microcentrifuge (Eppendorf®, Brinkmann Instruments, Inc., Westbury, NY) for 10 minutes. Following centrifugation, the supernatant was discarded. The pellet was then resuspended in 1.2 mL of the same sonication buffer. A mechanical pipet was used to aid in the resuspension process.

b. Sonication

Immediately prior to sonication, 10 µL of a 50 mM PMSF stock solution was added to the tube which was suspended in an ice water bath. A Misonix Inc. Ultrasonic Processor XL (Farmingdale, NY) was used at a setting of 3.5 for 15 seconds with a 45 second interval before the subsequent sonication step. This cycle was repeated three additional times for a total sonication time of 60 seconds. An additional 10 µL of a 50 mM PMSF stock solution was added post-sonication.

2. Purification

a. Pelletization of Membrane Debris

Post-sonication, the Flex-Tube® was spun at 10,000 x g in an Eppendorf® MiniSpin Microcentrifuge (Eppendorf®, Brinkmann Instruments, Inc., Westbury, NY) for 30 minutes at 4°C.

b. TH-GST Attachment to L-Glutathione-Modified Microscope Slides

Ten L-glutathione-modified microscope slides were each placed into separate 15 mL Fisherbrand disposable, screw cap centrifuge tubes (Fisher Scientific, Waltham,

MA). Five mL of 0.050 M Tris buffer, pH 7.40 was added to each tube. The supernatant solution from the preceding pelletization step, containing the expressed TH-GST fusion protein, was divided equally [ca. 120 μL each] among the slides. The capped tubes were placed on a Rocker II Model 260350 platform rocker (Boekel Scientific, Feasterville, PA) set at 20 cycles/min and incubated at 4°C for 30 minutes.

c. Excess TH-GST Supernatant Removal

Following incubation, the slides were each rinsed with 3.00 mL 0.050 M Tris buffer (pH 7.40), followed each time by decanting, three times to remove excess TH-GST supernatant.

d. Preparation of TH-GST Microscope Slides for Assay Standards and Blanks

Two of the purified TH-GST modified slides were placed in a boiling water bath for 30 minutes prior to use in an experiment. These slides were used for the standard and blank.

e. Preparation of a Representative Batch of Slides for SDS-PAGE Analysis

The expression and purification of TH-GST with the glutathione-modified slides was monitored at pertinent stages using SDS-PAGE. The SDS-PAGE monitoring procedure was identical to that previously described in Chapter 3, Section III-E for monitoring the expression and glutathione-agarose purification of TH-GST.

D. TH-GST Activity Assay

Each activity experiment included a minimum of six test tubes: two controls (standard and blank) and four activity samples. The details of the experiments are similar to those discussed in Chap 3, Section III. F. The logistics of the experiments using modified glass microscope slides are illustrated in Figure 4-7. The differences between use of modified agarose and modified microscope slides are discussed below.

Figure 4-7. TH activity experiment logistics.

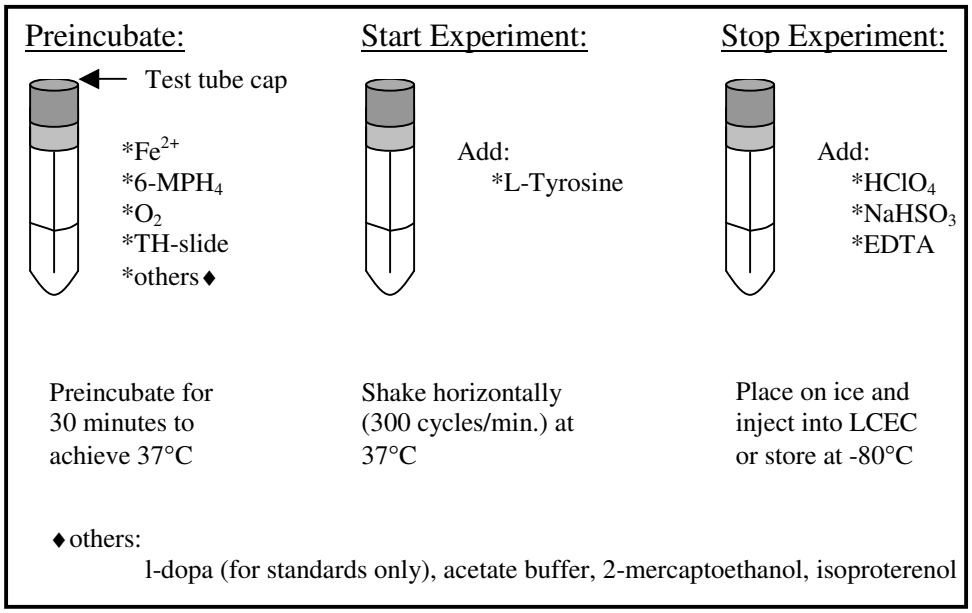

1. Preincubation of Assay Components

Prior to an assay for TH activity, it was necessary to equilibrate all the components necessary for the hydroxylation of L-tyrosine to L-dopa to achieve the

optimum reaction temperature of 37°C. This process was described in Chap 3, Section III. F. 1. Now, however, since TH-GST was bound to microscope slides rather than agarose beads, the volume of water added to each activity test tube was increased by 100 μL.

2. Preincubation of TH-GST Modified Microscope Slides

It was also necessary to equilibrate the TH-GST modified slides prior to placement in the TH activity test tubes. A 400 mL Pyrex® beaker was filled with 350 mL of a 0.050 M Tris buffer (pH 7.40) solution to which a magnetic stir bar and a Scienceware® round rack (Fisher Scientific, Fairlawn, PA) was added to support the microscope slides while allowing space for the magnetic stir bar. This microscope incubation apparatus was incubated in a Sherer Controlled Environment Chamber Model CEL 37-14 (Sherer-Gillett Co., Marshall, MI) to achieve 37°C. All ten microscope slides were placed on the rack in the beaker. The temperature of the solution was measured every 30 seconds using a Fluke 50 Series II Thermometer with an immersion temperature probe (Fluke Corporation, Everett, WA).

3. Assay for TH Activity

Once the assay solution and TH-GST modified microscope slides had achieved an equilibrated temperature of 37°C, the slides were carefully blotted dry with Kimwipes® (Kimberly-Clark, Roswell, GA) and placed in each of the activity test tubes. L-Tyrosine was added to begin the activity assay.

IV. Results and Discussion

A. Results

The expression and purification of TH-GST when L-glutathione-modified slides were used was monitored using SDS-PAGE. This process verified that we did express TH-GST and that the enzyme was bound to the microscope slides. In addition, TH-GST is readily purified and remains functional as later shown by the retention of its enzyme activity observed following the modified microscope slide purification process.

Prior to an assay of the TH immobilized on the slides for activity, a study was performed to determine the amount of preincubation time required for the microscope slides to attain the 37°C necessary for subsequent placement in the reaction test tubes. The procedure was discussed in Section III. D. 2., above. As Figure 4-8 illustrates, the buffer solution, which was initially at 37°C dropped to 26°C after the addition of the cold slides. It took 30 minutes for the solution and the slides to once again reach 37°C. Thus, a 30 min preincubation was subsequently used for all assays employing microscope slides.

Figure 4-8. Preincubation of microscope slides.

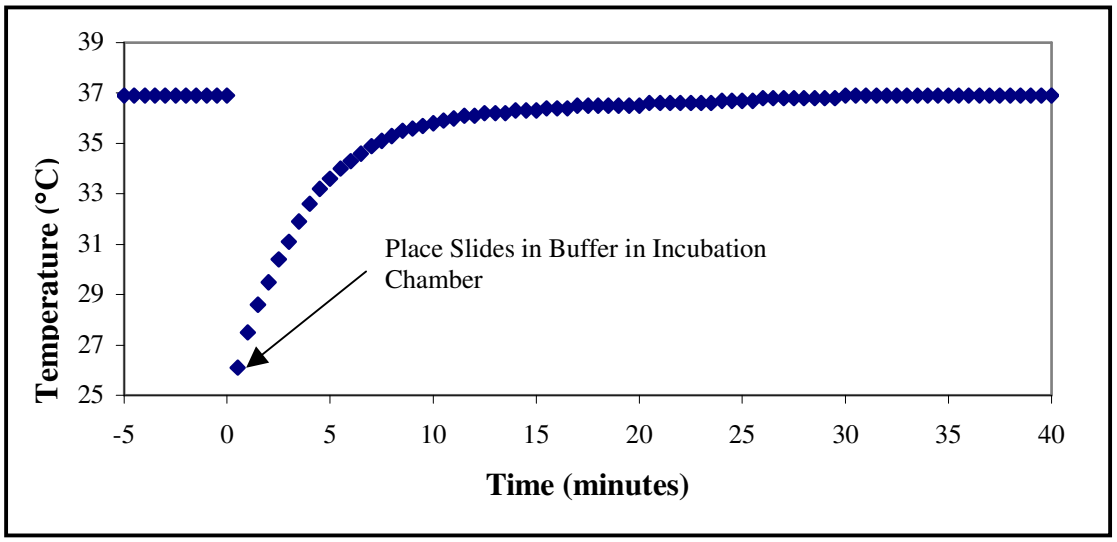

Once the expression of TH-GST was confirmed through SDS-PAGE, and the preincubation time was determined, an assay for activity was performed. The procedure developed for determining TH activity with agarose bead-attached TH-GST was used except the beads were replaced with slide-attached TH-GST.

As can be seen in Table 4-5, the TH-GST was successfully attached to the L-glutathione-modified slides, and the enzyme was shown to retain its activity. The data presented in the table represents four different assays repeated using the same batch of enzyme and the same batch of newly silanized L-glutathione-modified slides. The slides were initially used on the day of glutathione modification (Day 0) and the remainder of the slides were stored in a dessicator at 4°C until used subsequently for purification and activity assays of TH. Day 1 slides were stored for 24 hours, while Day 7 and Day 30 slides were stored for 7 and 30 days, respectively, before use.

Table 4-2. TH-GST activity on L-glutathione-modified slides and slide stability.

Days of Storage	TH Activity*
0	1165 ± 32
1	1152 ± 38
7	1157 ± 24
30	1172 ± 36

* TH activity presented as ng L-dopa/test tube (mean ± s.d.; n=4)

Following analysis of the above data, it was obvious that active TH-GST was successfully attached to L-glutathione-modified slides and that storage of the newly silanized L-glutathione-modified slides for up to a month resulted in no significant deterioration of slides, $F(3,12) = 0.286$, $p = 0.05$.

V. Conclusions

The use of the thiol/disulfide exchange reactions to attach substrates to silane-modified solid surfaces is a well-established technique which has many applications including covalent chromatography, DNA microarrays and protein microarrays.[122-124] However, no mention of this technique could be found in the literature for use in immobilization of the TH-GST protein and subsequent utilization of the associated TH activity. We employed this immobilization technique to covalently attach a L-glutathione

moiety to the surface of microscope slides to mimic L-glutathione-agarose, which is more commonly used to purify GST and GST-fusion proteins.

In order to confirm that TH-GST was attached to the modified microscope slides, we demonstrated that the protein cleaved from the surface of the slides was identical to that of the originally purified protein by gel electrophoresis. Then, to demonstrate that the attached protein maintained its fundamental TH activity, we successfully obtained activity using the previously employed TH activity assay procedure.

Storage conditions for the silanized L-glutathione-modified glass microscope slides were examined, and it was notably shown that storage of these slides for up to one month resulted in no significant deterioration in functionality.

Tyrosine Hydroxylase Activity in the Presence of a Strong Electric Field

Chapter 5

I. Introduction

Tyrosine hydroxylase exists in both cytosolic and membrane-bound within a typical neuron, where the latter is associated with the neuronal cell membrane.[50] The membrane-bound form of TH is exposed to strong electric fields by virtue of its proximity to both the transmembrane potential and the surface potential. Detailed information concerning the structure of cell membranes, the associated electric fields, and the relationship of TH to the neuronal membrane can be found in Chapter 1, Sections IV and V.

We hypothesized that the activity of the membrane-bound form of tyrosine hydroxylase would be affected by the presence of such strong electric fields and that these fields, thus, might be able to act as a short-term regulation mechanism. We have designed and performed novel experiments specifically to test this hypothesis.

We initially established a successful method for expressing active TH as a fusion protein with GST (Chap 2) and a unique and previously unreported technique that

resulted in enzymatically active TH-GST bound to a microscope slide, mimicking the membrane-bound form of TH (Chaps 3 and 4). We then focused our attention on measuring the activity of the bound TH in a strong electric field having a directionally controlled orientation.

II. The Electric Field Exposure Apparatus

A. Introduction/Design

The proper design and construction of a novel device for the purpose of exposing TH to large electric fields was essential for his work. Not only did the apparatus need to expose TH to an electric field, but it also had to provide a mechanism for TH to access the necessary cofactors and substrates in an appropriate aqueous mixture for the conversion of L-tyrosine to L-dopa. Since we had previously performed all of these experiments using test tubes containing the microscope-bound TH and its cofactors/substrates, the electric field apparatus was designed and built to house these same test tubes. Figure 5-1 illustrates the electric field apparatus designed by our lab.

Figure 5-1. Electric field apparatus (top view).

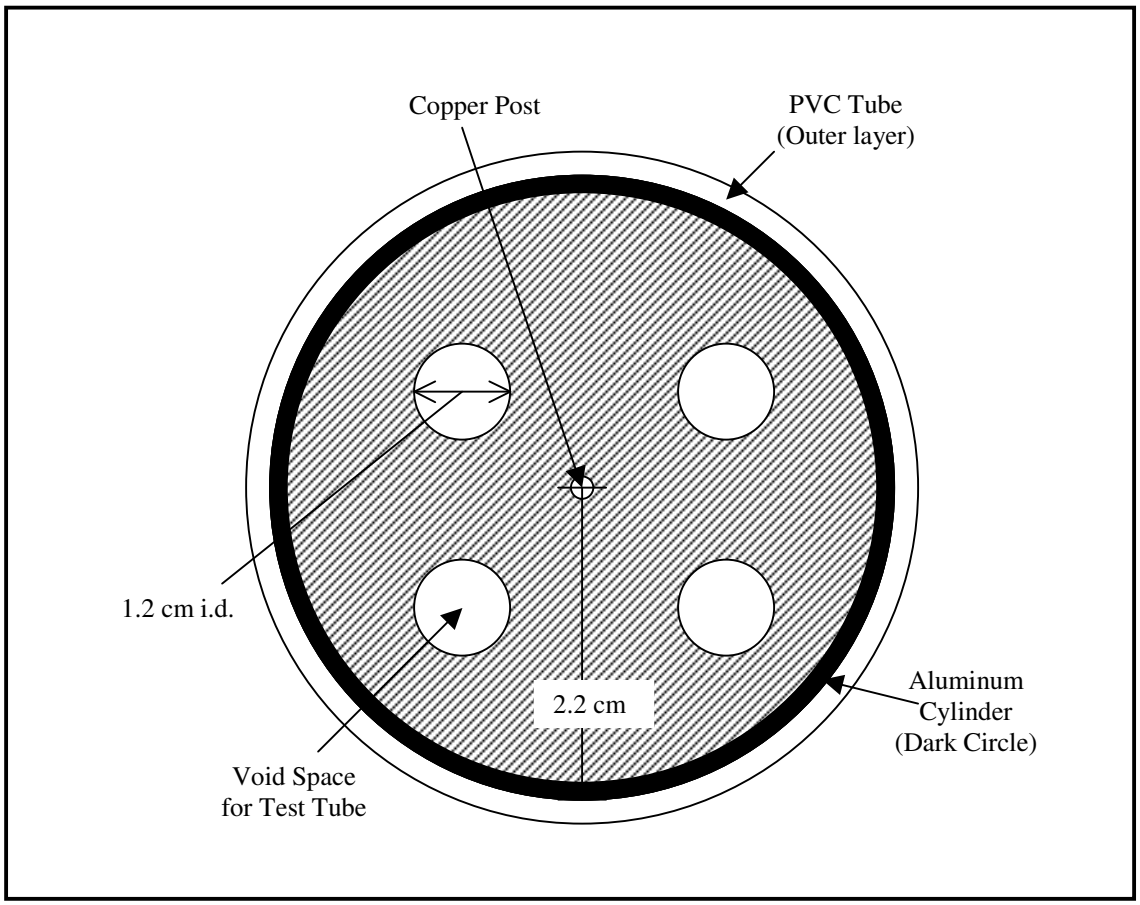

As can be seen in Figure 5-1, the apparatus was constructed within a PVC tube. An aluminum cylinder with an inner radius, b, of 2.2 cm was placed inside the PVC housing and the entire inner void was filled with epoxy. Before the epoxy hardened, a copper post with a radius, a, of 0.25 cm was positioned in the center of the apparatus. Four holes, void spaces for the test tubes, with individual diameters, d, of 1.2 cm were drilled equidistant around the center of the apparatus, with the center of each hole being placed 1.25 cm from the center of the apparatus.

Figure 5-2 shows a side view of the apparatus. For clarity, the solid aluminum tube is shown as a coil in this figure, allowing the internal copper post and test tube holes to be seen. The apparatus was constructed with a square epoxy base having imbedded threaded posts and a corresponding epoxy lid. The lid was secured with wing nuts attached to the threaded posts. A section of the aluminum cylinder material was used to provide an electrical contact to the external power supply at Input 1. This connector from the outer cylinder to Input 1 was constructed to be inside the epoxy base. The copper post was separately attached through the base to the external power supply at Input 2.

Figure 5-2. Electric field apparatus (side view).

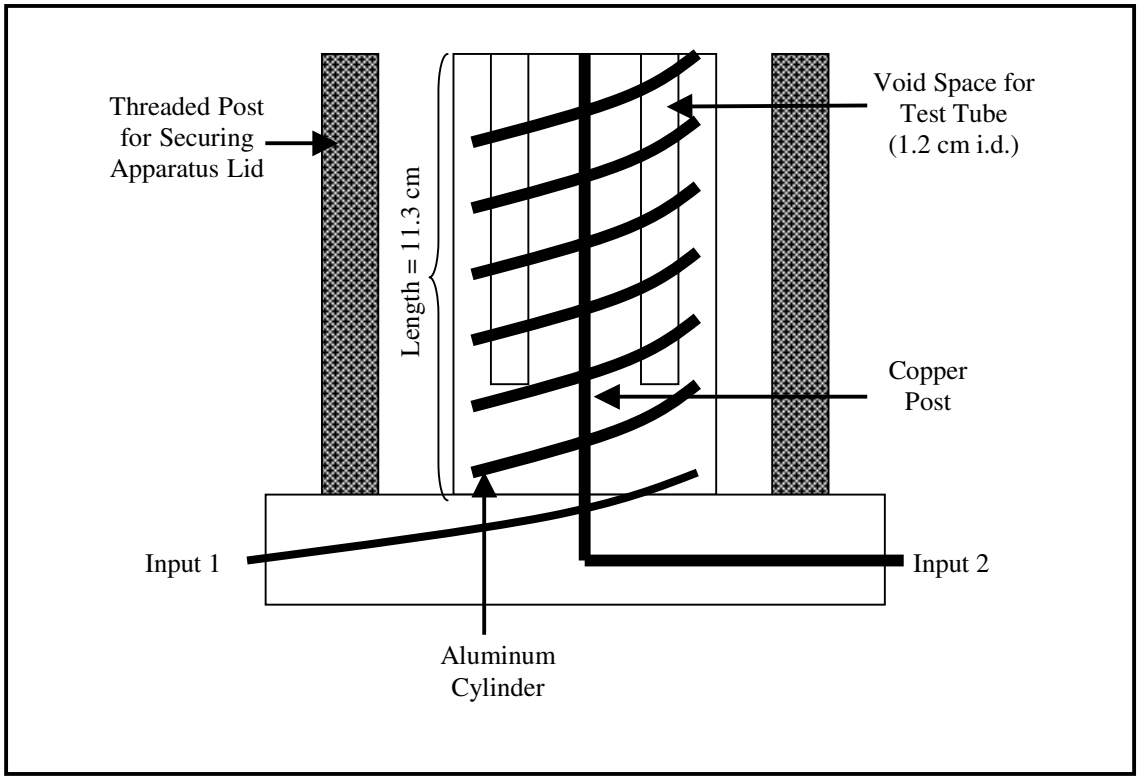

B. Electric Field Generation

Following construction of the electric field exposure apparatus, it was necessary to secure an instrument to reliably generate and maintain the necessary electric field(s). Since the membrane-bound enzyme could feasibly be exposed to fields as high as 100,000 V/cm, it was imperative that this power supply provide a relatively large electric field.

We employed a Yui Da high voltage power supply (Yui Da Electrics Co, Ltd., Jhongli City, Taiwan) that was specified to be capable of generating electric potentials up to 20,000 V. Figure 5-3 shows some of the related and basic components of this high voltage power supply.

Figure 5-3. High voltage power supply.

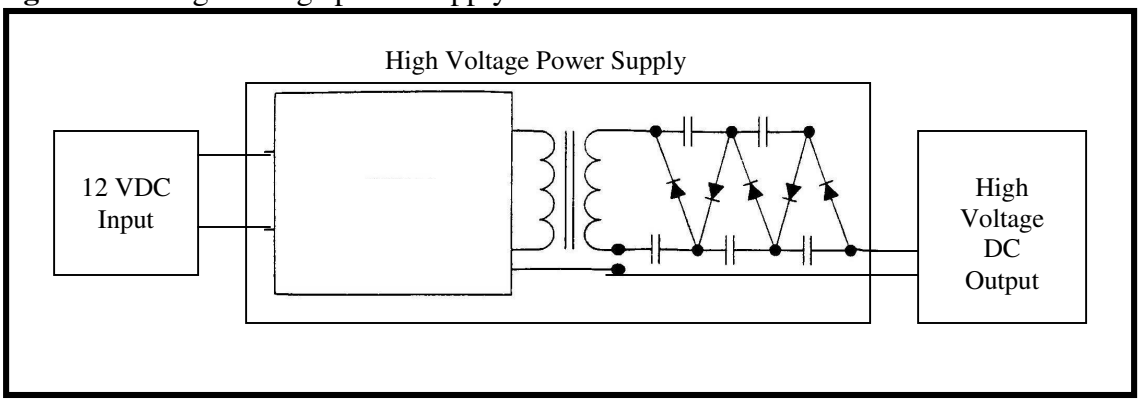

The specifications provided with the high voltage power supply stated that a 12 VDC input would produce a 20,000 VDC output. However, it was discovered that an 18 VDC input was actually necessary to produce the desired 20,000 VDC output. An

HP 6237B variable power supply (Hewlett Packard, Palo Alto, CA) capable of providing 0 - 24 VDC was subsequently used as the input to the high voltage power supply unit.

Precise measurement and monitoring of the generated electric field was necessary for our experiments. However, there were no readily available digital multimeters that contained sufficient internal resistance to monitor 20,000 VDC. Therefore, a voltage divider connected to a Fluke 8050A digital multimeter (Fluke, Everett, WA) was constructed for this purpose. This device proved capable of routinely monitoring the output of the high voltage power supply with a high degree of accuracy. The Yui-Da high voltage power supply and the associated measurement voltage divider were housed in a nonconductive container to minimize the opportunity for arcing. Figure 5-4 illustrates the relationship between the electric field generator, the voltage monitor, and the high voltage electric field sample exposure apparatus.

Figure 5-4. Electric field system.

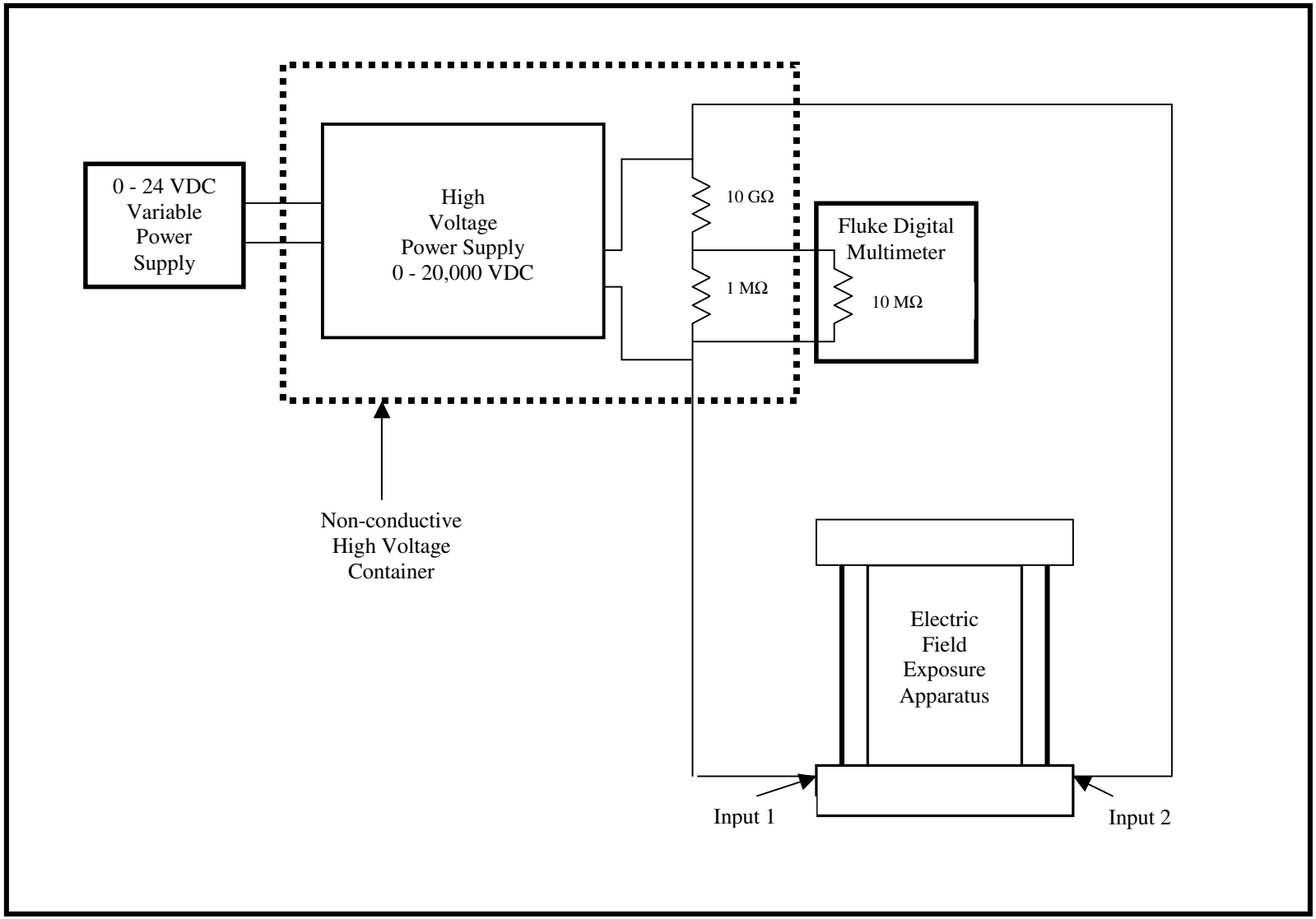

Only a small portion of the actual generated high voltage was detected by the digital multimeter due to the resistance shunt supplied by the voltage divider. The relationship between the digital multimeter reading and the actual voltage from the high voltage power supply, was calculated by

$$V_{meter} = \frac{R_2}{R_1 + R_2} V_{actual} \qquad \textbf{Equation 5-1}$$

where, as shown in Figure 5-4, R_1 = 10.00 GΩ and R_2 was the parallel combination of the shown 1.000 MΩ resistor and the stated meter resistance of 10.00 MΩ. In this case, V_{meter} is the voltage reading of the digital multimeter and V_{actual} is the output from the high voltage power supply. The calculated value of R_2 is given as

$$R_2 = \frac{10.00(1.000)}{10.00 + 1.000} M\Omega = 0.909 M\Omega \qquad \textbf{Equation 5-2}$$

Considering the 10.00 GΩ resistor, R_1, the voltage displayed on the digital multimeter when 20,000 V is generated from the high voltage power supply is calculated to be

$$V_{meter} = \frac{0.909 M\Omega}{10.00 x 10^3 M\Omega + 0.909 M\Omega}(20{,}000V) = 1.818V \qquad \textbf{Equation 5-3}$$

Conversely, to monitor the output from the high voltage power supply (V_{actual}), we can rearrange equation 5-1 to solve for V_{actual}.

$$V_{actual} = \left(\frac{10.00x10^3 + 0.909}{0.909} \right) (V_{meter}) = 11{,}001(V_{meter}) \qquad \textbf{Equation 5-4}$$

C. Electric Field Calculations

Gauss' Law was used to derive the electric displacement and the electric field produced at various locations within the electric field apparatus. The electric field apparatus was viewed to be a coaxial capacitor consisting of two conductors (an inner copper post and an outer aluminum cylinder) separated by an insulator, which is primarily epoxy resin in our case. Once attached to a power source, the two conductors are presumed to have equal but opposite charges. Since the constructed electric field apparatus acts as a coaxial capacitor filled with a dielectric material (epoxy resin), the gaussian surface at any given radius from the center through which the electric field penetrates is also a cylinder.

Electric displacement describes the displacement of charge at various points within the dielectric of the capacitor and primarily depends only on the free charge on the capacitor, not the bound charge within the dielectric.[127]

The total free charge on the capacitor plates, Q_f, within the apparatus can be calculated by

$$Q_f = D\int_0^{SA_{cyl}} dA = 2\pi rLD \qquad \textbf{Equation 5-5}$$

where D is the electric displacement, SA_{cyl} is the surface area of the cylinder, r is the radius measured from the center of the cylindrical capacitor, and L is the length (or height) of the cylindrical capacitor. Therefore, the electric displacement, D, experienced by our immobilized enzyme can be calculated for our coaxial capacitor[128] at a radius of r = 1.25 cm (the location of the glass-immobilized enzyme) within the electric field apparatus by substituting the surface area for our gaussian surface (cylinder) into the equation at that radius and rearranging to solve for D

$$D = \frac{Q_f}{2\pi rL} = \frac{Q_f}{2\pi(1.25)L} \qquad \textbf{Equation 5-6}$$

The electric field at radius r from the center of the capacitor is related to the electric displacement by

$$E_r = \frac{D}{\varepsilon_{er}} = \frac{Q_f}{2\pi rL\varepsilon_{er}} \qquad \textbf{Equation 5-7}$$

where ε_{er} is permittivity of the epoxy resin.

Referring back to Figures 5-1 and 5-2, the potential difference, V_{app}, between the two cylinders at a radius r from the center of the apparatus we used, in the region between

the outside edge of the central copper post (a) and the inside edge of the concentric aluminum cylinder (b), or in the region of a < r < b, is given as

$$V_b - V_a = -V_{app} = -\int_{r=a}^{r=b} E_r dr \qquad \textbf{Equation 5-8}$$

where E_r is the electric field along any cylindrical surface located at radius r. The negative sign in this equation arises from the fact that we usually connected the positive electrical lead to the copper post (+Q at r = a) and the negative electrical lead to the aluminum cylinder (-Q at r = b). We ignore the sign below in the derivation and focus only on the magnitude of the related voltage. Substituting Equation 5-7 into Equation 5-8 yields

$$V_{app} = \frac{Q_f}{2\pi L \varepsilon_{er}} \int_a^b \frac{dr}{r} = \frac{Q_f}{2\pi L \varepsilon_{er}} \ln\left(\frac{b}{a}\right) \qquad \textbf{Equation 5-9}$$

Solving for Q_f,

$$Q_f = \frac{V_{app} 2\pi L \varepsilon_{er}}{\ln\left(\frac{b}{a}\right)} \qquad \textbf{Equation 5-10}$$

The capacitance, C, for a given capacitor is a constant and is defined as the ratio of the magnitude of charge on one "plate" of a given capacitor to the potential difference across

the capacitor:

$$C = \frac{Q}{V_o} \qquad \textbf{Equation 5-11}$$

Thus, as the charge increases, the potential difference between the plates of a given capacitor must also correspondingly increase. V_o in equation 511 corresponds to V_{app} in our apparatus. Using this and substituting equation 5-10 into equation 5-11, we obtain

$$C = \frac{2\pi L \varepsilon_{er}}{\ln\left(\frac{b}{a}\right)} \qquad \textbf{Equation 5-12}$$

The permittivity of the epoxy resin dielectric ε_{er} is related to ε_o, the permittivity of free space (8.8542×10^{-12} C^2/Nm^2), through the dielectric constant κ_{er} for the epoxy resin as

$$\varepsilon_{er} = \kappa_{er} \varepsilon_o \qquad \textbf{Equation 5-13}$$

where κ_{er}=3.6.[129] For our electric field apparatus where the inside radius of the aluminum cylinder (b) is at a radius of 2.2 cm and the outside radius of the copper post (a) is 0.25 cm , the capacitance per unit length, can be approximated to be

$$\frac{C}{L} = \frac{2\pi\kappa_{er}\varepsilon_o}{\ln\left(\frac{b}{a}\right)} = \frac{2\pi(3.6)\left(8.8\frac{pF}{m}\right)}{\ln\frac{2.2cm}{0.25cm}} = 92\frac{pF}{m} \qquad \textbf{Equation 5-14}$$

Given that the cylindrical capacitor had a measured length, L, of 0.113 meters, we can use equation 5-14 to predict an approximate capacitance of 10.1 pF. Actual measurements of the capacitance of our device showed a capacitance of 4.4 pF with nothing placed in the four test tube holder holders. When test tubes filled with distilled water were employed in the unit, the measured capacitance was 4.5 pF. This outcome was gratifying in that the theoretically calculated and actual observed values were equal within, roughly, a factor of two to three. Indeed, we were well aware that our Gaussian model of an infinitely long (i.e., no edge effects) concentric cylindrical capacitor with a homogeneous dielectric could well have provided a calculated capacitance which varied by a factor of even five or ten from the actual measured value. Thus, the agreement within a factor of 2.3 was a welcome one. Secondly, we were happy to see that inclusion of the solution-filled incubation test tubes did not substantially alter the measured capacitance of the high voltage exposure unit. The difference between 4.4 and 4.5 pF in this case was deemed relatively insignificant.

Returning to equation 5-6, we focus our attention on the electric displacement and associated electric field experienced by the immobilized enzyme, located at r = 1.25 cm from the center of the cylinder. For this situation, the displacement experienced by the

immobilized enzyme, D_{enz}, is given as

$$D_{enz} = \frac{Q_f}{2\pi rL} = \frac{CV_o}{2\pi rL} \qquad \textbf{Equation 5-15}$$

or

$$D_{enz} = \frac{C_{app}V_{ab}}{2\pi rL} \qquad \textbf{Equation 5-16}$$

where C_{app} is the measured capacitance of the exposure unit (4.5 pF), and V_{ab} is the applied high voltage. Substituting appropriate values (r = 1.25 cm, L = 0.113 m), we obtain

$$D_{enz} = \frac{(4.5pF)V_o}{2\pi(0.0125m)(0.113m)} = 5.1x10^{-10}(V_o)\frac{C}{m^2} \qquad \textbf{Equation 5-17}$$

Since the electric displacement does not depend on the dielectric constant of the immobilized enzyme, it is considered by some to provide the best representation of the "electric field" generated within our apparatus and, thus, experienced by the protein. However, we note that the electric field at the radius in the apparatus where the protein is located can also be calculated from the following relationship

$$D_{enz} = \varepsilon_{enz}E_{enz} = \kappa_{enz}\varepsilon_o E_{enz} \qquad \textbf{Equation 5-18}$$

Or, rearranged,

$$E_{enz} = \frac{D_{enz}}{\kappa_{enz}\varepsilon_o} \qquad \textbf{Equation 5-19}$$

where κ_{enz} is the dielectric constant of the enzyme. Thus, an estimation of the magnitude of the electric field can be calculated using the fact that known dielectric constants for proteins fall in the range from 1 to 15.[59,130-133] While we do not know the dielectric constant for the immobilized TH protein, we can assume this value to be $\kappa_{enz} = 4$. This assumption, given the fact that the reported values of κ for proteins fall between 1 and 15, means that our subsequent estimates of the electric field experienced by the immobilized enzyme, E_{enz}, will be expected to deviate, at most, by a factor of four from the actual value.

Table 5-1 below shows the relationship between the applied external voltage and both the electric displacement and the electrical field experienced by the immobilized protein. The applied voltages correspond to experimentally employed values.

Table 5-1. Electric displacements and electric fields experienced by the immobilized TH enzyme at various applied potentials.*

Applied Voltage (V)	Electric Displacement, D_{enz} (C/m^2)	Electric Field, E_{enz}** (V/cm)
5,000	$2.6x10^{-6}$	720
10,000	$5.1x10^{-6}$	1400
15,000	$7.7x10^{-6}$	2200
20,000	$1.0x10^{-5}$	2900

* Values of D_{enz} and E_{enz} calculated using r = 1.25 cm, L = 11.3 cm and C= 4.5 pF

** Values of E_{enz} calculated using κ_{enz}=4

III. Experimental Design and Methods

A. Chemicals and Solutions

Double deionized water (ddH_2O) was used to prepare all aqueous solutions. A wall-mounted Milli-Q® Ultrapure Water System (Millipore® Corporation, El Paso, TX) was used to create the ddH_2O from water previously subjected to reverse osmosis (RO). All of the chemicals used for preparation of the glass slides and attachment of the fusion protein to the glass slides are listed in Chap 3, Section III. A. and Chap 4, Section III. A. All solutions were made on the day of use unless otherwise noted.

B. Tyrosine Hydroxylase Activity

Expression and purification of TH-GST on glutathione-modified microscope slides was performed as discussed in Chapters 3 and 4. Figure 5-5 summarizes the procedure and various constituents involved for the blanks, standards and activity assay samples used in the determination of TH activity in each experiment.

Figure 5-5. TH activity experimental logistics.

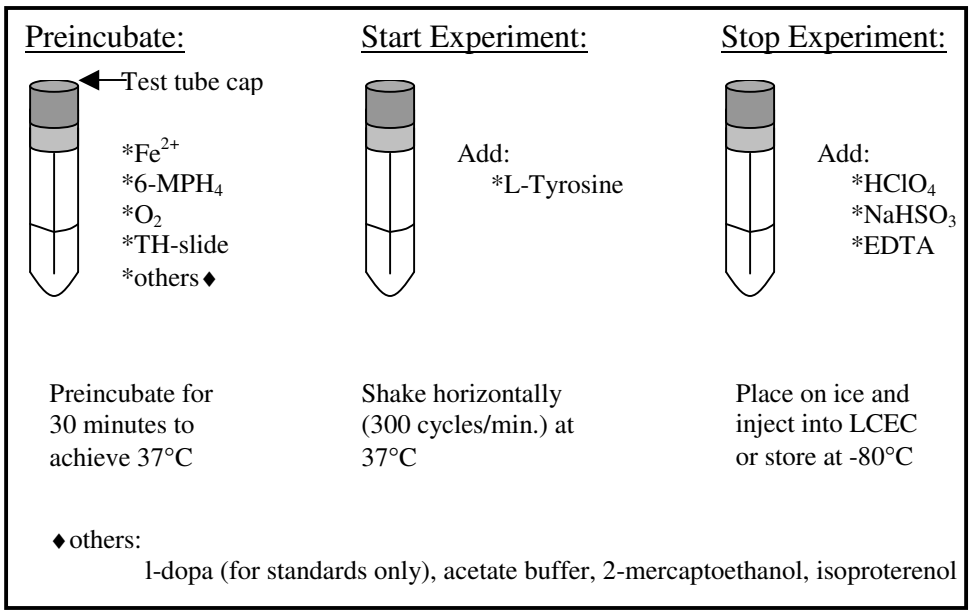

Each TH activity experiment employed ten fundamental incubation tubes: 1 standard, 1 blank, 4 TH-activity samples (no applied field) and 4 additional TH-activity samples (with applied field).

The caps used to seal the test tubes extended into the tubes and served the additional function of physically holding the microscope slides firmly in place, preventing the slides from rotating within the tubes. Once capped, the test tubes were placed in the electric field exposure apparatus so the enzyme-coated surface of the slides always faced the center copper post and were perpendicular to the externally applied electric field. For the majority of experiments reported in this dissertation, the negative lead from the high voltage power supply was connected to Input 1 (aluminum cylinder), and the positive lead was connected to Input 2 (copper post).

1. Possible Solution Heating Due to High Voltage Electric Field

Enzyme kinetics typically change significantly due to changes in temperature. Therefore, we initially determined what effect, if any, the applied electric field might have on the temperature of the solution inside the test tube. For these experiments, a test tube was prepared to contain all of the components normally employed for the investigation of TH activity: an acetate buffer of pH=6.0, ferrous sulfate, 6-MPH_4, 2-mercaptoethanol, isoproterenol, L-dopa, a TH-modified microscope slide and L-tyrosine. The test tube was placed in the Sherer Controlled Environment Chamber Model CEL 37-14 (Sherer-Gillett Co., Marshall, MI), which had been preheated to 37°C. During exposure to the large (20,000 V) electric field, the temperature of the solution was measured every 30 seconds using a Fluke 50 Series II Thermometer with an immersion temperature probe (Fluke Corporation, Everett, WA).

2. Effect of Shaker Speed on Measured Enzyme Activity

During preliminary experiments, it became apparent that shaking the high voltage exposure apparatus at a speed high enough to promote mixing could also cause the electrical leads to disconnect and/or arc resulting in a loss of the electric field. We thus decided to investigate the possibility of slowing the shaker to one half of the original speed to prevent this problem. However, it was not known whether sufficient mixing occurred at this speed.

An experiment was devised to examine possible use of a slower shaker speed. Two sets of four test tubes were exposed to 20,000 V in the electric field apparatus for the usual 20 minute experiment. Shaking was done for the two sets at 320 and 160 cycles/minute, respectively, and the results were compared.

3. Effect of the Electric Field Strength on TH Activity

A series of experiments were designed and performed to determine the TH activity when exposed to various electric field strengths.

Each experiment included ten test tubes: two controls (standard and blank), four activity samples not exposed to the electric field and four additional activity samples used within the electric field apparatus. Each experiment was performed for 20 minutes. The externally applied electric field strength for the individual experiments, in volts, were: 0, 5,000, 10,000, 15,000 and 20,000 V.

4. Effect of Incubation Time on TH Activity in an Electric Field

A series of experiments were designed and performed to investigate TH activity upon exposure to 20,000 V for various lengths of time.

Each individual experiment included ten test tubes: two controls (standard and blank), four activity samples not exposed to the electric field and four additional activity samples used within the electric field apparatus. Individual experiments were performed for a total of 10, 15, 20 and 30 minutes, respectively. The applied electric field was held constant at 20,000 V for the duration of each of these experiments.

5. Effect of Electric Field Reversal on TH Activity

Since, up to this point, the side of the glass slide containing the immobilized enzyme had been oriented in only one direction relative to the externally applied electrical field, we decided to determine whether the orientation of this enzyme attachment within the electric field might have an effect on its activity. We, thus, ran two sets of experimental samples for 15 minutes of external electric field exposure to 20,000 V. The first set was run under normal conditions. For the second set of experiments, we reversed the leads on inputs 1 and 2 of the electric field exposure apparatus, connecting the (+) lead of the high voltage source to the aluminum outer cylinder instead of the usual copper inner post and connecting the (-) lead to the copper post.

6. Effect of Intermittent Electric Field Exposure on TH Activity

We decided to investigate whether there was any apparent lag time required for conformational changes of TH associated with its "activation" and "deactivation," respectively, in being exposed to an electric field and having that electric field be turned off.

Two experiments were designed and performed for 10 and 15 minutes, respectively. A set of eight test tubes was prepared for each experiment. These test tubes consisted of a standard (test tube 1), a blank (test tube 2) and six enzyme activity test tubes (test tubes 3 through 8). The standard, blank and test tubes 3 and 4 were never exposed to the electric field. Test tubes 5 and 6 were exposed to a 20,000 V applied electric field for the entire experiment. Test tubes 7 and 8 were alternately exposed and not exposed to a 20,000 V applied electric field using 5 minute intervals starting with the electric field on in the first 5 minute interval. In both experiments, we began by incubating all test tubes for 5 minutes with tubes 5, 6, 7 and 8 being exposed to the 20,000 V externally applied electric field. After the initial 5 minute exposure, we removed tubes 7 and 8 from the applied field and continued incubation for a further 5 minutes. At the end of the second 5 minute interval, experiment 1 was completed. For experiment 2, however, we reinserted tubes 7 and 8 into the applied field and continued incubation of all tubes for a further 5 minute incubation period. At the end of the third 5 minute interval, experiment 2 was terminated. This is summarized in Table 5-2.

Table 5-2. Electric field exposure schedule.

Experiment	Total Experiment Time (min)	Electric Field Exposure for Successive Five Minute Intervals Test Tube Number 1, 2, 3, 4	5, 6	7, 8
1	10	Off/Off	On/On	On/Off
2	15	Off/Off/Off	On/On/On	On/Off/On

7. Effect of Substrate and Cofactor Concentration on TH Activity

As mentioned in Chapter 1, TH generally follows Michaelis-Menton kinetics. Since TH activity was affected by an electric field, we designed a series of kinetic experiments to further investigate exactly how the electric field altered the observed enzyme activity. We first investigated the relationship of the substrate concentration to the activity of TH with and without electric field exposure. We next investigated the enzyme activity alterations in an electric field as a function of cofactor concentration.

a. K_m and V_{max} Determinations for the L-Tyrosine Substrate

This study used ten test tubes: two controls (standard and blank), four activity samples not exposed to the electrical field, and four activity samples exposed to the 20,000 V electric field. The duration of the experiment was 15 minutes.

To evaluate the K_m and V_{max}, a series of experiments were performed varying the concentrations of L-tyrosine (0.25 mM, 0.10 mM, 0.20 mM, 0.30 mM, 0.50 mM and 0.75 mM) while maintaining the concentration of 6-MPH_4 at 2.0 mM.

b. K_m and V_{max} Determinations for the 6-MPH_4 Cofactor

This study also used ten test tubes: two controls (standard and blank), four activity samples not exposed to the external electrical field, and four activity samples exposed to 20,000 V. The duration of the experiment was 15 minutes.

To evaluate the K_m and V_{max}, a series of experiments were performed varying the concentration of 6-MPH_4 (0.50 mM, 0.75mM, 1.0 mM, 1.25 mM, 1.5 mM, 2.0 mM, 2.5 mM, 5.0 mM and 10.0mM) while maintaining the concentration of L-tyrosine at 0.50 mM.

IV. Results and Discussion

A. Results

We were initially concerned that we would have a sufficient pre-incubation time to raise the sample from room temperature to the desired incubation temperature of 37°C. Possible heating of the incubation solutions due to the electric field was also a concern. We, thus, decided to perform an experiment which would simultaneously address both of these concerns. In this investigation, we started the experiment, inserted room temperature samples, waited until the temperature of 37°C was achieved (30 minutes later), and then applied the 20,000 V external field. After application of the field, we observed the temperature for an additional 25 minutes.

As illustrated in Figure 5-6, it took approximately 30 minutes for the solution in the test tube to reach 37°C. Following application of the electric field, the temperature was recorded every 30 seconds for an additional 25 minutes. As shown in the same Figure 5-6, the solution inside the tube remained constant at 37°C for the remainder of the readings, verifying that no heating had occurred due to exposure of the sample to the 20,000 V external electrical field.

Figure 5-6. Determination of pre-incubation time and investigation of possible solution heating due to applied external electric field.

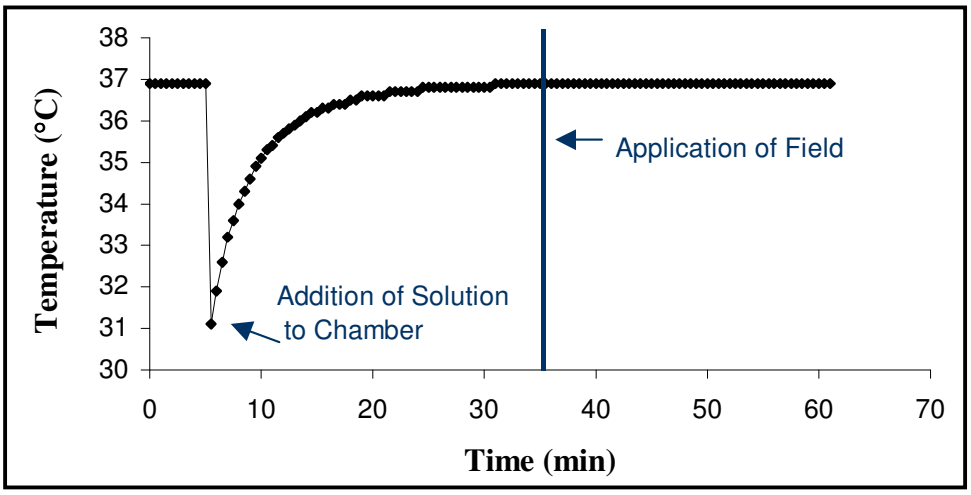

Once the functional pre-incubation time had been established and, simultaneously, it had been shown that the electric field would not lead to solution heating, we proceeded to investigate the shaker speed. During preliminary experiments, the test tubes had been vigorously shaken at a rate of 320 cycles/min to ensure a sufficient supply of oxygen for the enzymatic reaction. Due to the violence of the

320 cycles/min shaking rate, however, the leads to the electric field apparatus occasionally experienced electrical arcing and/or physical disconnection. A reduction in the shaking rate to 160 cycles/min was, thus, attempted. It was hoped that this reduced rate would prevent the previously observed undesirable physical disruption associated with the electrical leads while still maintaining saturated oxygenation of the solution. Table 5-3 contains the results of these experiments.

Table 5-3. TH activity at two different shaker speeds.

External Applied Electric Field, V	TH Activity*	
	Shaker Speed 160 cycles/min	**Shaker Speed 300 cycles/min**
0	920 ± 18	940 ± 31
20,000	1537 ± 22	1525 ± 25

* Activity presented as ng L-dopa formed during 15 min incubation period (mean ± s.d., n = 4)

As can be seen in Table 5-3, reduction of shaker speed had no significant effect on its activity. This outcome was true in both the absence ($t(6) = 1.62$, $p = 0.05$) and presence ($t(6) = 0.721$, $p = 0.05$) of an externally applied electric field. Moreover, the reduced shaker speed eliminated the problem of jarring the leads, which had led to both arcing and disconnection of the electric field. For all remaining experiments, therefore, the shaker speed was reduced to 160 cycles/min.

The next series of experiments investigated the relationship between the strength of the applied electric field and the observed activity of TH. Table 5-4 and Figure 5-7 demonstrate the results of these experiments.

Table 5-4. Effect of electric field strength on tyrosine hydroxylase activity.

External Applied Electric Field, V	TH Activity*
0	1181 ± 33
5,000	1427 ± 17
10,000	1632 ± 26
15,000	1948 ± 22
20,000	2292 ± 34

* Activity presented as ng L-dopa formed during 20 min incubation period (mean ± s.d., n = 4)

Figure 5-7. TH activity vs. applied external electric field.

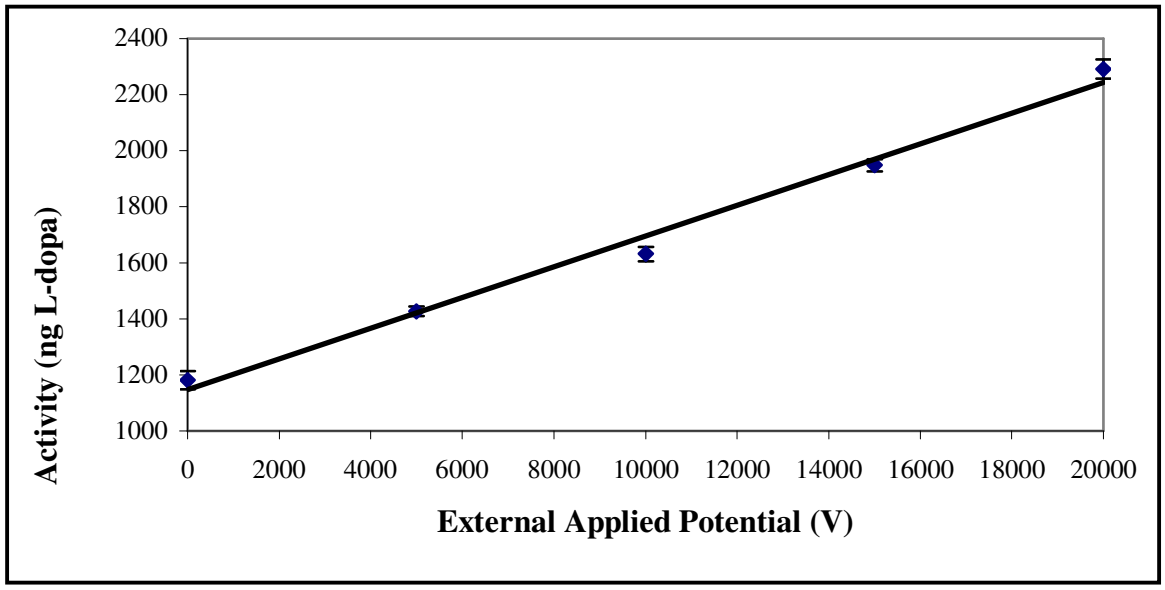

The investigation of the effect of the external applied electric field on the enzyme activity clearly showed that TH activity increased with increasing values of applied external electric field. As can be seen, application of an external electric field of 20,000 V nearly doubled the amount of L-dopa produced by this enzyme when compared to the amount produced in the absence of an external electric field. This data was fitted to the straight line equation y = m x + b, where y = TH activity (ng L-dopa produced) and x = external applied potential, V. The data fit the equation y = 0.055 x + 1150 with a correlation coefficient (R^2) of 0.99.

We then examined whether the amount of L-dopa produced was proportional to incubation time in the absence and presence of an externally applied 20,000 V electric field. In these experiments, samples incubated without and with the external field were

examined at 8.0, 13.0, 18.0 and 28.0 minutes of incubation, respectively. The data were plotted against the incubation time. Figure 5-8 represents the results of this experiment.

Figure 5-8. Tyrosine hydroxylase activity as a function of incubation time in the presence and absence of an applied 20,000 V electric field.

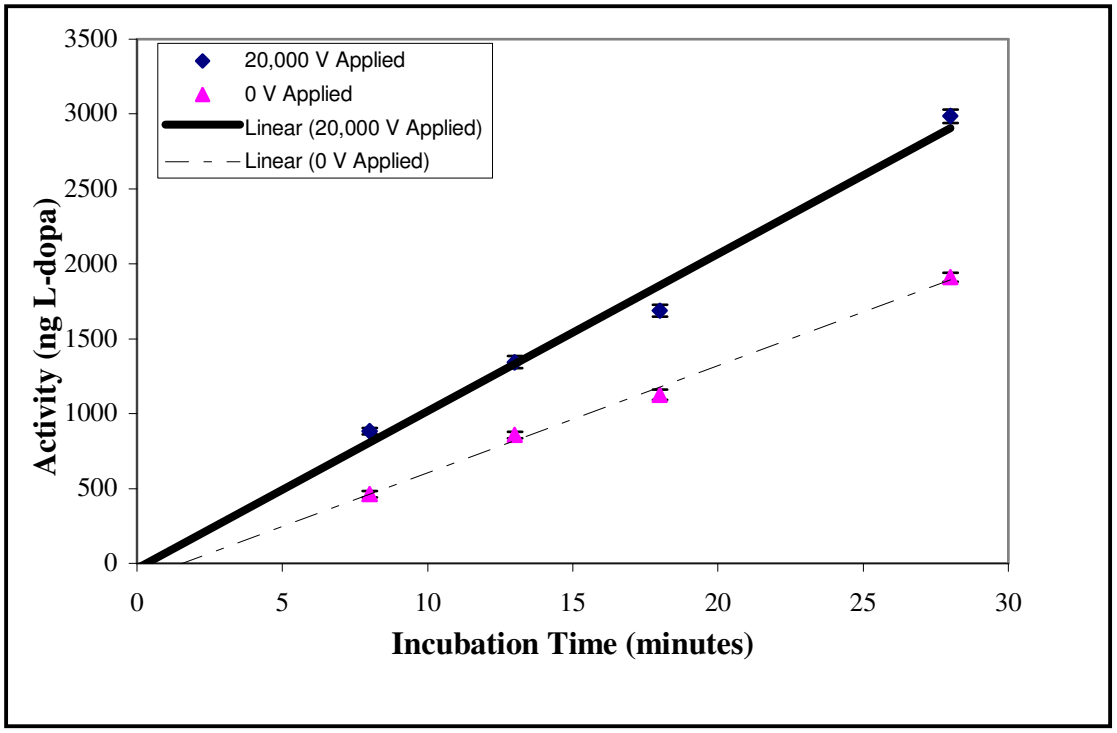

As seen in Figure 5-8, the TH activity for the glass slide immobilized enzyme is completely linear with incubation time for up to at least 28 minutes of incubation in both the absence ($y = 71.5 x - 109$; $R^2 = 0.996$) and presence ($y = 104.9 x - 31.9$; $R^2 = 0.983$) of the externally applied electrical field. Further, from the slopes of the two lines, it is seen that the TH activity in the presence of the 20,000 V field is 1.5 times greater than in the absence of the field. These two conditions, i. e., with the applied electric field and

without the applied electric field, could be equated to "on" and "off" or "active" and "inactive" states of the enzyme, respectively.

In another set of experiments, we examined the importance of the orientation of the tether linking the TH fusion protein to the glass slide in relationship to the applied external electric field. These experiments included two sets of samples. The first set of samples was assayed with the usual attachment of the (+) lead of the externally applied 20,000 V to the copper post and the (-) lead attached to the concentric aluminum cylinder. The second set was assayed under identical conditions except the (+) and (-) electrical leads were reversed**.** This completely reversed the orientation of the enzyme attachment within the applied electric field in the second set of experiments. As the data in table 5-5 shows, however, reversal of the external applied field did not have a significant effect ($t(6) = 0.696$, $p = 0.05$) on the measured activity of the enzyme in the presence of the 20,000 V externally applied field.

Table 5-5. Effect of reversing the orientation of the external applied electrical field on the tyrosine hydroxylase activity.

	TH Activity*	
External Applied Electric Field, V	**Normal Field Orientation****	**Reverse Field Orientation****
0	982 ± 28	975 ± 18
20,000	1563 ± 33	1549 ± 23

* Activity presented as ng L-dopa formed during 20 min inbubation period (mean ± s.d., n = 4)

** Normal orientation had (+) lead connected to center copper post. Reverse orientation had (-) lead connected to center copper post

This somewhat unexpected outcome from the reversal of the external electric field suggests that the "activated" enzyme conformation observed in the presence of the applied external field is somehow achieved independent of the orientation of the attached portion of the fusion protein to the glass slide relative to the applied field. Apparently, the region of the enzyme responsible for the increase in activity in the applied high voltage field is sufficiently remote from the point of attachment to the glass slide to allow the enzyme to maneuver into the higher activity conformation completely independent of the orientation of the externally applied electric field.

There is, presumably, some conformational change in TH when it is exposed to an electric field as witnessed by the effect of the externally applied electric field on the observed activity. The next set of experiments was designed to investigate any possible lag time between the application or removal of the external field and the subsequent conformational reorientation of the protein. In this series of experiments the electric field was turned on for 5 minutes, turned off for 5 minutes, and then turned back on for the last 5 minutes of the experiment. If it took a relatively long time for the enzyme to relax from the more active state back to the less active, the data for the samples in the second sequential time group would be skewed toward higher activity. Subsequently, if it took a relatively long time for the enzyme to change its conformation to the more active form when the electric field was turned back on, the data for the samples from the third sequential time group should be skewed toward lower activity. Table 5-6 contains the results of this series of experiments.

Table 5-6. The effect of intermittent electric field exposure on TH activity.

Experiment	Total Experiment Time (min)	TH Activity*		
		External Applied Electric Field Continuously Off	External Applied Electric Field Continuously On**	Intermittent External Applied Electric Field**
1	10	624 ± 24	1008 ± 28	824 ± 23
2	15	888 ± 21	1404 ± 41	1252 ± 25

* Activity presented as ng L-dopa formed during the 10 and 15 minute inbubation periods (mean ± s.d., n = 4)

** External applied 20,000 V electric field applied for intermediate samples in successive 5 min intervals in Experiments 1 and 2, respectively, as ON/OFF and ON/OFF/ON

For the 10 minute experiment, there were three distinct sample sets: 1.) no electric field exposure for the entire 10 minute experiment, 2.) electric field exposure for the entire 10 minute experiment and 3.) electric field exposure for the initial 5 minutes and then no electric field for the final 5 minutes. If the conformation change to and from the more active state was instantaneous, the intermittent exposure samples should have achieved activities approximately midway between the other two samples. The predicted value for this case, an average of the two activities (off and on), was 816 ± 37 ng L-dopa. If it took a significant time for the enzyme to change conformations, the data would be skewed. The result of the intermittent exposure experiment resulted in an activity of 824 ± 23 ng L-dopa. A students' t-test was performed, and it was determined that these two values were not significantly different ($t(6) = 0.367$, $p = 0.05$).

For the 15 minute experiment, there were also three sets of samples: 1.) no electric field exposure for the entire 15 minute experiment, 2.) electric field exposure for the entire 15 minute experiment and 3.) electric field exposure for 5 minutes, then no electric field for the next 5 minutes and then the electric field was turned back on for the last 5 minutes. Since the intermittent exposure samples were exposed to the electric field for two thirds of the experiment, if the conformation change to and from the more active state was instantaneous, these samples would have achieved activities approximately two thirds that of samples that were exposed to the field for the entire 15 minutes plus one third that of the the samples not exposed to the electric field for the entire 15 minutes. This predicted value was calculated to be 1232 ± 46 ng L-dopa. The experimental result for the intermittent experiment produced a TH activity of 1252 ± 25 ng L-dopa. A students' t-test confirmed that the predicted and experimental values were not significantly different ($t(6) = 0.764$, $p = 0.05$).

Next, kinetic studies were undertaken to determine better understand why strong electric fields led to increased TH activity. A series of experiments were performed to determine the K_m and V_{max} values for both the substrate (L-tyrosine) and cofactor (6-MPH_4) of TH while 1.) not being exposed and 2.) being exposed to an externally applied electric field.

The kinetic data was initially plotted as the observed TH activity as a function of the concentration of substrate or concentration of cofactor as illustrated in Figures 5-9 and 5-10.

Since TH follows Michaelis-Menton kinetics, the data was subsequently plotted using a Lineweaver-Burk double reciprocal approach to derive the values for K_m and

V_{max}. The V_{max} was calculated from the inverse of the y-intercept, and the K_m was calculated as the negative reciprocal of the x-intercept. The Lineweaver-Burk plots for L-tyrosine and 6-MPH_4 are illustrated in Figures 5-11 and 5-12, respectively, while the derived K_m and V_{max} values are listed in Table 5-7.

Figure 5-9. Effect of L-tyrosine concentration on TH activity.

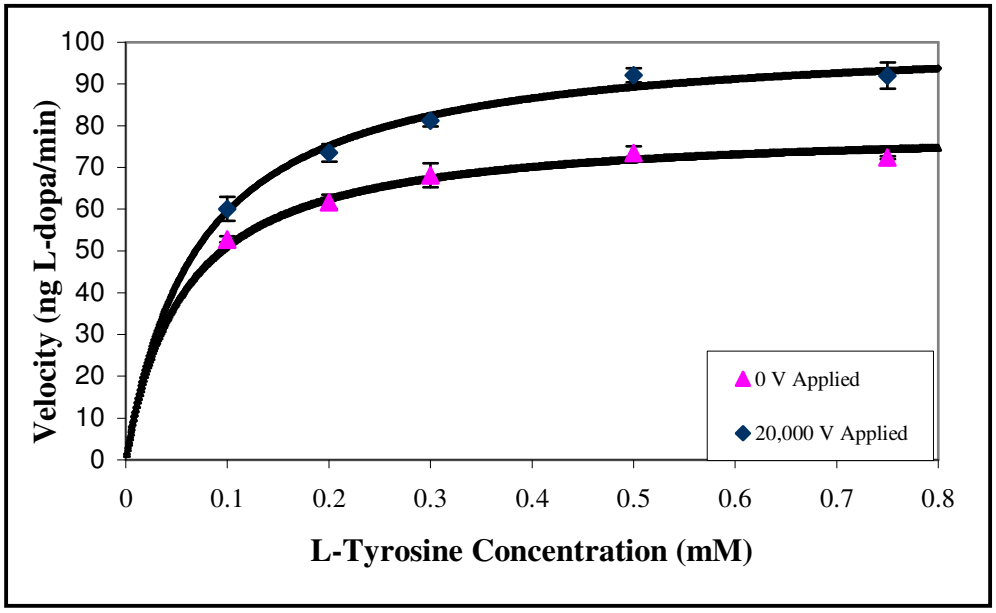

Figure 5-10. Effect of 6-MPH_4 concentration on TH activity.

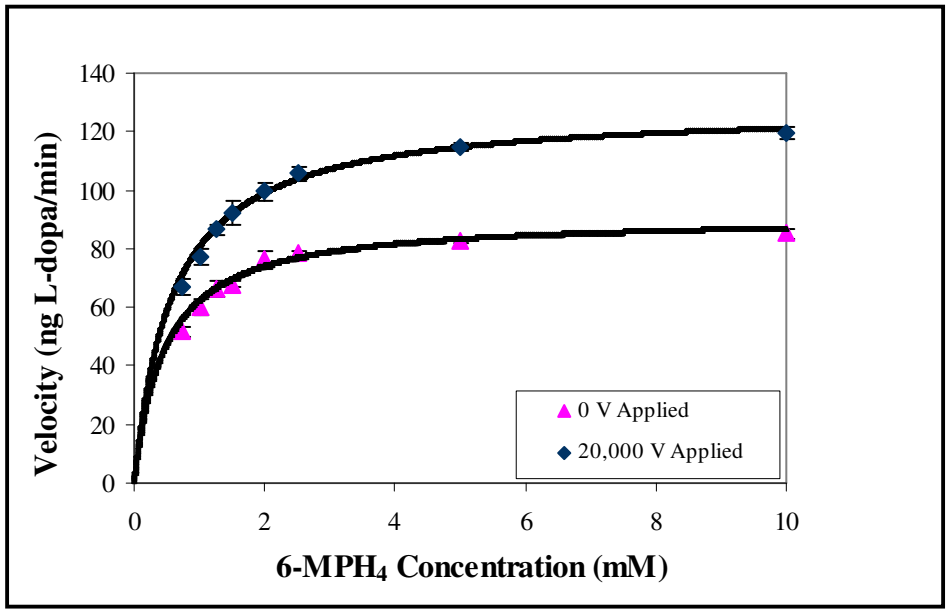

Figure 5-11. Representative Lineweaver-Burk plot for L-tyrosine.

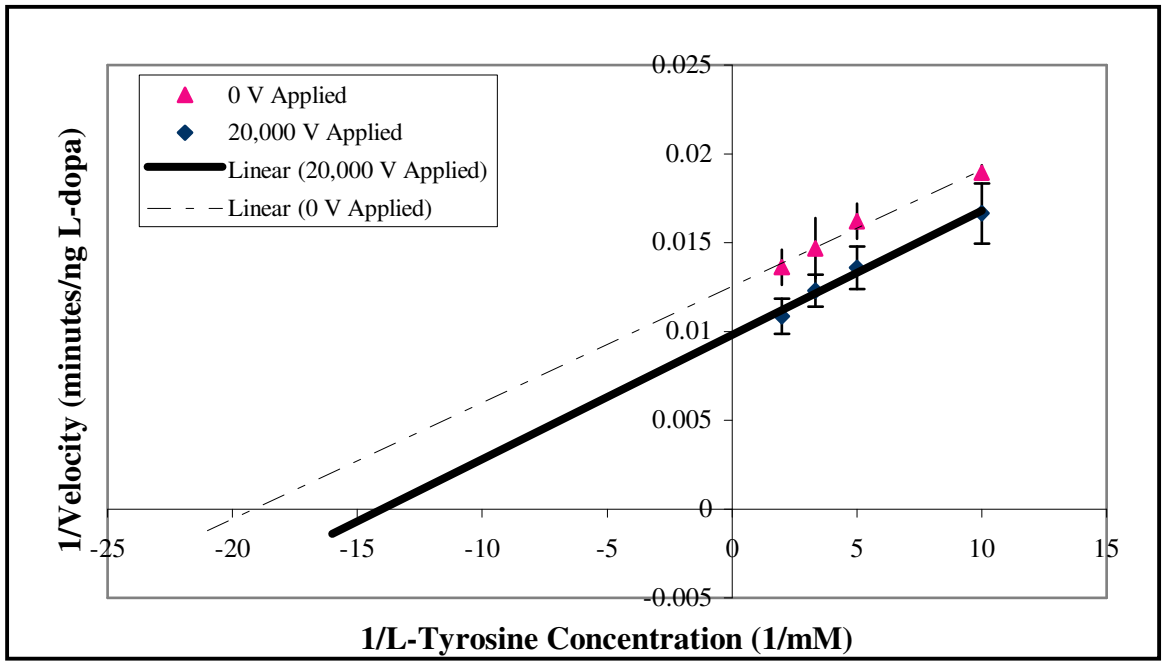

Figure 5-12. Representative Lineweaver-Burk plot for 6-MPH_4.

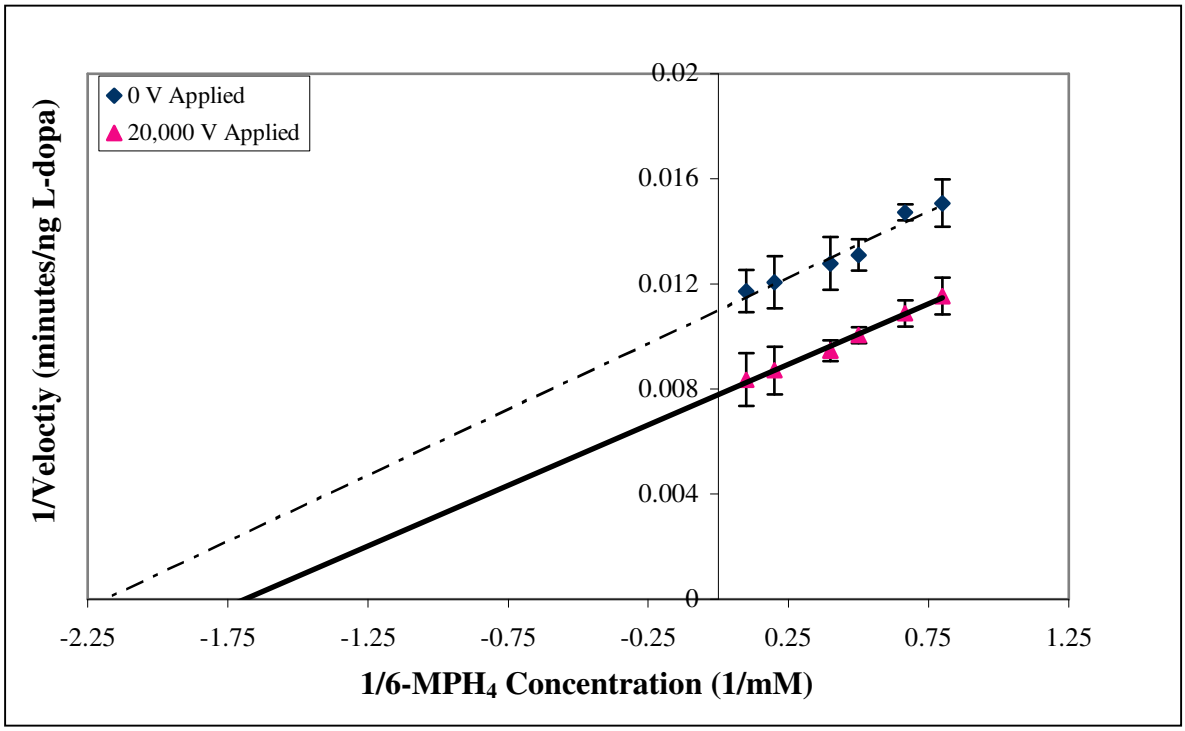

Table 5-7. Kinetic values for L-tyrosine.

Applied Electric Field (V)	K_m* (mM)	V_{max}**	k_{cat}* (sec^{-1})	V/K* (sec^{-1})
0	0.055 ± 0.001	80 ± 2	0.403 ± 0.004	$9.46x10^{-5}$ ± $0.004x10^{-5}$
20,000	0.070 ± 0.002	102 ± 5	0.512 ± 0.007	$9.47x10^{-5}$ ± $0.06x10^{-5}$

* Values reported as mean ± s. d. (n = 2)
** V_{max} values reported as mean ± s. d. (n = 2) in ng L-dopa/min

Table 5-8. Kinetic values for 6-MPH_4.

Applied Electric Field (V)	K_m* (mM)	V_{max}**	k_{cat}* (sec^{-1})	V/K* (sec^{-1})
0	0.455 ± 0.007	91 ± 8	0.463 ± 0.005	$1.30x10^{-5}$ ± $0.03x10^{-5}$
20,000	0.590 ± 0.006	128 ± 9	0.653 ± 0.007	$1.41x10^{-5}$ ± $0.02x10^{-5}$

* Values reported as mean ± s. d. (n = 2)
** V_{max} values reported as mean ± s. d. (n = 2) in ng L-dopa/min

Since K_m is equal to the concentration of the substrate necessary to achieve half the value of the maximum velocity obtainable by the enzyme, K_m is a measure of the efficiency of the enzyme. From the values listed in Tables 5-7 and 5-8, it is seen that even though TH becomes less efficient for the use of both L-tyrosine and 6-MPH_4 in the presence of an electric field, V_{max} increases.

The turnover number, k_{cat}, describes the number of substrate molecules converted to product in a given amount of time per enzyme molecule when the substrate is saturating. It can be seen in Tables 5-7 and 5-8 that the turnover numbers for TH associated with both L-tyrosine and 6-MPH_4 increase when the enzyme is exposed to an electric field. In fact, the k_{cat} for L-tyrosine increased by 27% while the k_{cat} for 6-MPH_4 increased by 40%.

The last parameter in Tables 5-7 and 5-8 is V/K which describes the rate of binding of substrate molecules by the enzyme into productive complexes.[134] Since the units of V_{max} are ng L-dopa/min and the units of K_m are mM, the units of V_{max} were first converted to mM/sec before calculating the ratio. The data shows that exposure of TH to an electric field does not change the rate of binding of L-tyrosine into productive complexes ($t(2) = 0.235$, $p = 0.05$); however, the rate of binding 6-MPH_4 into productive compleses is increased in the presence of an electric field ($t(2) = 31.24$, $p = 0.05$).

V. Conclusions

We developed an apparatus that would allow for the exposure of tyrosine hydroxylase (TH) to a strong electric field with controlled orientation of the field relative to the fixed orientation of the point of attachment of the immobilized enzyme. The apparatus was capable of generating fields with applied potentials ranging from 0 to 20,000 V. Using this electric field apparatus and the techniques developed in Chapters 3 and 4, we established that the activity of TH is affected by exposure to a strong electric field. The activity of TH is increased within the electric field independent of the orientation of the field. In fact, the activity of TH increases linearly with increasing electric field strength.

Kinetic analysis revealed that the binding affinity of TH for both the L-tyrosine substrate and the 6-MPH_4 cofactor decreased in the presence of the electric field. However, the observed V_{max} increased in the presence of the electric field for both the

substrate and the cofactor. Suprisingly, the increase in V_{max} in both cases was sufficient to overcome the decreased affinity of the enzyme for both the substrate and cofactor.

The formation of a more active/productive form of TH within an electric field could be imagined to be due to any number of factors. We briefly speculate on possible sources of this outcome here to provide future investigators possible paths for pursuit.

First, we note that the values of k_{cat} show an increase in the presence of the applied electric field. This would imply that there was an increased efficiency in the conversion of substrate molecules into product molecules in a given amount of time for each enzyme molecule. But, the reasons why this has occurred are less obvious.

The ratio of V_{max} to K_m for 6-MPH_4 may also help explain the increased activity of TH in the presence of the electric field. The V_{max} to K_m ratio increased in the presence of the applied field relative to the absence of the field, with the t-test comparison showing the two values to be significantly different ($p < 0.05$). This indicates that the rate of formation of the enzyme/cofactor complexes leading to successful production of the ultimately desired L-dopa product were increased in the presence of the electric field.

The inhibition of the enzyme by the L-dopa product could also possibly be involved in the observed enhancement of TH activity in the strong electric field. In this case, the molecular oxygen is known to oxidize the essential ferrous ion to the ferrate ion, rendering the enzyme inactive. The biopterin, or in our case the 6-MPH_4, cofactor then typically reduces the Fe^{3+} to Fe^{2+}, which reactivates the enzyme. However, L-dopa binding to the active site can effectively block this reduction of the Fe^{3+} to Fe^{2+} by the cofactor.[126, 137] Typical K values for this feedback inhibition by L-dopa are in the range of 40-50 micromolar, which are very comparable to the 5-10 micromolar values

achieved in our typical TH incubation mixture.[126] Thus, in the presence of an electric field, this feedback inhibition could feasibly be reduced due to a decreased affinity of the enzyme for the L-dopa product as involved in this mechanism. Such a decreased affinity could obviously be brought about by changes in the active site environment due to the electric field.

Alternative explanations could involve possible active site alterations, which would include simple enzyme conformational changes and/or altered electrostatic interactions. Such factors could lead to the observed changes in TH activity all by themselves. Such changes could also lead to thermodynamic and/or kinetic factors, which could explain the observations. A simple decrease in the activation energy or alteration in the free energy change involved would suffice for a kinetic and/or thermodynamic explanation. However, any such explanations via changes in thermodynamics and/or kinetics simply beg the question as to the underlying source of the observed changes.

Conformational changes leading to a more “open” active site could possibly explain why the V_{max} for both substrate and cofactor increased even though the K_m values for both, seemingly paradoxically, were decreased. In a more open arrangement, even though the affinities for the substrate and cofactor may be less, the active site of the enzyme could be envisioned to be much more accessible to each of these essential components.

Based on these results obtained in our kinetic experiments in particular, the originally hypothesized additional "short-term" regulation effect of the large electric field on TH seems less likely and/or less applicable at this time. On the other hand, the current

results could quite reasonably be seen to apply to situations associated with the process of aging and other potential related concerns. The catecholamine neurotransmitter levels are clearly affected by the rate of TH activity. Likewise, these transmitters are known to be involved in learning, memory, sleep-wake cycle and regulation of cerebral blood flow.[6] The results obtained could help explain the physiological development of deficiencies in learning, appearance of memory loss, sleep disturbance, pain threshold alteration, disturbed thermoregulation and even development of Parkinson's disease. All of these difficulties are clearly associated primarily with and/or exacerbated by aging.[135] Aging membranes have altered structures, notably including increased cholesterol content. The increased cholesterol content is accompanied by a decrease in the overall percentage of lipids, leading to a decreased surface charge per unit area.[135] Since a substantial portion of TH is bound to the neuronal membrane, it would of course be affected by the associated electric field. We have shown in this dissertation that alterations in such electric fields unquestionably alter the enzymatic activity of TH, and thus any change in the membrane that could lead to changes in these electric fields would clearly affect TH activity.

A concern raised by the current studies is associated with the selection and utilization of the acetate buffer for the enzyme incubations. Since the incubation pH of 6.80 is considerably removed from the pK_a value of 4.74 for acetic acid, there is some concern about the limited buffering capacity of the incubation mixtures and the possible effects this could have had on the outcomes observed. While acetate buffer has been traditionally used for TH assays, it may lead to complicating factors in studies like those undertaken here. Thus, this might be worth further investigation. Similarly, the

isoelectric points of various pertinent functional groups involved in the catalytic process may have been initially near the pH of the incubation mixture and, then, substantially altered due to a lack of buffer capacity and/or changes in the group(s) themselves.

Field induced effects on many other physical phenomena could also be involved in the results obtained in our investigations. There could be electric field induced alterations in pK_a values of the active site moieties, the substrate, the cofactor, and/or the solution components. Electric fields could lead to substantial orientation of "freely" mobile molecules, like the substrate and cofactor, through their endogenous charge and/or dipolar orientations that would lead to an enhanced fraction of the time being spent in a favorable orientation for interaction with the enzyme's active site. Mobility of various ionic species would almost certainly be affected by strong electric fields. Many of the pertinent molecular species involved in the enzymatic activity are obviously ions or have appropriately alterable mobility factors. One might even consider the possibility of obliquely related things like substantially enhanced charge hopping, a phenomenon observed in xerography in amorphous glasses due to large applied electric fields.[138,139]

In short, we are very excited to have been able to develop both physical and biochemical techniques in our laboratory which have clearly demonstrated the substantial enhancement of immobilized tyrosine hydroxylase activity in a strong electric field. Yet, there remain many questions and many different possibilities as to the source of this observation.

References

1. Laverty, R. Catecholamines: Role in health and disease. *Drugs.* **16:**418-40 (1978).

2. Meissner, W., Harnack, D., Reese, R., et al. High-frequency stimulation of the subthalamic nucleus enhances striatal dopamine release and metabolism in rats. *J of Neurochem.* **85:**601-09 (2003).

3. Schierle, G.S. and Brundin, P. Excitotoxicity plays a role in the death of tyrosine hydroxylase- immunopositive nigral neurons cultured in serum-free medium. *Exp Neurol.* **157:**338-48 (1999).

4. Matsushita, N., Okada, H., Yasoshima, Y., et al. Dynamics of tyrosine hydroxylase promoter activity during midbrain dopaminergic neuron development. *J of Neurochem.* **82:**295-304 (2002).

5. Rowley, M., Bristow, L.J., and Hutson, P.H. Current and novel approaches to the drug treatment of schizophrenia. *J Med Chem.* **44:**477-501 (2001).

6. Siegel, G.J., Agranoff, B.W., Albers, R.W., et al., *Basic neurochemistry: Molecular, cellular and medical aspects*, 6th ed. (Lippincott-Raven Publishers, Philadelphia, PA, 1999).

7. Cooper, J.R., Bloom, F.E., and Roth, R.H., *The biochemical basis of neuropharmacology*, 7th ed. (Oxford University Press, New York, 1996).

8. Nestler, E.J., McMahon, A., Sabban, E.L., et al. Chronic antidepressant administration decreases the expression of tyrosine hydroxylase in the rat locus coeruleus. *Proc Nat Acad Sci USA.* **87:**7522-6 (1990).

9. Martinez-Mir, I., Palop, V., Morales-Olivas, F.J., et al. The effects of epinine on arterial blood pressure and regional vascular resistances in anesthetized rats. *Gen Pharmacol.* **31:**75-9 (1998).

10. Lehninger, A.L., Nelson, D.L., and Cox, M.M., *Principles of biochemistry*, 2nd ed. (Worth Publishers, New York, NY, 1993).

11. Molinoff, P.B. and Axelrod, J. Biochemistry of catecholamines. *Ann Rev Biochem.* **40:**465-500 (1971).

12. Kaufman, S. New tetrahydrobiopterin-dependent systems. *Ann Rev Nutrit.* **13:**261-86 (1993).

13. Almas, B., Toska, K., Teigen, K., et al. A kinetic and conformational study on the interaction of tetrahydropteridines with tyrosine hydroxylase. *Biochem.* **39:**13676-86 (2000).

14. Goodwill, K.E., Sabatier, C., Marks, C., et al. Crystal structure of tyrosine hydroxylase at 2.3 angstroms and its implications for inherited neurodegenerative diseases. *Nat Struct Bio.* **4:**578-85 (1997).

15. Fitzpatrick, P.F. Mechanistic studies of tyrosine hydroxylase. *Adv Exp Med Bio.* **338:**81-86 (1993).

16. Maass, A., Scholz, J., and Moser, A. Modeled ligand-protein complexes elucidate the origin of substrate specificity and provide insight into catalytic mechanisms of phenylalanine hydroxylase and tyrosine hydroxylase. *Eur J Biochem.* **270:**1065-75 (2003).

17. Fitzpatrick, P.F. Tetrahydropterin-dependent amino acid hydroxylases. *Ann Rev Biochem.* **68:**355-81 (1999).

18. Kappock, T.J. and Caradonna, J.P. Pterin-dependent amino acid hydroxylases. *Chem Rev.* **96:**2659-756 (1996).

19. Nagatsu, T. and Ichinose, H. Comparative studies on the structure of human tyrsosine hydroxylase with those of the enzyme of various mammals. *Comp Biochem Phys.* **98:**203-10 (1991).

20. Dunkley, P.R., Bobrovskaya, L., Graham, M.E., et al. Tyrosine hydroxylase phosphorylation: Regulation and consequences. *J Neurochem.* **91:**1025-43 (2004).

21. Kumer, S.C. and Vrana, K.E. Intricate regulation of tyrosine hydroxylase activity and gene expression. *J of Neurochem.* **67:**443-62 (1996).

22. Zigmond, R.E. A comparison of the long-term and short-term regulations of tyrosine hydroxylase activity. *J Physiol.* **83:**267-71 (1989).

23. Nagatsu, T., Levitt, M., and Udenfriend, S. Tyrosine hydroxylase: The initial step in norepinephrine biosynthesis. *J Bio Chem.* **239:**2910-17 (1964).

24. Krauss, G., *Biochemistry of signal transduction and regulation*, 4th ed. (Wiley-VCH Verlag GMBH KGaA, Germany, 2008).

25. Zigmond, R.E., Schwarzschild, M.A., and Rittenhouse, A.R. Acute regulation of tyrosine hydroxylase by nerve activity and by neurotransmitters via phophorylation. *Ann Rev Neurosci.* **12:**415-61 (1989).

26. Perez, R.G., Waymire, J.C., Lin, E., et al. A role for alpha-synuclein in the regulation of dopamine biosynthesis. *J Neurosci.* **22:**3090-9 (2002).

27. Haycock, J.W. and Haycock, D.A. Tyrosine hydroxylase in rat brain dopamine nerve terminals. *J Bio Chem.* **266:**5650-57 (1991).

28. Tachikawa, E., Tank, A.W., Weiner, D.H., et al. *J Neurochem.* **48:**1366-76 (1987).

29. Campbell, D.G., Hardie, D.G., and Vulliet, P.R. Identification of the four phosphorylation sites in the n-terminal region of tyrosine hydroxylase. *J Biol Chem.* **261:**10489-92 (1986).

30. Bevilaqua, L.R., Graham, M.E., Dunkley, P.R., et al. Phosphorylation of ser(19) alters the conformation of tyrosine hydroxylase to increase the rate of phosphorylation of ser(40). *J Biol Chem.* **276:**40411-6 (2001).

31. Thompson, T.L., Colby, K.A., and Patrick, R.L. Activation of striatal tyrosine hydroxylase by in vivo electrical stiumlation: Comparison with cyclic amp-mediated activation. *Neurochem Res.* **15:**1159-66 (1990).

32. Daubner, S.C., Lauriano, C., Haycock, J.W., et al. Site-directed mutagenesis of serine 40 of rat tyrosine hydroxylase. Effects of dopamine and camp-dependent phosphorylation on enzyme activity. *J Biol Chem.* **267:**12639-46 (1992).

33. Ribeiro, P., Wang, Y., Citron, B.A., et al. Regulation of recombinant rat tyrosine hydroxylase by dopamine. *Proc Nat Acad Sci USA.* **89:**9593-7 (1992).

34. Ramsey, A.J. and Fitzpatrick, P.F. Effects of phosphorylation of serine 40 of tyrosine hydroxylase on binding of catecholamines: Evidence for a novel regulatory mechanism. *Biochem.* **37:**8980-6 (1998).

35. Royo, M., Daubner, S.C., and Fitzpatrick, P.F. Specificity of the map kinase erk2 for phosphorylation of tyrosine hydroxylase. *Arch Biochem Biophys.* **423:**247-52 (2004).

36. Haycock, J.W., Ahn, N.G., Cobb, M.H., et al. Erk1 and erk2, two microtubule-associated protein 2 kinases, mediate the phosphorylation of tyrosine hydroxylase at serine-31 in situ. *Proc Nat Acad Sci USA.* **89:**2365-9 (1992).

37. Liu, N., Cigola, E., Tinti, C., et al. Unique regulation of immediate early gene and tyrosine hydroxylase expression in the odor-deprived mouse olfactory bulb. *J Biol Chem.* **274:**3042-7 (1999).

38. Vetillard, A., Benanni, S., Saligaut, C., et al. Localization of tyrosine hydroxylase and its messenger rna in the brain of rainbow trout by immunocytochemistry and in situ hybridization. *J Comp Neurol.* **449:**374-89 (2002).

39. Kilbourne, E.J., Nankova, B.B., Lewis, E.J., et al. Regulated expression of the tyrosine hydroxylase gene by membrane depolarization. *J Bio Chem.* **267:**7563-69 (1992).

40. Montminy, M., Gonzalex, G., and Yamamoto, K. Regulation of camp-inducible genes by creb. *Trend Neurosci.* **13:**184-88 (1990).

41. Bear, M.F., Connors, B.W., and Paradiso, M.A., *Neuroscience: Exploring the brain*, 2nd ed. (Lippincott Williams and Wilkins, Baltimore, 2001).

42. Coyle, J.T. and Wooten, G.F. Rapid axonal transport of tyrosine hydroxylase and dopamine- -hydroxylase. *Brain Res.* **44:**701-4 (1972).

43. Thoenen, H., Mueller, R.A., and Axelrod, J. Phase difference in the induction of tyrosine hydroxylase in cell body and nerve terminals of sympathetic neurones. *Proc Nat Acad Sci USA.* **65:**58-62 (1970).

44. Ito, R., Asami, S., Kagawa, S., et al. Usefulness of tyrosine hydroxylase mrna for diagnosis and detection of minimal residual disease in neuroblastoma. *Biol Pharm Bull.* **27:**315-8 (2004).

45. Michaelis, L. and Menten, M.L. *Biochem.* **49:**333-69 (1913).

46. Rao, D.N. Enzyme kinetics? Elementary, my dear... *Resonance.* **3:**38-44 (1998).

47. Reguzzoni, M., Cosentino, M., Rasini, E., et al. Ultrastructural localization of tyrosine hydroxylase in human peripheral blood mononuclear cells: Effect of stimulation with phytohaemagglutinin. *Cell Tissue Res.* **310:**297-304 (2002).

48. Kaufman, S. Tyrosine hydroxylase. *Adv Enzymol Relat Areas Mol Biol.* **70:**103-220 (1995).

49. Pickel, V.M., Joh, T.H., and Reis, D.J. Ultrastructural localization of tyrosine hydroxylase in noradrenergic neurons of brain. *Proc Nat Acad Sci USA.* **72:**659-63 (1975).

50. Kuczenski, R.T. and Mandell, A.J. Regulatory properties of soluble and particulate rat brain tyrosine hydroxylase. *J Bio Chem.* **247:**3114-22 (1972).

51. Doskeland, A.P. and Flatmark, T. Ubiquitination of soluble and membrane-bound tyrosine hydroxylase and degradation of the soluble form. *Eur J Biochem.* **269:**1561-9 (2002).

52. McGeer, E.G., McGeer, P.L., and Wada, J.A. Distribution of tyrosine hydroxylase in human and animal brain. *J Neurochem.* **18:**1647-58 (1971).

53. Kuczenski, R.T. and Mandell, A.J. Regulatory properties of soluble and particulate rat brain tyrosine hydroxylase. *J Biol Chem.* **247:**3114-22 (1972).

54. Singer, S.J. and Nicolson, G.L. The fluid mosaic model of the structure of cell membranes. *Science.* **175:**720-31 (1972).

55. Tsong, T.Y. and Astumian, R.D. Electroconformational coupling and membrane protein function. *Prog Biophys Mol Biol.* **50:**1-45 (1987).

56. Tsong, T.Y. and Astumian, R.D. Electroconformational coupling: How membrane-bound atpase transduces energy from dynamic electric fields. *Annu Rev Physiol.* **50:**273-90 (1988).

57. Bezanilla, F., Taylor, R.E., and Fernandez, J.M. Distribution and kinetics of membrane dielectric polarization. 1. Long-term inactivation of gating currents. *J Gen Physiol.* **79:**21-40 (1982).

58. Goldman, D.E. Potential, impedenance and rectification in membranes. *J Gen Physiol.* **27:**37-60 (1943).

59. Kamp, F., Chen, Y., and Westerhoff, H.V. Energization-induced redistribution of charge carriers near membranes. *Biophys Chem.* **30:**113-32 (1988).

60. Pannese, E., *Neurocytology: Fine structure of neurons, nerve processes, and neuroglial cells*. (Thieme Medical Publishers, Inc., New York, 1994).

61. Dillon, P.F., Root-Bernstein, R.S., Sears, P.R., et al. Natural electrophoresis of norepinephrine and ascorbic acid. *Biophys J.* **79:**370-76 (2000).

62. McLaughlin, S. and Harary, H. Phospholipid flip-flop and the distribution of surface charges in excitable membranes. *Biophys J.* **14:**200-08 (1974).

63. Thórólfsson, M., Døskeland, A.P., Muga, A., et al. The binding of tyrosine hydroxylase to negatively charged lipid bilayers involves the n-terminal region of the enzyme. *FEBS Letters.* **519:**221-26 (2002).

64. Johnson, J.E. and Cornell, R.B. Amphitropic proteins: Regulation by reversible membrane interactions (review). *Mol Mem Biol.* **16:**217-35 (1999).

65. Hol, W.G.J., van Duijnen, P.T., and Berendsen, H.J.C. The alpha-helix dipole and the properies of proteins. *Nature.* **273:**443-46 (1978).

66. Ettre, L.S. and Sakodynskii, K.I. M. S. Tswett and the discovery of chromatography i; early work (1899-1903). *Chromatographia.* **35:**223-31 (1993).

67. Ettre, L.S. and Sakodynskii, K.I. M. S. Tswett and the discovery of chromatography ii: Completion of the development of chromatography (1903–1910) *Chromatographia.* **37:**329-38 (1993).

68. Craveo, P. and Podhradsky, D. High-performance liquid chromatography of amino acids after derivatization with 9-isothiocyanatoacridine *J Biochem Biophys Meth.* **30:**145-52 (1996).

69. Kiyokatsu, J., Muramatsua, T., Saitoa, Y., et al. Analysis of pesticides in environmental water samples by solid-phase micro-extraction—high-performance liquid chromatography *J Chrom A.* **754:**137-44 (1996).

70. Skoog, D.A. and Leary, J.J., *Principles of instrumental analysis*, 4th ed. (Harcourt Brace College Publishers, Orlando, FL, 1992).

71. Kissinger, P.T., Refshauge, C., Dreiling, R., et al. An electrochemical detector for liquid chromatography with picogram sensitivity. *Anal Lett.* **6:**465-77 (1973).

72. Refshauge, C., Kissinger, P.T., Dreiling, R., et al. New high performance liquid chromatographic analysis of brain catecholamines. *Life Sci.* **14:**311-22 (1974).

73. Kissinger, P.T. and Heineman, W.R. eds., *Laboratory techniques in electroanalytical chemistry*. (Marcel Dekker, New York, 1984).

74. William, R., *Pulsed electrochemical detection*. (John Wiley and Sons, Inc., New York, 1997).

75. Weber, S.G. and Purdy, W.C. Electrochemical detectors in liquid chromatography. *Ind Eng Chem Prod Res Dev.* **20:**593 (1981).

76. Blank, C.L. and Pike, R.L. A novel, inexpensive, and sensitive method for analysis of tyrosine hydroxylase activity in tissue samples. *Life Sci.* **18:**859-66 (1976).

77. Gramsbergen, J.B., Sandberg, M., Moller Dall, A., et al. Glutathione depletion in nigrostriatal slice cultures: Gaba loss, dopamine resistance and protection by the tetrahydrobiopterin precursor sepiapterin. *Brain Res.* **935:**47-58 (2002).

78. He, H., Stein, C.M., Christman, B., et al. Determination of catecholamines in sheep plasma by high-performance liquid chromatography with electrochemical detection: Comparison of deoxyepinephrine and 3,4-dihydroxybenzylamine as internal standard. *J Chrom B.* **701:**115-19 (1997).

79. Naoi, M., Takahashi, T., and Nagatsu, T. Simple assay procedure for tyrosine hydroxylase activity by high-performance liquid chromatography employing coulometric detection with minimal sample preparation. *J Chromatogr.* **427:**229-38 (1988).

80. Kato, T., Horiuchi, S., Togari, A., et al. A sensitive and inexpensive high-performance liquidchromatographic assay for tyrosine hydroxylas. *Experientia.* **37:**809-11 (1981).

81. Nagatsu, T., Oka, K., and Kato, T. Highly sensitive assay for tyrosine hydroxylase activity by high-performance liquid chromatography. *J Chromatogr.* **163:**247-52 (1979).

82. D'Sa, C.M., Arthur, R.E., Jr., and Kuhn, D.M. Expression and deletion mutagenesis of tryptophan hydroxylase fusion proteins: Delineation of the enzyme catalytic core. *J Neurochem.* **67:**917-26 (1996).

83. Saluta, M. and Bell, P.A.Troubleshooting GST Fusion Protein Expression in E. coli. Amersham Biosciences. 1998.

84. Svenson, A., Carlsson, J., and Eaker, D. Specific isolation of cysteine peptides by covalent chromatography on thiol agarose derivatives. *FEBS Letters.* **73:**171-74 (1977).

85. Girardini, J., Amirante, A., Zemzoumi, K., et al. Characterization of an omega-class glutathione s-transferase from schistosoma mansoni with glutaredoxin-like dehydroascorbate reductase and thiol transferase activities. *Eur J Biochem.* **269:**5512-21 (2002).

86. Simons, P.C. and Vander Jagt, D.L. Purification of glutathione s-transferases by glutathione-affinity chromatography. *Methods Enzymol.* **77:**235-7 (1981).

87. Simons, P.C. and Vander Jagt, D.L. Purification of glutathione s-transferases from human liver by glutathione-affinity chromatography. *Anal Biochem.* **82:**334-41 (1977).

88. Toribio, F., Martinez-Lara, E., Pascual, P., et al. Methods for purification of glutathione peroxidase and related enzymes. *J Chromatogr B Biomed Appl.* **684:**77-97 (1996).

89. Robyt, J.F. and White, B.J., *Biochemical techniques: Theory and practice*. (Waveland Press, Inc., Prospect Heights, IL, 1987).

90. Swank, R.T. and Munkres, K.D. Molecular weight analysis of oligopeptides by electrophoresis in polyacrylamide gel with sodium dodecyl sulfate. *Anal Biochem.* **39:**462-77 (1971).

91. Girardini, J., Amirante, A., Zemzoumi, K., et al. Characterization of an mega-class glutathione s-transferase from schistosoma mansoni with glutaredoxin-like dehydroascorbate reductase and thiol transferase activities. *Eur J Biochem.* **269:**5512-21 (2002).

92. Winayanuwattikun, P. and Ketterman, A.J. Catalytic and structural contributions for glutathione-binding residues in a delta class glutathione s-transferase. *Biochem J.* **382:**751-57 (2004).

93. Vararattanavech, A. and Ketterman, A.J. Multiple roles of glutathione binding-site residues of glutathione s-transferase. *Prot Pep Lett.* **10:**441-48 (2003).

94. Di Simplicio, P., Jensson, H., and Mannervik, B. Identification of the isozymes of glutathione transferase induced by trans-stilbene oxide. *Acta Chem Scand B.* **37:**255-7 (1983).

95. Townsend, D.M. and Tew, K.D. The role of glutathione-s-transferase in anti-cancer drug resistance. *Oncogene.* **22:**7369-75 (2003).

96. Frangioni, J.V. and Neel, B.G. Solubilization and purification of enzymatically active glutathione s-transferase (pgex) fusion proteins. *Anal Biochem.* **210:**179-87 (1993).

97. Axen, R., Drevin, H., and Carlsson, J. Preparation of modified agarose gels containing thiol groups. *Acta Chem Scand B.* **29:**471-74 (1975).

98. Guan, K.L. and Dixon, J.E. Eukaryotic proteins expressed in escherichia coli: An improved thrombin cleavage and purification procedure of fusion proteins with glutathione s-transferase. *Anal Biochem.* **192:**262-7 (1991).

99. KunLiang, G. and Dixon, J.E. Eukaryotic proteins expressed in escherichia coli: An improved thrombin cleavage and purification procedure of fusion proteins with glutathione s-transferase. *Anal Biochem.* **192:**262-67 (1991).

100. Wrona, M. Interpersonal Communication. Jun. 2005.

101. Smith, D.B., Davern, K.M., Board, P.G., et al. Mr 26,000 antigen of schistosoma japonicum recognized by resistant wehi 129/j mice is a parasite glutathione s-transferase. *Proc Nat Acad Sci USA.* **83:**8703-7 (1986).

102. Smith, D.B., Rubira, M.R., Simpson, R.J., et al. Expression of an enzymatically active parasite molecule in escherichia coli: Schistosoma japonicum glutathione s-transferase. *Mol Biochem Parasitol.* **27:**249-56 (1988).

103. Vasser, M., Comstock, L.J., and de Boer, H.A. The tac promoter: A functional hybrid derived from the trp and lac promoters. *Proc Nat Acad Sci USA.* **80:**21-25 (1983).

104. Phillips, T.A., VanBogelen, R.A., and Neidhardt, F.C. Lon gene product of escherichia coli is a heat-shock protein. *J Bacteriol.* **159:**283-7 (1984).

105. D'Sa, C.M., Arthur, R.E., Jr., States, J.C., et al. Tryptophan hydroxylase: Cloning and expression of the rat brain enzyme in mammalian cells. *J Neurochem.* **67:**900-6 (1996).

106. Paliy, O. and Gunasekera, T.S. Growth of e. Coli bl21 in minimal media with different gluconeogenic carbon sources and salt contents. *Appl Microbiol Biotechnol.* **73:**1169-72 (2007).

107. Terpe, K. Overview of bacterial expression systems for heterologous protein production: From molecular and biochemical fundamentals to commercial systems. *Appl Microbiol Biotechnol.* **72:**211-22 (2006).

108. Feng, X.J., Wang, J.H., Shan, A.S., et al. Fusion expression of bovine lactoferricin in escherichia coli. *Protein Expr Purif.* **47:**110-7 (2006).

109. Luria, S.E. and Burrous, J.W. Hybridization between escherichia coli and shigella. *J Bacteriol.* **74:**461-76 (1955).

110. Tortora, G.J., Funke, B.R., and Case, C.L., *Microbiology: An introduction*, 5th ed. (The Benjamin/Cummings Publishing Company, Inc.Redwood City, CA, 1995).

111. Ruegg, U.T. and Rudinger, J. Reductive cleavage of cystine disulfides with tributylphosphine. *Methods Enzymol.* **47:**111-6 (1977).

112. Getz, E.B., Xiao, M., Chakrabarty, T., et al. A comparison between the sulfhydryl reductants tris(2-carboxyethyl)phosphine and dithiothreitol for use in protein biochemistry. *Anal Biochem.* **273:**73-80 (1999).

113. Umezawa, H. Structures and activities of protease inhibitors of microbial origin. *Methods Enzymol.* **45:**678-95 (1976).

114. Zimmerman, U.J. and Schlaepfer, W.W. Characterization of a brain calcium-activated protease that degrades neurofilament proteins. *Biochem.* **21:**3977-82 (1982).

115. Kuramochi, H., Nakata, H., and Ishii, S. Mechanism of association of a specific aldehyde inhibitor, leupeptin, with bovine trypsin. *J Biochem.* **86:**1403-10 (1979).

116. Weber, K. and Osborn, M. The reliability of molecular weight determinations by dodecyl sulfate-polyacrylamide gel electrophoresis. *J Biol Chem.* **244:**4406-12 (1969).

117. Schagger, H., Aquila, H., and Von Jagow, G. Coomassie blue-sodium dodecyl sulfate-polyacrylamide gel electrophoresis for direct visualization of polypeptides during electrophoresis. *Anal Biochem.* **173:**201-5 (1988).

118. Splittgerber, A.G. and Sohl, J. Nonlinearity in protein assays by the coomassie blue dye-binding method. *Anal Biochem.* **179:**198-201 (1989).

119. Bradford, M.M. A rapid and sensitive method for the quantitation of microgram quantities of protein utilizing the principle of protein-dye binding. *Anal Biochem.* **72:**248-54 (1976).

120. Wong, P.K. Development of Methodology for the Determination of Catecholamines, Indoleamines, and Related Hydroxylating Enzymes. Dissertation. (University of Oklahoma, 1980).

121. Rogers, Y.H., Jiang-Baucom, P., Huang, Z.J., et al. Immobilization of oligonucleotides onto a glass support via disulfide bonds: A method for preparation of DNA microarrays. *Anal Biochem.* **266:**23-30 (1999).

122. Perret, E., Leung, A., Morel, A., et al. Versatile decorationof glass surfaces to probe individual protein-protein interactions and cellular adhesion. *Langmuir.* **18:**846-54 (2002).

123. Carlsson, J. and Batista-Viera, F. Solid-phase disulfide oxides: A new approach to reversible immobilization and covalent chromatography of thiol compounds. *Biotech App Biochem.* **14:**114-20 (1991).

124. Grunwell, J.R., Glass, J.L., Lacoste, T.D., et al. Monitoring the conformational fluctuations of DNA hairpins using single-pair fluorescence resonance energy transfer. *JACS.* **123:**4295-303 (2001).

125. Halliwell, C.M. and Cass, A.E. A factorial analysis of silanization conditions for the immobilization of oligonucleotides on glass surfaces. *Anal Chem.* **73:**2476-83 (2001).

126. Arkles, B., Steinmetz, J.R., Zazyczny, J., et al., in *Silanes and other coupling agents*, edited by Mittal, K.L.a.P., E. P. (Utrecht, VSP, 1992), pp. 91-104.

127. Chirgwin, B.H., Plumpton, C., and Kilmister, C.W., *Elementary electromagnetic theory. Volume 1: Steady electric fields and currents*. (Pergamon Press Ltd., Headington Hill Hall, Oxford, 1971).

128. Ryan, S.R. Interpersonal Communication. Feb. 2007.

129. Lide, D.R. ed., *CRC Handbook of Chemistry and Physics*. (CRC Press, Boca Raton, FL, 1995).

130. Warshel, A., Russell, S.T., and Churg, A.K. Macroscopic models for studies of electrostatic interactions in proteins: Limitations and applicability. *Proc Nat Acad SciUSA.* **81:**4785-9 (1984).

131. Kirkwood, J.G. and Shumaker, J.B. The influence of dipole moment fluctuations on the dielectric increment of proteins in solution. *Proc Nat Acad Sci USA.* **38:**855-62 (1952).

132. Nakamura, H., Sakamoto, T., and Wada, A. A theoretical study of the dielectric constant of protein. *Prot Eng.* **2:**177-83 (1988).

133. Gilson, M.K., Rashin, A., Fine, R., et al. On the calculation of electrostatic interactions in proteins. *J Mol biol.* **184:**503-16 (1985).

134. Northrop, D.B. On the meaning of km and v/k in enzyme kinetics. *J Chem Ed.* **75:**1153-57 (1998).

135. Yehuda, S., Rabinovitz, S., Carasso, R.L., et al. The role of polyunsaturated fatty acids in restoring the aging neuronal membrane. *Neurobiol Aging.* **23:**843-53 (2002).

136. Moreland, J.L., Gramada, A., Buzko, O.V., Zhang, Q. and Bourne, P.E. The Molecular Biology Toolkit (mbt): A Modular Platform for Developing Molecular Visualization Applications. *BMC Bioinformatics.* **6:**21 (2005).

137. Ramsey, A.J., Hillas, P.J., and Fitzpatrick, P.F. Characterization of the Active Site Iron in Tyrosine Hydroxylase. *J Biol Chem.* **271:**24395-400 (1996).

138. Lygaitis, R., Getautis, V. and Grazulevicius, J.V. Hole-Transporting Hydrzazones. *Chem Soc Rev.* **37:**770-88 (2008).

139. Zallen, R., *The Physics of Amorphous Solids*. (John Wiley and Sons, Inc.New York, NY 1983).